ANNUAL REPORT 2010

Laboratoire Leon Brillouin

TABLE OF CONTENTS

The Laboratoire Léon Brillouin:

the French National Neutron Facility

Fig. 1 : View of the Orphee reactor, guide hall and laboratory buildings.

The Laboratoire Léon Brillouin is a French Research Infrastructure jointly supported by the *Commissariat à l'Energie Atomique et aux Energies Alternatives* (CEA) and the *Centre National de la Recherche Scientifique* (CNRS); it constructs and operates spectrometers around Orphée, a 14MW reactor operated by the CEA since 1980. The LLB is rather unique among neutron centers worldwide because it was specified from the outset to operate as both a large-scale facility open to a user community as well as a research institute in charge of developing its own research programs. In view of the duality of its mission, the objectives of the LLB are to perform research in its own scientific programs, to promote the use of diffraction and neutron spectroscopy, to welcome and assist experimentalists, subsequently ensuring training and education, and providing access for industrial partners. These activities are enduring and complementary to international centers, such as the Institute Laue-Langevin or the future European Spallation Source in Sweden and cooperation programs with other national centers.

As a **service institute,** the LLB makes its facilities and expertise available to visiting scientists from France and foreign countries, in Europe and abroad, through two calls for proposals per year reviewed by five peer-committees of international experts. About 110 people are currently working at the laboratory, 70% having a permanent position and 30% as non-permanent staff.

Every year, LLB welcomes about 500 visiting scientists with 30% being foreigners (20% European, 10% other countries). About 450 experiments selected by the scientific review committees are performed annually. Moreover, the LLB benefits from the exceptional scientific environment provided by the "*Plateau of Saclay*", which includes the Synchrotron source SOLEIL and many renowned Universities, research centers and engineering schools. LLB is a leading hub for neutron scattering at the national and European levels, and a part of the European network, thus involved in the NMI3 project under the Seventh Framework Program of the European Union Commission.

The neutron source, Orphé**e** is a 14-MW "pool" type reactor, with a compact, light-water moderated, core which delivers up to 3×10^{14} $n.cm^{-2}s^{-1}$ thermal flux in the surrounding heavy water reflector tank. The heavy water tank is equipped with three local moderators: two cold sources (liquid hydrogen at 20K) and one hot source (graphite at 1400 K). The experimental areas are located around the reactor, either in the reactor building or along the neutron guides of the guide hall. One experimental area with specific radiological

shielding has been designed for industrial neutronography (mostly used by the aeronautical or space industry).

The reactor safety was reassessed by a panel of experts, nominated by the French safety authorities, who published their evaluation on October 23rd 2010 in a status report given to the CEA. Though some improvements in safety were required, the report points out that the initial reactor safety features remain appropriate to up-to-date safety practices; the cost of this improvement was planned by additional funding, spread over a few years. All these maintenance operations will enable us to keep the Orphée reactor in a very good functioning state and open up a future of at least ten more years of operations.

LLB's neutron scattering instruments are distributed in six experimental groups responsible for the operation of the instruments and for providing expertise in data analysis: Triple Axis Spectrometry, Powder and Liquids Diffraction, Single Crystal Diffraction, Small Angle Scattering, Reflectometry and Quasi-elastic Scattering . The experimental support for running and developing instruments is provided by four technical groups: Instrument Development, Sample Environment, Electronics, and Information Technology. Common platforms have been implemented to ensure and support specific research activities (Biology, Chemistry, High pressure and Cryogenics). Moreover, one instrument is a Collaborative Research Group Instrument (CRG) with the Karlsruhe Institute of Technology (KIT), a German University of the State of Baden-Württemberg and National Laboratory of the Helmholtz Association. New objectives in research led to the instrumental development program CAP2015. The goal of this program is the modernization or construction of nearly half of the laboratory's instruments by 2015, accounting for the need of the scientific community. In the years to come, this will give LLB an excellent quality of instrumentation at the disposal of the French and European communities.

Another part of LLB's main assignments is the **Organization of Training sessions,** in addition to its own training activity through research programs for PhD students. This follows from the fact that neutron scattering experiments cannot be conducted elsewhere than on medium and large-scale facilities. The LLB participates in the education and information of students, scientists and the general public about both the capabilities of neutron scattering *per se* and the scientific advances achieved thanks to the use of this probe. This consists in taking part in national and international conferences, presenting the technique at local meetings or at all levels of University courses, hosting advanced neutron scattering schools and sponsoring workshops, jointly working with other large-scale facilities and in close collaboration with the French Neutron Scattering Society (SFN). Several other ongoing actions are publications, displays, website, books, but a major one is the supervision of PhD students.

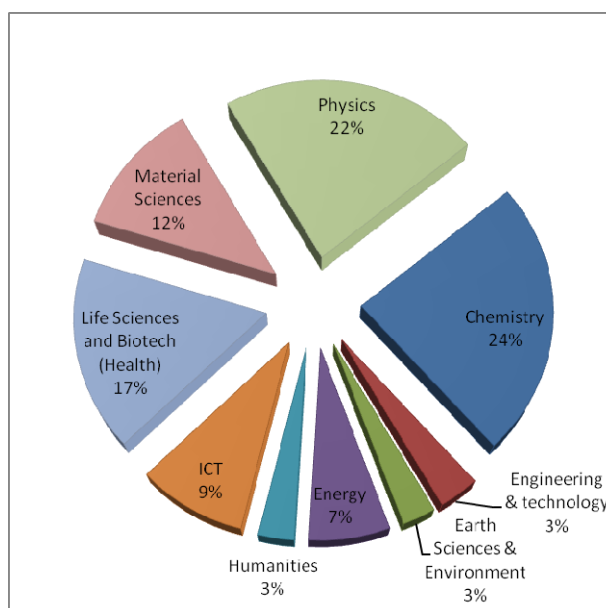*Fig.2 ; Poster announcing the 2011 FANs training session (http://www-llb.cea.fr/fan).*

Fig. 3 : Scientific domains and societal issues explored at the LLB.

The laboratory also proposes its own training session, called « *les FANs du LLB* » (*Formation **A** la **N**eutronique,* see Fig.2), each year in autumn. The aim is to provide young researchers with a first simple contact to real experimental neutron scattering. Students and post-docs working in all scientific areas where neutrons can provide valuable insights are welcome, with newcomers to neutrons scattering being given priority.

A specific feature of the school is that most students come with their own samples which are tested during the training sessions together with our demonstration samples. This ensures a strong and efficient participation in the courses. Moreover tutorial sessions are organized, in connection with several Masters Courses. The objective is to inform students in Physics, Chemistry, Biology and other disciplines of the potential of neutron scattering for their particular field of research.

As a research laboratory, the LLB teams are successfully running their own research program. LLB researchers have a strong international visibility and recognition: the scientific results lead to 578 publications between 2008 and 2010 from which 10-15% are accepted in highly ranked journals (Nature, Science, Angewandte Chemie, Physical Review Letters, and others), equivalent to 70% of the scientific production of the French Neutron Scattering Community. In terms of societal impact, the financed projects are distributed among various domains, Fig. 3 illustrates the multidisciplinary aspects of our work. Some of them belong to the French National Strategy of Research and Innovation (SNRI) such as Health and Biology, Energy or Environmental issues.

Due to the central use of neutron scattering and its multidisciplinary applications for exploring condensed matter, the research of LLB teams is performed among three main axes, covering most of the domains of current interests: -

- Strongly Correlated Quantum Materials and Magnetism,

- Materials and Nanosciences: Fundamental Studies and Applications,

- Soft Matter and Biophysics.

They are shorly described in the "Highlights" section.

Highlights
2010

AXE 1
Strongly Correlated Quantum Materials and Magnetism

The "strongly correlated electron systems" denote a class of materials and physical phenomena which cannot be described in terms of the standard theory for a Fermi gas of non-interacting electrons. Such situations mainly occur in compounds containing transition-metal or rare-earth elements, because d and f orbitals have a more pronounced localized character. One common feature in many of these materials is the coexistence of several degrees of freedom associated with the electron- (charge, spin, orbital) or lattice sub-systems, whose interplay is responsible for a large variety of ground states and excitation spectra. Well-known examples studied at LLB, both experimentally and theoretically, include cuprate or ferropnictide high-T_c superconductors, "giant magnetoresistance" manganites, compounds with short-range magnetic interactions subject to geometrical frustration (multiferroics, spin-ices, etc.), lanthanide-based heavy-fermion systems and "Kondo insulators", as well as a number of materials in which unconventional orders occurs, such as the "magnetic blue phase" of MnSi, or the multipole-order states found in rare-earth hexaborides. Because neutrons interact with both the atom nuclei and their electron shells, neutron scattering is one of the best tools to study this type of physics involving interplay of lattice and magnetic properties. Polarized neutron beams, implemented on several spectrometers at LLB, further enhance the potential of neutron experiments for studying strong correlation phenomena in condensed matter.

- *MAGNETOCALORIC PROPERTIES AND MAGNETIC STRUCTURES OF THE NEW TERNARY SILICIDES $RE_6Co_{1.67}Si_3$ (RE = Nd, Gd, Tb)*
  S. Tencé, E. Gaudin, G. André, B. Chevalier

- *NORMAL-STATE SPIN DYNAMICS AND TEMPERATURE-DEPENDENT SPIN RESONANCE ENERGY IN AN OPTIMALLY DOPED IRON ARSENIDE SUPERCONDUCTOR*
  D. S. Inosov, J. T. Park, P. Bourges, D. L. Sun, Y. Sidis, A. Schneidewind, K. Hradil, D. Haug, C. T. Lin, B. Keimer and V. Hinkov

- *NOVEL MAGNETIC STATE IN THE INCIPIENT KONDO SEMICONDUCTOR $CeRu_2Al_{10}$*
  J. Robert, J-M. Mignot, G. André, T. Nishioka, R. Kobayashi, M. Matsumura, H. Tanida, D. Tanaka, and M. Sera

- *PRESSURE INDUCED FERROMAGNETIC TO ANTIFERROMAGNETIC TRANSITION IN $BiMnO_3$ MULTIFERROIC*
  S. E. Kichanov O. L. Makarova, I. Mirebeau, D.P. Kozlenko, and A. A. Belik

- *MULTIFERROIC BFO FILMS*
  J. Allibe, I.C Infante, H. Béa, B. Dupé, D. khil, K. Bouzehouane, S. Fusil, E. Jacquet, G. Geneste, F. Ott, S. Petit, M. Bibes, and A. Barthélémy

- *EVIDENCE OF THE SPIN MELTING IN THE SPIN LIQUID $Tb_2TI_2O_7$ PYROCHLORE*
  P. Sazonov, A. Gukasov, I. Mirebeau, and P. Bonville.

MAGNETOCALORIC PROPERTIES AND MAGNETIC STRUCTURES OF THE NEW TERNARY SILICIDES $RE_6Co_{1.67}Si_3$ (RE = Nd, Gd, Tb)

S. Tencé[1, 2], E. Gaudin[1], G. André[2], B. Chevalier[1]

[1] CNRS, Université de Bordeaux, ICMCB, 87 avenue du Docteur Albert Schweitzer, 33608 Pessac Cedex, France
[2] CEA, IRAMIS, LLB, 91191 Gif-sur-Yvette Cedex, France

During the past ten years, the interest for the magnetic refrigeration as a new solid state cooling technology competitive with the conventional compression-evaporation cycle for room-temperature applications has grown considerably. Among the magnetocaloric materials, the family of ferromagnetic ternary silicides $RE_6Co_{1.67}Si_3$ (RE = Ce, Pr, Nd, Gd, Tb or Dy) [1], crystallizing with the hexagonal $Ce_6Ni_{1.67}Si_3$–type structure, has been recently discovered by us. These compounds present significant magnetic entropy change ΔS_m, in the vicinity of their ferromagnetic ordering temperature T_C, depending on the RE element. For instance, $Gd_6Co_{1.67}Si_3$ which orders ferromagnetically at T_C = 294 K [2] close to that determined for Gd the reference compound for the magnetic refrigeration, exhibits a ΔS_m value reaching -5.72 J kg^{-1} K^{-1} at T_C for a magnetic field change ΔH from 0 to 4.8 T (*Fig. 1*).
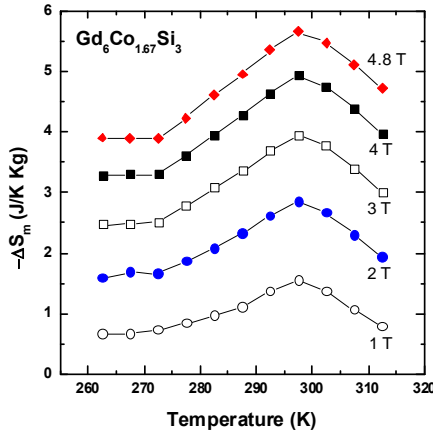

Fig. 1: Temperature dependence of the magnetic entropy of $Gd_6Co_{1.67}Si_3$ measured at various fields.

This ΔS_m value, determined by magnetization measurements, is smaller than that reported for pure gadolinium (-9.5 J kg^{-1} K^{-1} using the same conditions). But as $Gd_6Co_{1.67}Si_3$ shows a broad distribution of the ΔS_m peak, its refrigerant capacity is larger than those of some magnetocaloric materials having a first-order magnetic phase transition. Also, it is interesting

to note that this ternary silicide $Gd_6Co_{1.67}Si_3$ presents no hysteresis in its magnetization *versus* temperature or applied magnetic field, which is highly desired in the magnetic refrigeration cycle.

Magnetization measurements have revealed that other compounds as $Nd_6Co_{1.67}Si_3$ and $Tb_6Co_{1.67}Si_3$ order ferromagnetically at 84 K and 183 K respectively [1] and present below these T_C Curie temperatures additional magnetic transitions, not observed for $Gd_6Co_{1.67}Si_3$, suggesting that the magnetism of these ternary compounds based on Nd and Tb is quite complex. These last transitions appear: (i) at T_1 = 38 K for $Nd_6Co_{1.67}Si_3$ and (ii) near T_1 = 168-170 K for $Tb_6Co_{1.67}Si_3$. Moreover, isothermal magnetization M measurements have revealed complex magnetic behaviors for both compounds highlighted by unusual field cycling with multiple steps in the M *versus* H curves at low temperatures (*Fig. 2*).
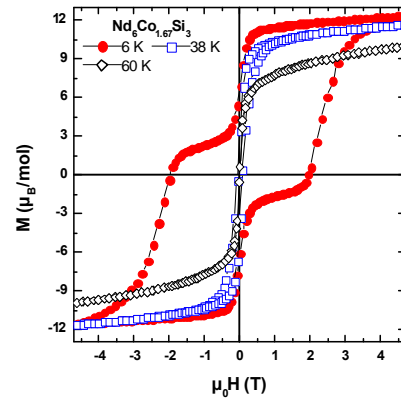

Fig. 2: Field dependence of the magnetization of $Nd_6Co_{1.67}Si_3$ measured at various temperatures below T_C = 84 K.

In particular, at 6 K a field-induced first order transition appears in the isothermal magnetization of $Nd_6Co_{1.67}Si_3$ [3]. Consequently, neutron powder diffraction investigations were required for both ternary silicides in order to explain their magnetic

behaviors and especially the nature of each magnetic transition [4].

Neutron powder diffraction studies have enabled to determine the magnetic structures of $Nd_6Co_{1.67}Si_3$ and $Tb_6Co_{1.67}Si_3$ which present some common points: at 1.5 K both magnetic structures are canted ferromagnetically with a magnetic cell corresponding to the nuclear cell ($\mathbf{k} = (0\ 0\ 0)$) (*Fig. 3*).
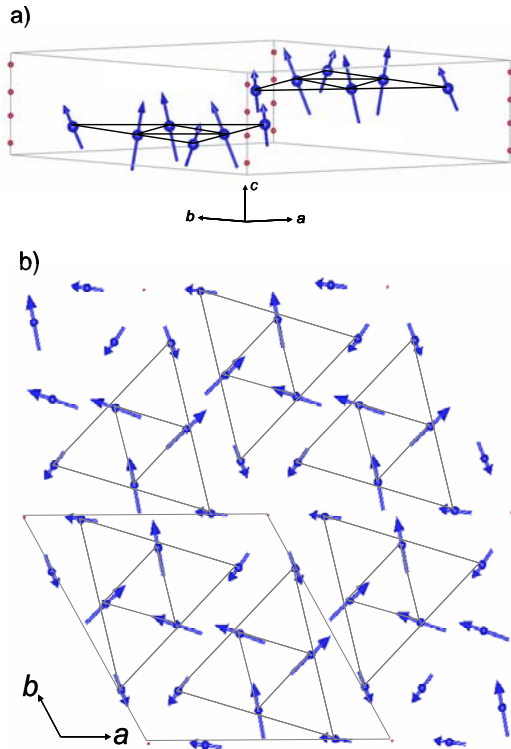
a)

b)

Fig. 3: a) Magnetic structure of $Nd_6Co_{1.67}Si_3$ at 1.5 K and b) Its projection in the (a, b)-plane. For clarity, the Nd-moment value in the projection has been multiplied by 2 compared with the 3D picture.

Magnetic moments have a ferromagnetic component along the *c*-axis and a component into the (*a, b*)-plane with moments at 60° from each other. Moreover, both *RE* sublattices order at the same T_C temperature and the magnetic moment value is higher on the *RE*2 atom than on the *RE*1 atom at any temperature in agreement with the existence of the Co atomic disorder around *RE*1 atom. However, for $Nd_6Co_{1.67}Si_3$, the magnetic structure below $T_C = 84$ K is purely ferromagnetic and the transition at $T_1 = 38$ K corresponds to the beginning of a moment reorientation leading to a canted ferromagnetic structure. $Tb_6Co_{1.67}Si_3$ already has below $T_C = 183$ K a non-collinear ferromagnetic structure and $T_1 = 171$ K corresponds to a spin reorientation with the

onset of two different canting angles for Tb1 and Tb2 atoms. The occurrence of these magnetic structures is discussed on the basis of the atomic disorder existing for Co atom in the ternary silicides around the Nd1 and Tb1 atoms. Nevertheless, neutron diffraction experiments in variable magnetic fields need to be performed in order to understand the nature of the field-induced transitions observed in the isothermal magnetization measurements [3]. In particular, it would be interesting to determine whether the field-induced first-order magnetic transition at low temperature is driven by a simultaneous structural transition or it is from purely magnetic origin.

References

[1] B. Chevalier *et al.* J. Alloys Compd. **442**, 149-151, (2007).
[2] E. Gaudin *et al.* Chem. Mater. **20**, 2972-2979, (2008).
[3] E. Gaudin *et al.* 2008 Solid State Sci. **10**, 481-485, (2008).
[4] S. Tencé *et al.* J. Phys. D: Appl. Phys. **42,** 165003 (10pp), (2009).

NORMAL-STATE SPIN DYNAMICS AND TEMPERATURE-DEPENDENT SPIN RESONANCE ENERGY IN AN OPTIMALLY DOPED IRON ARSENIDE SUPERCONDUCTOR

D. S. Inosov[1], J. T. Park[1], P. Bourges[2], D. L. Sun[1], Y. Sidis[2], A. Schneidewind[3], K. Hradil[3], 4 D. Haug[1], C. T. Lin[1], B. Keimer[1] and V. Hinkov[1]

[1] Max-Planck-Institut für Festkörperforschung, Heisenbergstraße 1, 70569 Stuttgart, Germany
[2] Laboratoire Léon Brillouin, IRAMIS,CEA-CNRS, CEA Saclay, 91191 Gif-sur-Yvette.
[3] Forschungsneutronenquelle Heinz Maier-Leibnitz (FRM-II), TU München, D-85747 Garching, Germany

In conventional superconductors like mercury or niobium, the electronic system gains energy by establishing a superconducting condensate consisting of electron pairs (Cooper pairs) bound by the exchange of virtual phonons. Other elementary excitations also have the potential to mediate pairing: In heavy-fermion superconductors like $CeIrIn_5$ or UPd_2Al_3, antiferromagnetic (AFM) spin excitations are likely to be involved in the pairing mechanism. However, coupling of itinerant carriers to the quasi-localized rare-earth *f*-electrons introduces a complexity hitherto preventing a satisfactory theory.

In cuprate high-*Tc* superconductors, AFM spin excitations are also among the most promising contenders for the pairing boson. However, strong electron correlations and complications arising from a pseudogap state have precluded commonly accepted theories. Typically, the normal-state pseudogap arises from one or more competing phases with the superconductivity: these novel phases include incommensurate spin- and charge-modulated phases or circulating current phases.

The recently discovered iron arsenide superconductors [1] also derive from AFM parents compounds. They are characterized by the omnipresence of AFM correlations throughout the phase diagram, often coexisting with superconductivity deep into the superconducting dome. Besides, it was shown that electron-phonon coupling is too weak to explain the high superconducting critical temperature, *T*c, up to 56 K, which turns the spotlight onto the magnetic coupling channel again. Furthermore, iron arsenides remain itinerant at all doping levels [2], rendering Fermi-liquid based approaches more promising than in the cuprates.
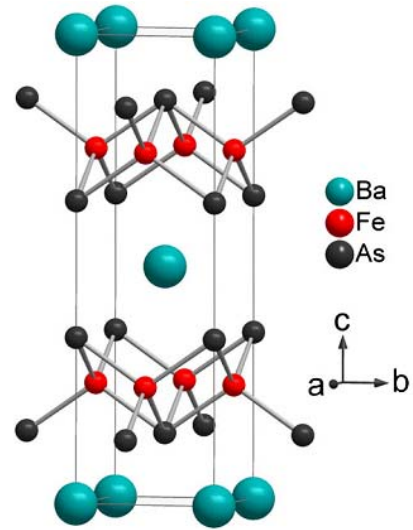

Fig. 1: Nuclear structure of the parent compound BaFe₂As₂ with antiferromagnetic structure. Upon substitution of Fe by Co, one obtains an electron doped metal where the AFM state disappears with an appearance of a superconducting phase for 15 % of Co with a critical temperature of 25 K.

In several of these unconventional superconductors, a redistribution of AFM spectral weight in the superconducting state into a "resonance peak" at an energy $h\omega = h\omega_{res}$ smaller than the superconducting gap 2Δ heralds the onset of superconductivity. Since the intensity of this mode is determined by coherence factors in the superconducting gap equation, it is only expected to occur for particular gap symmetries and was one of the first indications for *d*-wave superconductivity in the cuprates. The recent discovery of a resonant mode in both hole-doped $Ba_{1-x}K_xFe_2As_2$ and electron-doped $BaFe_{2-x}(Ni, Co)_xAs_2$ is therefore an important achievement. While the existence of a resonance was shown to be compatible with a sign-reversed $s^{+/-}$-wave superconducting gap [3], it is a consequence of the opening of the gap and hence does not *per se* constitute

evidence of a magnetic pairing mechanism. Since a pairing boson of sufficient spectral weight must be present already above Tc, detailed knowledge of both the spectrum in the normal state and its redistribution below Tc is a prerequisite for a quantitative assessment of theoretical models.
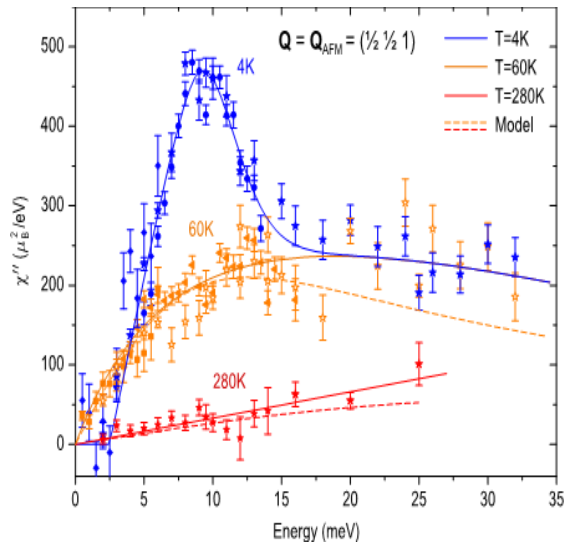

Fig. 2: Imaginary part of Spin susceptibility, Imχ (Q_{AFM}, $h\omega$,) in $BaFe_{1.85}Co_{0.15}As_2$ at the AFM wavevector. The solid lines are guides to the eye. The dashed lines represent global fits of the formula for nearly antiferromagnetic metals [5].

Here we report the spin excitations in a single crystal of optimally electron-doped $BaFe_{1.85}Co_{0.15}As_2$ (Tc =25 K) at temperatures up to T = 280 K and energies up to $h\omega$ = 32 meV (>4Δ) [4]. We perform momentum scans at various energies on both thermal beam triple-axis 2T at LLB and PUMA and FRMII-Garching. At all measured energies, the magnetic spectrum remains commensurate and the measured **Q**-width does not change appreciably with the energy. The Fig. 2 shows the imaginary part of the spin susceptibility Imχ(Q_{AFM}, $h\omega$). One of the central results of our study is that we can present Imχ(Q_{AFM}, $h\omega$) in absolute units by calibrating the magnetic spectrum with the phonons branches for which one can compute the absolute scattering magnitude.

In the superconducting state at 4 K, we observed a peak at $h\omega_{res}$= 9.5 meV in agreement with previous reports. That peak

corresponds to the magnetic resonance peak in that system and signs the opening of the superconducting gap. We also show [4] that the temperature evolution of that resonance energy monotonically follows the closing of the superconducting energy gap s$^{+/-}$ as expected from conventional Fermi-liquid approaches. The simplicity of this behavior is in notable contrast to its counterpart in the cuprates.

In the normal state at 60 K, we observe a broad spectrum of gapless excitations with a maximum around 20 meV and a linear dependence at low energy. Increasing T to 280 K suppresses the intensity and presumably shifts the maximum to higher energies, while the low-energy linearity is preserved. That normal state spectrum carries a weight comparable to underdoped cuprates. However, in contrast to cuprates, the spectrum agrees well with the predictions of the theory of nearly antiferromagnetic metals [5]. This observation points towards a surprisingly simple theoretical description of the spin dynamics in the iron arsenides.

Our comprehensive set of data [4] provides a solid foundation for models of spin fluctuations-mediated superconducting pairing for the iron arsenides. In particular, based on our absolute unit calibration of *Imχ(Q_{AFM},$h\omega$)*, it is now possible to compare the total exchange energy of the electron system below Tc to the condensation energy determined by specific-heat measurements. Independent information about the spin-fermion coupling strength can also be derived from a comparison of the measured spin fluctuation spectrum and the fermionic self-energy extracted from photoemission spectroscopy

References

[1] X.H. Chen *et al*, Nature **453**, 761–762 (2008).
[2] F. Rullier-Albenque *et al,* Phys. Rev. Lett. **103**, 057001 (2009).
[3] *see e.g.* M.M. Korshunov and I. Eremin, Phys. Rev. B **78**, 140509 (2008).
[4] D. S. Inosov, *et al*, Nature Phyics **6**, 178 (2010).
[5] T. Moriya, *Spin Fluctuations in Itinerant Electron Magnetism* (Springer-Verlag, Berlin Heidelberg, 1985).

NOVEL MAGNETIC STATE IN THE INCIPIENT KONDO SEMICONDUCTOR $CeRu_2Al_{10}$

J. Robert[1], J-M. Mignot[1], G. André[1], T. Nishioka[2], R. Kobayashi[2], M. Matsumura[2], H. Tanida[3], D. Tanaka[3], and M. Sera[3]

[1] LLB, CEA-CNRS, CEA/Saclay, 91191 Gif sur Yvette, France
[2] Graduate School of Integrated Arts and Science, Kochi Univ., Kochi 780-8520, Japan
[3] Dept. of Quantum Matter, ADSM, Hiroshima University, Higashi-Hiroshima 739-8530, Japan

The low-temperature behavior of intermetallic cerium compounds is dominated by the competition between several interaction channels (intraatomic couplings, on-site Coulomb repulsion, hybridization between local f-electron states and itinerant conduction-band states) forming the basis of the well-known, highly successful, Anderson model. This gives rise to a variety of ground states, from long-range magnetic order to heavy-electron Fermi liquid, or unconventional superconductivity. Meanwhile, numerous studies have been devoted to Ce-based materials that do not seem to fit into this general framework. Recently, compounds of the CeM_2Al_{10} family (M = Ru, Os, Fe) have been reported to exhibit intriguing properties [1], and became the subject of considerable interest. In both $CeRu_2Al_{10}$ and $CeOs_2Al_{10}$, the transport coefficients below room temperature are indicative of an incipient Kondo-insulating behavior, with a thermally activated variation of the electrical resistivity [1,2]. In this regime, the magnetic susceptibility exhibits a large anisotropy, with the easy direction parallel to the orthorhombic a axis. A phase transition takes place at T_0 = 27 K in $CeRu_2Al_{10}$ (29 K in $CeOs_2Al_{10}$), below which the behavior of the material changes dramatically. In $CeRu_2Al_{10}$, the resistivity shows a positive jump just below T_0, then goes through a maximum and finally drops to a constant, metalliclike, but rather high residual value below 10 K. Huge pressure effects have also been reported. There is ongoing controversy over the mechanism of this transition and its order parameter. The initial assumption [1] that some type of magnetic order took place, accompanied by the opening of a gap at the Fermi surface, was substantiated by the observation of a (quite weak) internal field in μ+SR experiments [3], but subsequent ^{27}Al nuclear quadrupole resonance (NQR) measurements [4] failed to reveal any broadening or splitting of the resonance line imputable to an internal field below the ordering temperature. Alternative scenarios have also been proposed, such as a charge-density wave, a spin-density wave or a dimerization of the Ce sites producing a singlet state, but none of them could be convincingly established. It is noteworthy that the transition temperature T_0 is much higher that the Néel temperature in $GdRu_2Al_{10}$ (T_N = 16.5 K). Neutron scattering studies were thus undertaken at LLB to answer the above questions [5].
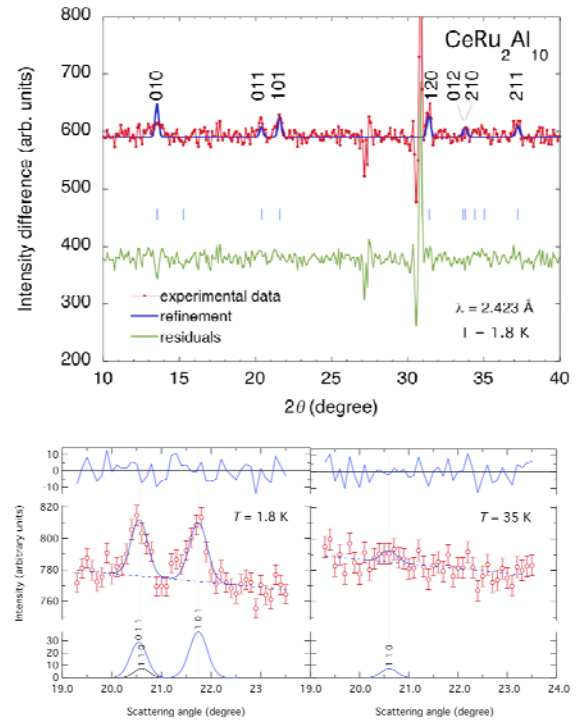
Fig. 1: (top) Powder diffraction pattern measured in the ordered state of $CeRu_2Al_{10}$. (bottom) Enlarged view of the low-angle satellites; note: (110) is a weak nuclear peak.

Superstructure peaks (Fig. 1) observed at the forbidden positions of the base-centered orthorhombic *Cmcm* structure in neutron powder diffraction measurements (G4-1) provided the first experimental evidence for the onset of *long-range order* below T_0. Since the origin of

14

the satellites was difficult to ascertain from the powder data alone, owing to the very weak peak intensities, single-crystal diffraction experiments with polarization analysis were carried out on 4F1.
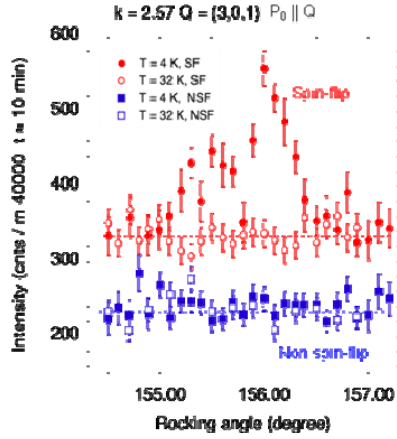

Fig. 2: Polarized single-crystal diffraction intensities from the (3,0,1) satellite, measured in the spin-flip and non–spin-flip channels below and above T_0.
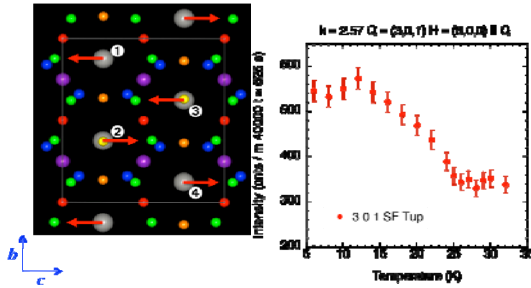

Fig. 3 : (left) AFM (k = [1, 0, 0]) structure in $CeRu_2Al_{10}$, as determined from unpolarized and polarized neutron diffraction. (right) Temperature dependence of the intensity of the (3,0,1) magnetic satellite.

The results indicate that, for an incident neutron polarization oriented parallel to the scattering vector ($P_0 \parallel Q$), the signal associated with the Bragg satellites is purely spin-flip (Fig. 2), i.e. the scattering is unambiguously *magnetic*. Taken together, unpolarized and polarized measurements support the antiferromagnetic (AFM) structure displayed in Fig. 3, in which the Ce magnetic moments are aligned along the c axis, with a low magnitude of 0.34(2) μ_B. Triple-axis measurements of low-energy excitation spectra in $CeRu_2Al_{10}$ powder revealed a strong, broadened excitation centered around 8 meV at T = 15 K, which disappears on heating to T_0 and thus reflects the dynamics of the ordered state. Experiments on single crystals

are now underway to study its dispersion and see whether it can be ascribed to an AFM magnon with an anisotropy gap, or to a singlet-triplet-like mode as suggested by other works.
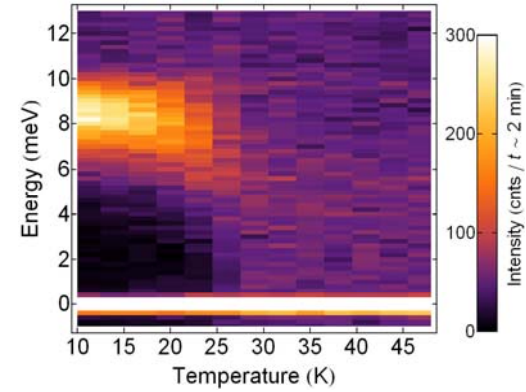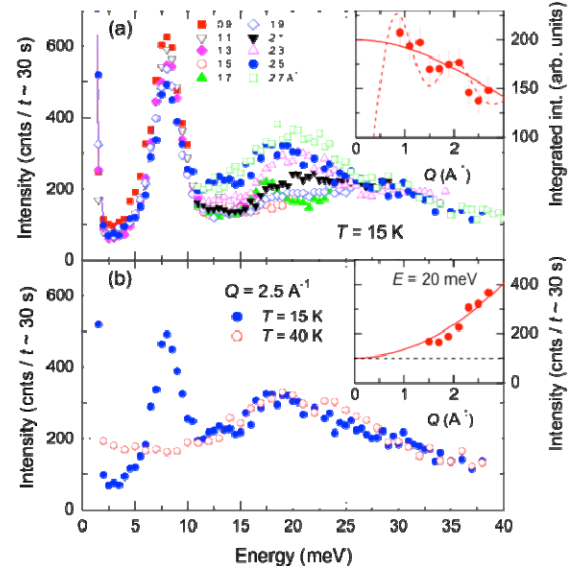
Fig. 4: (top) INS intensities measured on $CeRu_2Al_{10}$ powder as a function of (a) momentum transfer and (b) temperature. (bottom) Intensity map showing the suppression of the 8-meV excitation as T increases to T_0.

References

[1] A. M. Strydom. Physica B: Condens. Matt. **404**, 2981, (2009).

[2] T. Nishioka *et al.*, J. Phys. Soc. Jpn. **78**, 123705, (2009).

[3] S. Kambe *et al.*, J. Phys. Soc. Jpn. **79**, 053708, (2010).

[4] M. Matsumura *et al.*, J Phys Soc Jpn. **78**, 123713, (2009).

[5] J. Robert *et al.*, Phys. Rev. B **82**,100404(R), (2010).

PRESSURE INDUCED FERROMAGNETIC TO ANTIFERROMAGNETIC TRANSITION IN BiMnO₃ MULTIFERROIC

S. E. Kichanov[1], O. L. Makarova[2], I. Mirebeau[3], D.P. Kozlenko[1], A. A. Belik[4]

[1] Frank Laboratory of Neutron Physics, JINR, 14190, Dubna, Russia
[2] Russian Research Center, Kurchatov Institute, 123182 Moscow,
[3] CEA–CNRS, IRAMIS, Laboratoire Léon Brillouin, 91191 Gif-sur-Yvette Cedex, France
[4] International center for Materials Nanoarchitektonics, (MANA), National Institute for Material Science (MINS) 1-1 Namiki, Tsukuba, Ibaraki, 305-0044, Japan

The $RMnO_3$ manganese oxides show many interesting phenomena, such as giant magneto-resistance, insulating-metal transition, and multiferroic properties. Orthorhombic (R=Tb, Dy, Gd) and hexagonal (R=Y, Lu, Er, Yb) compounds show ferroelectricity coexisting with long range magnetic orders of commensurate or incommensurate nature. The magnetic frustration which governs these complex magnetic orders is associated with a strong spin-lattice coupling, leading atomic displacements and dielectric anomalies at the magnetic transitions, as well as hybrid "phonon-magnons" excitations. It opens the possibility to switch the polarisation by a magnetic field, or the reverse, with promising applications for electronic devices.

Among the $RMnO_3$ multiferroics, $BiMnO_3$ is a rare example of a compound with collinear ferromagnetic (FM) ground state (T_{FM}=100K), possessing orbital order. The ferroelectric transition occurs at T_{FE}~770K, well above T_{FM}, and is accompanied by a structural change from an orbitally disordered C2 to an orbitally ordered C2/c monoclinic phase. The origin of the ferroelectricity in $BiMnO_3$ is related to lone pairs $6s^2$ of Bi^{3+} ions, which induce local structural distortions [1].

Due to the centrosymmetric character of the C2/c group, the nature of the magnetodielectric anomaly and ferroelectric loop observed in $BiMnO_3$ around T_{FM} remains unclear. A strong magnetoelastic coupling, which does not change the symmetry of the crystal structure, was observed in a previous neutron diffraction study [2]. It implies that the magnetoelectric properties should arise from structural distortions, breaking the average crystal symmetry at a local level. Theory [3] suggested a mechanism for the local symmetry breaking associated with a competition between ferromagnetic and antiferromagnetic (AFM) superexchange interactions.

Applying pressure allows one to study the magnetoelastic coupling by checking how changes in interatomic distances influence the magnetic order. Recent susceptibility and X-ray diffraction [4, 5] revealed a new magnetic phase transition at a pressure of 1 GPa in $BiMnO_3$. By performing magnetic neutron diffraction measurements under pressure, we show that this transition reflects the onset of an AFM phase and we determine its magnetic structure [6]. These neutron data were combined with those obtained in PSI (not described here), which yield the pressure induced change of the crystal structure.
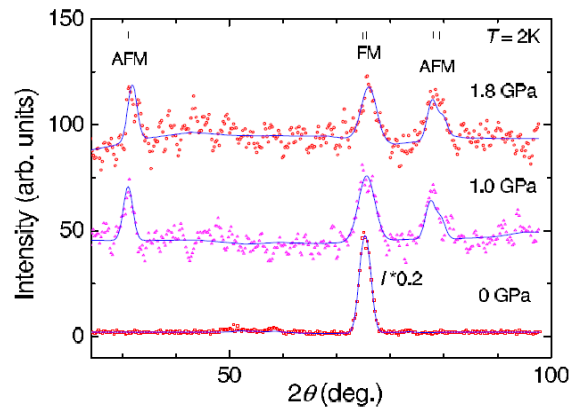
Fig. 1: Magnetic neutron diffraction patterns measured on G6-1 at T=2K, showing the onset of an antiferromagnetic phase under pressure. Solid lines are Fullprof refinements.

High pressure neutron diffraction measurements were performed on G61 diffractometer using the setup described in ref. [7]. The incident neutron wavelength was 4.74 Å. The sample of about 2mm³ was loaded into a sapphire anvil pressure cell, and the diffraction patterns collected in the range 0-3 GPa, down to 2K. The magnetic patterns (*Fig. 1*) were obtained by

subtracting a pattern in the paramagnetic region (T=120K). They clearly show the onset of AFM Bragg peaks under pressure, coexisting with FM ones. The two magnetic phases coexist at 1 and 1.8 GPa, but the FM contribution decreases with increasing pressure, at the expense of the FM one.

Fig. 2: BiMnO$_3$ antiferromagnetic structure.

At ambient pressure, Fullprof refinements yield a collinear ferromagnetic structure with moments of 3.4μ_B/Mn along the *b* axis, in agreement with previous results [2]. Under pressure, the AFM structure (*Fig. 2*) h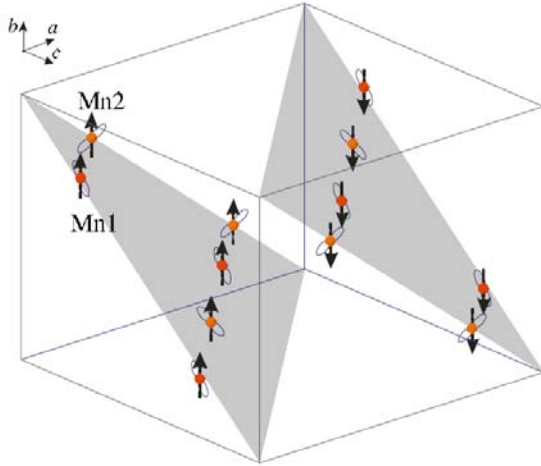as a propagation vector (½,½,½), with a magnetic unit cell doubled along the 3 cubic axes. The Mn moments form FM planes perpendicular to the <111> direction, with AFM coupling between adjacent planes. This structure connected with orbital ordering is similar to the A-type AFM structure of orthorhombic LaMnO$_3$ with Jahn-Teller distortion.
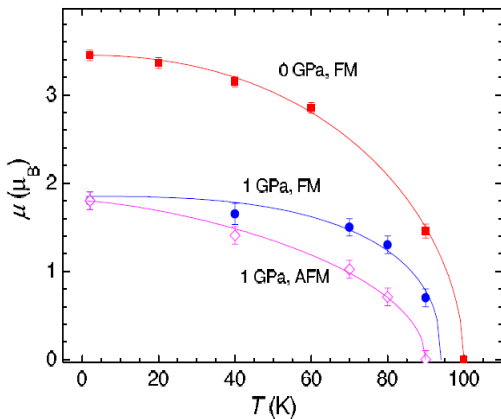

Fig. 3: Temperature dependence of the ordered magnetic moments in FM and AFM phases of BiMnO$_3$.

At 1 GPa, the ordered magnetic moments (Fig. 3) have similar values at 2K, of 1.8(1) and 1.7(1) μ_B/Mn for the FM and AFM phases respectively. Their different temperature dependences suggests a phase coexistence rather than a single canted or conical structure
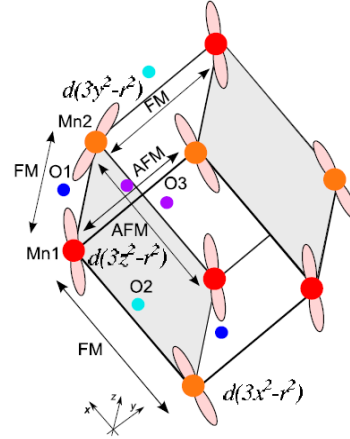
Fig. 3: a) Competing magnetic interactions in the perovskite sub-unit of BiMnO$_3$.

The pressure induced change of the magnetic ground state from FM to AFM can be qualitatively understood by a change in the balance between FM Mn$_1$-O$_2$-Mn$_2$ and AFM Mn$_1$-O$_3$-Mn$_2$ interactions, in favour of the latter ones (Fig. 4). It agrees with the change in the bond angles deduced from the evolution of the crystal structure under pressure [6]. The whole results support the mechanism previously proposed for the magneto dielectric effect, arising from local distortions of the Bi^{3+} environment, needed to optimize the competition of frustrated FM and AFM superexchange interactions.

References

[1] T. Kimura *et al.* Phys. Rev. B **67**, 180401 (R) (2003)
[2] E. Montanari *et al.* Phys. Rev. B **75**, 220101 (R) (2007).
[3] I. V. Solovyev and Z. V. Phelkina, New J. Phys. **10**, 073021, (2008).
[4] C. C. Chou *et al*. Phys. Rev. B **80**, 184426, (2009).
[5] A. A. Belik *et al*. Inorg. Chem. **48**, 1000, (2009).
[6] D.P. Kozlenko *et al*. Phys. Rev. B **82**, 014401, (2010).
[7] I. N. Goncharenko, High Pressure Research, **24**, 193, (2004).

MULTIFERROIC BFO FILMS

J. Allibe[1], I. C. Infante[1], H. Béa[1], B. Dupé[2], Dkhil[2], K. Bouzehouane[1], S. Fusil[1], E. Jacquet[1], G. Geneste[2], F. Ott[3], S. Petit[3], M. Bibes[1], A. Barthélémy[1]

[1] Unité Mixte de Physique CNRS/Thales, 1 av. Fresnel, Campus de l'Ecole Polytechnique, 91767 Palaiseau et Université Paris-Sud, 91405 Orsay
[2] Laboratoire Structures, Propriétés et Modélisation des Solides, UMR CNRS-Ecole Centrale Paris, Grande Voie des Vignes, 92295 Châtenay-Malabry
[3] Laboratoire Léon Brillouin, CEA/CNRS UMR12, 91191 Gif-sur-Yvette

The renaissance of multiferroics [1,2], materials in which at least two ferroic or antiferroic orders coexist, is motivated by fundamental aspects as well as by their possible application in spintronics [3]. Such compounds are rare and the very few that possess simultaneously a finite magnetization and polarization usually order below around 100 K. Ferroelectric antiferromagnets (FEAF) are less scarce, and some exhibit a coupling between their two order parameters. This magnetoelectric (ME) coupling allows the reversal of the ferroelectric (FE) polarization by a magnetic field [4] or the control of the magnetic order parameter by an electric field [5].

The practical interest of conventional antiferromagnets (AF) is mainly for exchange bias in spin-valve structures. The phenomenon of exchange bias (EB) manifests itself though a shift in the hysteresis loop of a ferromagnet (FM) in contact with an AF and arises from the exchange coupling at the FM/AF interface. Combining this effect with the ME coupling in a FEAF/FM bilayer can allow the reversal of the FM magnetization via the application of an electric field through the FEAF, as reported recently at 2 K in $YMnO_3$/NiFe structures [6].

To exploit these functionalities in devices, one needs to resort to ferroelectric antiferromagnets with high transition temperatures. $BiFeO_3$ (BFO) is a FE perovskite with a Curie temperature of 1043 K that orders antiferromagnetically below 643 K. BFO thin films have a very low magnetization (0.01 μ_B/Fe) compatible with an AF order, and remarkable FE properties with polarization values up to 100 $\mu C.cm^{-2}$. Recently, we reported that BFO films can be used to induce an EB on adjacent CoFeB layers at 300 K [7]. This observation, together with the demonstration of a coupling between the AF and FE domains, paves the way towards the room-temperature electrical control of

magnetization with BFO. However, several problems remain to be addressed before this can be achieved. Key issues are the magnetic structure of BFO thin films and the mechanisms of EB in BFO-based heterostructures.
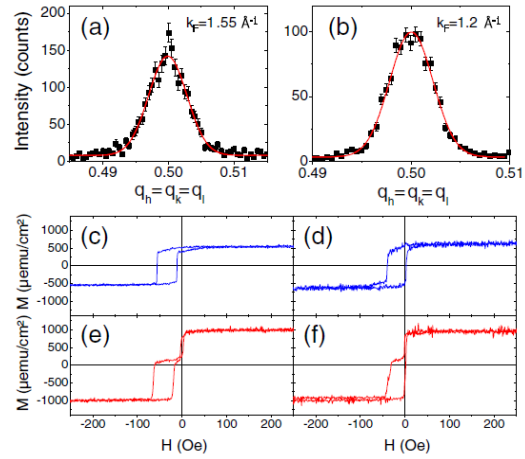
Fig. 1: (a), (b) Neutron diffraction scans close to the [½ ½ ½] for a 70 nm (001)- and a 300 nm (111)-oriented BFO films on STO, at 300 K. Magnetic field dependence of the magnetization of CoFeB/BFO(70 nm) (c), (d) and CoFeB/BFO(70 nm)/LSMO samples (e), (f) grown on (001)-oriented STO (c), (e) and (111)-oriented STO (d), (f), at 300 K.

A first key information that is usually required to analyze EB is the magnetic structure of the AF. Bulk BFO is known to have a *G*-type AF order with a superimposed cycloidal modulation [8]. In view of the strong sensitivity to strain of the properties of FE and magnetic oxides, one can anticipate that the magnetic order of BFO films might be different from that of the bulk. In order to determine their magnetic structure, selected (001)-and (111)-oriented BFO films were thus measured by neutron diffraction with the triple axis 4F1 spectrometer installed at the Orphée reactor of the Laboratoire Léon Brillouin (LLB). It is worth emphasizing that triple-axis spectrometers are usually used to investigate excitations; however, diffraction (elastic scattering)

experiments can also be performed, generally with an attractive low background thanks to the analyzer. This property is quite important in the case of thin films because of the small volume of the sample (the $1cm^2$ film is 70 nm thick), and the necessity to have an improved signal to noise ratio. In a *G*-type AF, superstructure peaks are expected to appear at [½ ½ ½]-type reflections. In Fig. 1(a) and 1(b), we show the corresponding diffracted intensities in BFO films grown on (001)- and (111)-oriented STO. Clearly an AF peak is observed for both films. No intensity was measured at [0 0 ½]-type or [½ ½ 0]-type reflections, which are characteristic of *A*-type and *C*-type antiferromagnetism respectively. This shows that both (001) and (111)-oriented films are bulk-like *G*-type AF. In other words, neither strain nor symmetry changes modify the type of magnetic order, besides destroying the cycloidal modulation [22].
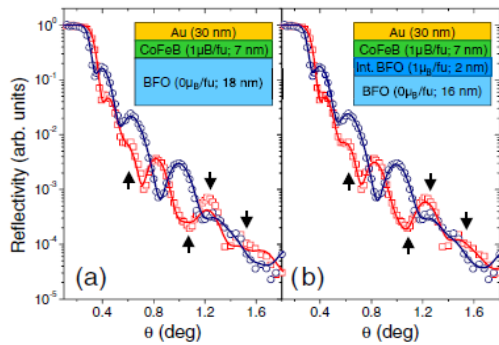

Fig. 2: Polarized neutron reflectivity data measured in a saturating field of 1.2 T.

To further investigate the EB phenomenon in the CoFeB/BiFeO3 system, we tried to detect the presence of a net magnetization in BFO close to the interface using polarized neutron reflectometry (PNR). The PNR measurements were carried out with the PRISM instrument of the LLB at room temperature. Spin-up and spin-down intensities (R_{++} and R_{--}) were collected and the data were corrected for the polarization efficiency (Fig 2). Our analysis, using the Simul-Reflec software, shows that the best fit is obtained by introducing a 2 +/- 0.5 nm layer carrying a magnetic moment of 1 +/- 0.5 μ_B/f.u. at the interface. This accounts for the existence of a large density of uncompensated spins at the CoFeB/BFO interface and is fully consistent with the observation of exchange bias and enhanced coercivity. As the ferroelectric domain structure can be easily controlled by an electric field, our results

strongly suggest that the electrical manipulation of magnetization should be feasible at room temperature in BFO-based exchange-bias heterostructures [9].

Furthermore, a great research effort is currently carried out to take further advantage of this ME coupling and discover novel ferroelectrics with better or additional properties. An active direction focuses on perovskites with strongly elongated unit cells [10], i.e., a large axial ratio (ratio of the long to the short axis of the pseudo-cubic unit cell c/a) [11]. Indeed, this structural property is expected to result in a polar charge distribution with a large dipolar moment. Another research route focuses on multiferroic materials, opening the door for novel spintronics devices. The combination of these two approaches should lead to the discovery of magnetic polar materials with giant axial ratio. Indeed, we reported recently on a clear ferroelectric behavior in epitaxial thin films of a monoclinic polymorph of BFO with a giant axial ratio (c/a ratio of 1.23) stabilized via epitaxial growth onto $LaAlO_3$. Furthermore, as shown by neutron diffraction carried out on 4F1, this phase is antiferromagnetic at 300 K and is thus the first example of a room-temperature multiferroic with a giant axial ratio [12,13].

References

[1] N. Spaldin and M. Fiebig, Science **309**, 391 (2005).
[2] W. Eerenstein, N. D. Mathur, and J. F. Scott, Nature (London) **442**, 759 (2006).
[3] M. Bibes and A. Barthélémy, IEEE Trans. Electron Devices **54**, 1003 (2007).
[4] T. Kimura *et al*. Nature (London) **426**, 55 (2003).
[5] T. Zhao *et al*. Nat. Mater. **5**, 823 (2006).
[6] V. Laukhin *et al*. Phys. Rev. Lett. **97**, 227201 (2006).
[7] H. Béa *et al*. Philos. Mag. Lett., **87**, 165 (2007)
[8] I. Sosnowksa *et al*. J. Phys. C **15**, 4835 (1982).
[9] H. Béa *et al*, Phys. Rev. Lett. **100,** 017204 (2008)
[10] Y. Uratani *et al*. Jpn. J. Appl. Phys. **44**, 7130 (2005).
[11] J. Iniguez *et al*. Phys. Rev. B **67**, 224107 (2003).
[12] H. Béa *et al*. Phys. Rev. Lett. **102**, 217603 (2009)
[13] I. C. Infante *et al*. Phys. Rev. Lett. **105**, 057601 (2010)

EVIDENCE OF THE SPIN MELTING IN THE SPIN LIQUID $Tb_2Ti_2O_7$ PYROCHLORE

A. P. Sazonov[1], A. Gukasov[1], I. Mirebeau[1] and P. Bonville[2]

[1] Centre de Saclay, DSM/IRAMIS/Laboratoire Léon Brillouin, CEA, F-91191 Gif-sur-Yvette, France

[2] Centre de Saclay, DSM/IRAMIS/Service de Physique de l'Etat Condensé, CEA, F-91191 Gif-sur-Yvette, France

Geometrically frustrated magnets show interesting magnetic ground states, either short-ranged or long ranged, stabilized by a subtle energy balance and often associated with low-energy excitations. In zero magnetic field, $R_2Ti_2O_7$ pyrochlores where the rare-earth ions R belong to a lattice of corner sharing tetrahedra (Fig. 1) and the Ti ions are not magnetic, show short range ordered ground states with extensive entropy, respectively known as spin liquid (R = Tb) [1] and spin ice (R = Ho) [2].
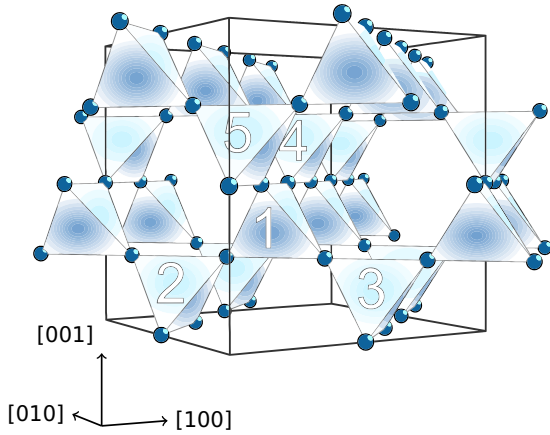

Fig. 1. *$R_2Ti_2O_7$ crystal structure. Only the rare-earth ions R are shown for simplicity.*

A magnetic field H applied along a [110] axis induces the long-range ordered magnetic structures both in the $Tb_2Ti_2O_7$ spin liquid and $Ho_2Ti_2O_7$ spin ice. The field splits the system into the so-called α and β chains, respectively along and perpendicular to H. The α chains have their local easy [111] axis at ~35° from H whereas in the β chains the easy axis is perpendicular to H. Although intensively studied, the field induced magnetic structures of the $Tb_2Ti_2O_7$ spin liquid were not fully understood up to now. They are quite complex and require a large amount of high quality data to be solved unambiguously. Moreover they crucially depend on the temperature T, the field

H and its precise orientation $\Delta\varphi$ with respect to the [110] axis.

Single crystal neutron diffraction using hot neutrons combined with symmetry analysis based on the theory of representations allowed us to solve this problem. Many Bragg peaks (typically ~300) were measured in $Tb_2Ti_2O_7$ for different (T, H, $\Delta\varphi$) condition. At the same time, the number of fitted parameters used in the refinement (moment values and angles) was significantly reduced by using symmetry constraints. This yields a quantitative and unique description of the magnetic order. Using these tools we showed that the $Tb_2Ti_2O_7$ field induced magnetic structures are of two types, with $k = 0$ and $k = (0,0,1)$ propagation vectors respectively [3,4]. The $k = 0$ structure has non-zero magnetization, whereas the $k = (0,0,1)$ one is antiferromagnetic. It is stabilized in a limited range of the phase diagram, above 2 T and below 2 K, coexisting with the $k = 0$ structure (Fig. 2).
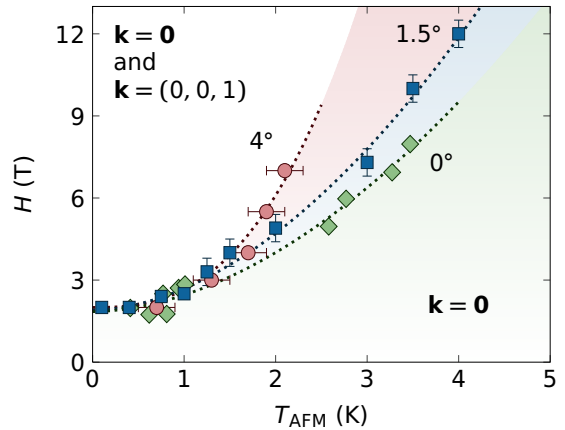

Fig. 2. *H-T_{AFM} phase diagram of $Tb_2Ti_2O_7$ at different field misalignment angles with respect to the [110] direction according to our measurements (circles [3], squares [4]) and literature data (diamonds [5]).*

Both $k = 0$ and $k = (0,0,1)$ magnetic structures strongly depend on the field alignment with

respect to the [110] axis. In the $k = 0$ structure the Tb-α moments slowly rotate from their local [111] easy axis toward the field direction when the field increases; their absolute values are practically independent of the field misalignment. As for the Tb-β moments, we found that for a well aligned field ($\Delta\varphi = 0.4°$), they are collinear to the field. Surprisingly, they flip from a direction opposite to H (A state, Fig. 3) to a direction parallel to H (B state in Fig. 3) at a critical field $H_{sf} = 1.5(5)$ T.
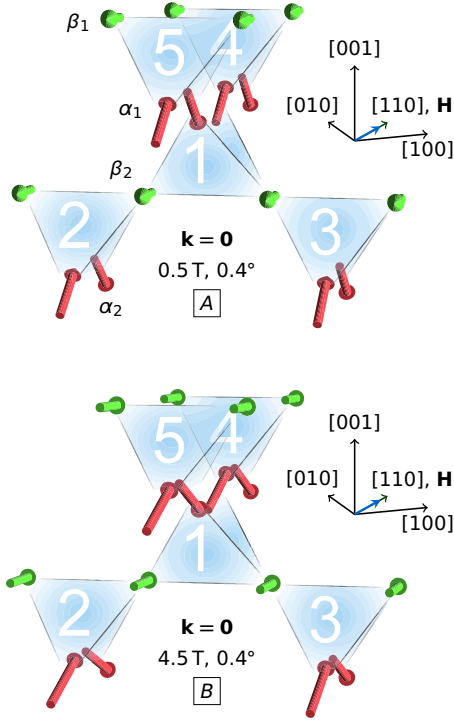

Fig. 3. *Tb$_2$Ti$_2$O$_7$ field-induced magnetic structure with $k = 0$ in the well aligned sample ($\Delta\varphi = 0.4°$) below (A) and above (B) the flip of the Tb-β moments.*

Moreover, the β moments show a minimum versus the field, decreasing to zero at H_{sf} (Fig. 4). This means that the spin flip occurs through a "melting" of the β moments. Namely, the β moments become paramagnetic at H_{sf} because the applied field exactly compensates the exchange field. This melting of the β moments disappears when the misalignment increases. All these features are well reproduced by a four sites self consistent mean-field model (solid lines in Fig. 4).

In addition, the antiferromagnetic structure with $k = (0,0,1)$ propagation vector, which is favoured in well aligned samples and involves mostly the β moments, rapidly disappears in the misaligned samples. In this structure, the β moments are antiferromagnetically coupled

along the chains. That is, in the spin liquid Tb$_2$Ti$_2$O$_7$ a state with two nearest neighbours Tb-β spins both pointing in (or out) of a tetrahedron is induced. This contrasts with the spin ice Ho$_2$Ti$_2$O$_7$, where ferromagnetic spin coupling within the β chains and antiferromagnetic coupling between nearest-neighbor β chains are found. We also note that a similar state with $k = (0,0,1)$ is induced in Tb$_2$Ti$_2$O$_7$ under uniaxial pressure or stress [6]. This suggests to relate the onset of magnetic ordering to a coupling of the magnetic field with the spins through the lattice, favored in Tb$_2$Ti$_2$O$_7$ by the giant magnetostriction and the low energy crystal field levels of the non Kramers Tb ion.
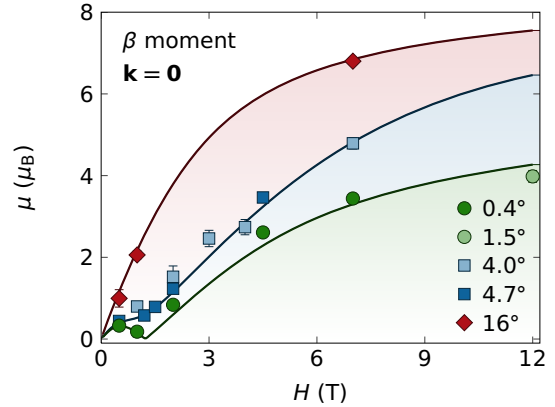
Fig. 4. *Tb$_2$Ti$_2$O$_7$ $k = 0$ structure at 1.6 K. Field dependences of the Tb-β moment values for different field misalignments ($\Delta\varphi$) with respect to the [110] direction. The solid lines are calculations using a four sites molecular field model with anisotropic exchange [4].*

References

[1]   J. S. Gardner, S. R. Dunsiger, B. D. Gaulin, M. J. P. Gingras, J. E. Greedan, R. F. Kiefl *et al.*, Phys. Rev. Lett. **82**, 1012 (1999).

[2] M. J. Harris, S. T. Bramwell, D. F. McMorrow, T. Zeiske, and K. W. Godfrey. Phys. Rev. Lett. **79**, 2554 (1997).

[3] H. Cao, A. Gukasov, I. Mirebeau, P. Bonville, and G. Dhalenne, Phys. Rev. Lett. **101**, 196402 (2008).

[4] A. P. Sazonov, A. Gukasov, I. Mirebeau, H. Cao, P. Bonville, B. Grenier, and G. Dhalenne, Phys. Rev. B **82**, 174406 (2010).

[5]   K. C. Rule, J. P. C. Ruff, B. D. Gaulin, S. R. Dunsiger, J. S. Gardner, J. P. Clancy *et al.*, Phys. Rev. Lett. **96**, 177201 (2006).

[6] I. Mirebeau, I. N. Goncharenko, G. Dhalenne, and A. Revcolevschi, Phys. Rev. Lett. **93**, 187204 (2004).

AXE 2
Materials and Nanosciences:
Fundamental Studies and Applications

The second axis "Materials and Nanosciences: Fundamental Studies and Applications", covers the activities related to the research in materials sciences and more generally in hetero-systems (interfaces, alloys, composites materials, confined systems). The studies cover detailed structures of nano-objects, interactions between nano-objects, and the role of nanostructures in composite materials. The length-scales which characterize the properties of the systems range between 1-100 nm. More specifically the following areas are addressed at the LLB: *Magnetic nanostructures* (metallic layers, oxide epitaxial layers, nanoparticles) studied by diffraction, SANS and reflectometry; *Composite materials* (polymer reinforcement by nano-particles, metallurgical composites) whose properties are studied by SANS; *Metallurgy* (both fundamental and industrial). Textures and Strain heterogeneities are studied by diffraction in various alloys or nuclear materials; *Confined systems* (microporous materials and organized guest-hosts systems, mesoporous materials and organized guest-hosts systems) in which the dynamics of the confined elements can be studied by inelastic scattering techniques; *Amorphous materials* (disordered systems – glasses). The local atomic order is also investigated by diffraction.

- *NANO-STRUCTURE OF AMPHIPHILES-BASED SYSTEMS USED IN CONSERVATION OF CULTURAL HERITAGE*
  M. Baglioni, D. Berti, J. Teixeira, P. Baglioni

- *LOCAL ORDER IN Te-RICH Te-Ge-X (X=Ga, I, Se) IR OPTICAL GLASSES*
  P. Jóvári, I. Kaban, B. Bureau, A. Wilhelm, P. Lucas, B. Beuneu , D. A. Zajac

- *DEFORMATION MECHANISMS OF A BCC STEEL UNDER UNIAXIAL LOADING STUDIED BY NEUTRON DIFFRACTION*
  V. Klosek, R. Dakhlaoui, L. Vincent, B. Marini, M.H. Mathon

- *EFFECT OF THE Pb2+ LONE ELECTRON PAIR IN THE STRUCTURE AND PROPERTIES OF THE DOUBLE PEROVSKITES $Pb_2Sc(Ti_{0.5}Te_{0.5})O_6$ and $Pb_2Sc(Sc_{0.33}Te_{0.66})O_6$: RELAXOR STATE DUE TO INTRINSIC PARTIAL DISORDER.*
  S.A Larrégola, J.A. Alonso, M. Algueró, R. Jiménez, E. Suard, F. Porcher, J.C. Pedregosa

- *GIANT MAGNETIC HARDNESS IN THE SYNTHETIC MINERAL FERRIMAGNET $K_2Co_3II(OH)_2(SO_4)_3(H_2O)_2$*
  S. Vilminot, P. J. Baker, S. J. Blundell, T. Sugano, G. André, M. Kurmoo

- *THE ISOTOPE EFFECT IN HYDRATION OF CEMENT*
  S. Mazumder, D. Sen, J. Bahadur, J. Klepp, H. Rauch, J. Teixeira.

NANO-STRUCTURE OF AMPHIPHILES-BASED SYSTEMS USED IN CONSERVATION OF CULTURAL HERITAGE

M. Baglioni[1], D. Berti[1], J. Teixeira[2], P. Baglioni[1]

[1]Dept of Chemistry and CSGI, University of Florence, via della Lastruccia 3 - Sesto Fiorentino, 50019 Florence, Italy
[2]Laboratoire Léon Brillouin, CEA-CNRS, CEA-Saclay, 91191 Gif-sur-Yvette, France

Until recently, serendipity and experimentation have been the most frequent design principles of formulations for either cleaning or consolidation of our Cultural Heritage. Accordingly, the past has witnessed a number of actively detrimental treatments, such as the application of acrylic and vinyl resins, whose ageing and degradation can irreversibly jeopardize the appearance (or even the continued existence) of irreplaceable works of art, as below illustrated for the copolymer film application to mural paintings in "Templo de los Nichos Pintados" in Mayapan (Yucatan, Mexico).

Fig. 1 – Damages caused by the inappropriate application of polymers to Mesoamerican mural paintings.

Often the degradation of these polymers makes them no more removable by organic solvents, whose use on painted layers is also not always advisable. The search for alternative, environmentally benign cleaning tools for the removal of polymeric films has therefore acquired an extraordinary relevance. In the last years we have designed, prepared and tested micellar and microemulsive formulations where solvents are dispersed in aqueous media, which are among the most effective systems available for the removal of several acrylic and vinyl resins.

A detailed characterization of structural features at the nanoscale is the key to achieve a predictive knowledge on their performances for a given application. As their structural complexity grows in response to many different requirements, scientists need more and more tailored tools to investigate them.

Illuminating examples are the systems obtained by adding to a SDS/1-pentanol (PeOH) aqueous dispersion either an immiscible oil (**a**) (xylene) or a mixture of partially water-miscible solvents (**b**) (ethyl acetate (EA) and propylene carbonate (PC)) [1, 2]. While the former is a classical microemulsion, the latter, was not yet defined, in terms of structural features. The **b** system provides better results in the removal of acrylic/vinyl coatings (removal tests of an ethylmethacrylate/methylacrylate 70/30 copolymer, Paraloid B72 from glass slides showed that in 90 minutes it removed ~90% of the polymer, while the **a** system only ~60%) [2, 3]. Since Paraloid has similar affinities for xylene and PC (or EA) the reason for different performance should be related to the composition and to the microstructure of the systems.
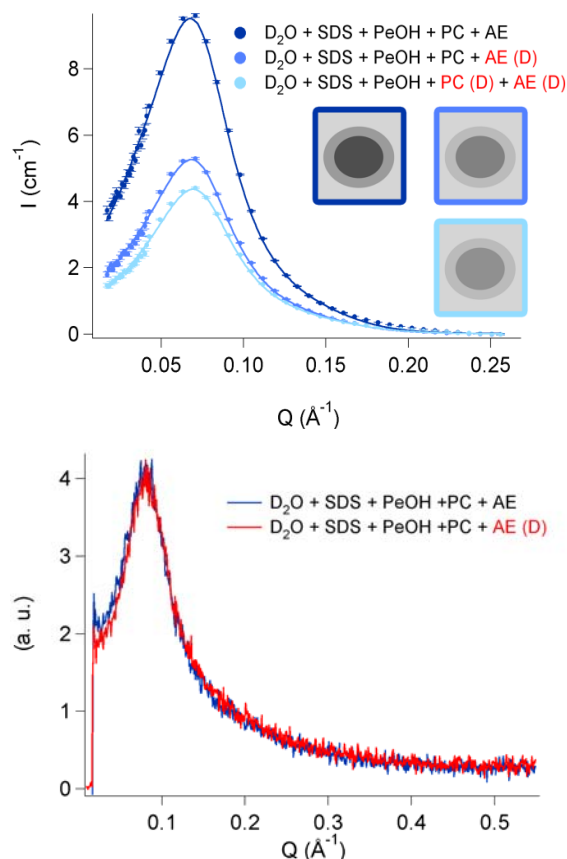

Fig. 2 – Top: a contrast series, recorded on the EA/PC system; the lines are the result of a global fitting analysis. Bottom: SAXS curves of two of the same samples.

For both systems, the interaction with a polymer film results in a "phase separation", where an aqueous micellar or oil-in-water microemulsive phase coexists with a polymer solution, constituted by a clearly defined blend of solvents, particularly enriched in PeOH, which is, in itself, a non-solvent for Paraloid.

The purpose of the work was to understand how the microstructural details are related to the different effectiveness in polymer removal and which factors drive the composition of the polymer-rich phase.

Small Angle Neutron Scattering (SANS) is a unique tool in this respect, because it lends itself to H/D isotopic substitution, without changing the chemical composition and properties of the system, but allowing to get information on different regions or domains [4], while SAXS is not as informative, being insensitive to isotopic composition (Fig. 2).

Using contrast variation series of samples, we have been able to precisely define and compare the microstructure of both systems, which were modeled as composed of monodisperse core-shell prolate aggregates, with effective charge Z and interacting with each other according to a screened Coulomb potential. The neutron scattering length density of the core and of the shell and the geometrical parameters of the aggregates have been determined through global fitting of each contrast variation series, giving access to the composition of each micellar domain [5].
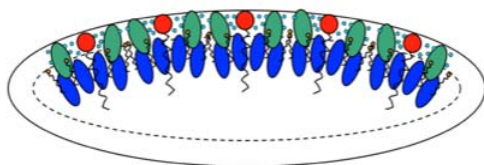

Fig. 3 – Schematic structure of the EA/PC system aggregates.

Experiments were also performed letting the EA/PC micelles and the xylene-in-water microemulsion in contact with known amounts of Paraloid B72 films for a few hours. As anticipated, for both systems the formation of a droplet of swollen polymer is observed, which, for a wide range of initial Paraloid content, has the same composition [3].

After the interaction with the polymer, the micellar aggregates lose about 30% of their initial volume, and, in particular, they are depleted of PeOH, which, as a neat solvent, does not solubilize Paraloid, but rather acts as a co-solvent for one of the two blocks constituting the copolymer.

We believe that the partition of PeOH, EA and PC between the aqueous and the micellar phase leads the initial swelling steps and determines the more efficient removal observed for the EA/PC micellar system..
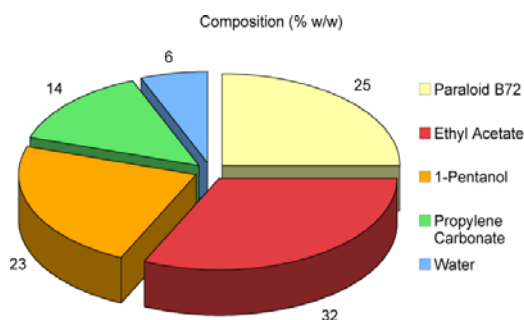
Fig. 4 – Compositon of the polymer-rich phase obtained after the interaction of the EA/PC system with Paraloid B72.
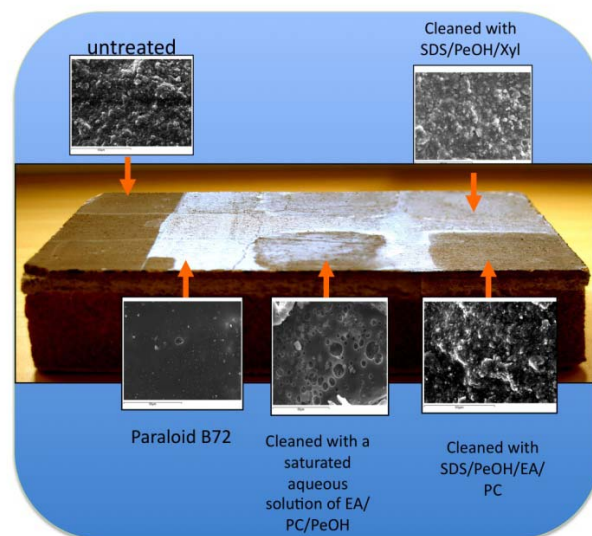
Fig. 5 – Removal tests of Paraloid B72 from laboratory fresco model samples. Glazing light picture and SEM images.

References

[1] E. Carretti, L. Dei and P. Baglioni, Langmuir, 2003, 19, 7867–7872.

[2] R. Giorgi, M. Baglioni, D. Berti, P. Baglioni, Accounts of Chemical Research, 2010, 43, 694-705 DOI: 10.1021/ar900193h.

[3] M. Baglioni, D. Rengstl, D. Berti, M. Bonini, R. Giorgi and P. Baglioni, Nanoscale, 2010, 2, 1723–1732.

[4] B. Cabane, Small Angle Scattering Methods, in Surfactant Solutions New Methods of Investigation, ed. R. Zana, Marcel Dekker, Inc., New York, 1987; Neutron, X-Ray and Light Scattering, ed. P. Lindner and Th. Zemb, North Holland, Amsterdam, 1991.

[5] M. Baglioni, J. Teixeira, R. Giorgi, P. Baglioni, D. Berti, to be submitted to Langmuir.

Note: no kinship exists among the authors.

LOCAL ORDER IN Te-RICH Te-Ge-X (X=Ga, I, Se) IR OPTICAL GLASSES

P.Jóvári[1], I Kaban[2], B Bureau[3], A.Wilhelm[3], P. Lucas[4], B. Beuneu[5],

D. A. Zajac[6]

[1]Research Institute for Solid State Physics and Optics, H-1525 Budapest, POB 49, Hungary
[2]IFW Dresden, Institute for Complex Materials, P.O.B. 270116, D-01171 Dresden, Germany
[3]Equipe Verres et Céramiques, Lab. Sciences Chimiques de Rennes UMR-CNRS 6226
[4]Dpt. of Material Science and Engineering, University of Arizona, Tucson, AZ, USA 85721
[5]Laboratoire Léon Brillouin, CEA-Saclay 91191 Gif sur Yvette Cedex France
[6]HASYLAB at DESY, Notkestrasse 85 D-22603 Hamburg, Germany

An important aim of research on telluride glasses is the design of single mode fibers guiding infrared light until 20 μm. Due to their excellent glass forming ability, selenium based glasses are extensively used in the mid infrared region. However the cut off of these glasses is near 14 μm, making them inappropriate for novel far infrared applications. The most straightforward strategy of shifting the cut off to longer wavelengths is the replacement of selenium by a heavier element e.g. tellurium. Unfortunately, tellurides are usually poor glass formers. Indeed, a critical cooling rate of only ~1 K/sec is enough to vitrify Se, while an extremely fast quenching of 10^6 K/sec is necessary to obtain small chips of vitreous Te. In order to shape lenses or fibers for optical devices, one has to improve the glass forming ability of such glasses by preventing Te from crystallizing.
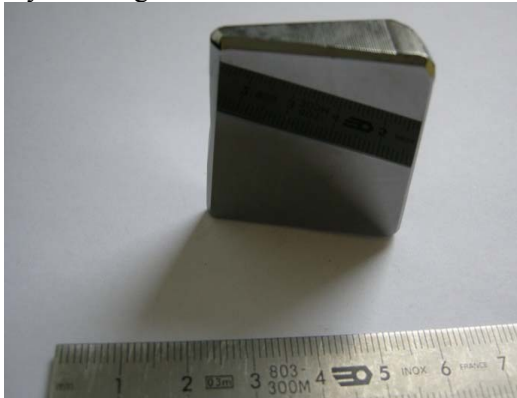

Fig. 1. A prism made of TGG ($Te_{78}Ge_{11}Ga_{11}$)

In the past, this has been achieved by adding halogens (Cl, Br or I) to pure Te. These materials (also known as TeX glasses) exhibit excellent optical properties, but their glass transition temperature T_g is low and the resulting poor thermal stability prevents their optical applications. Glasses with higher T_g can be obtained in the binary Ge_xTe_{100-x} system along a narrow compositional range at x≈15-25 [1], but these can only be vitrified using a cooling rate around 10^3 K/s, which restricts the sample size to about 0.05 mm thickness. Different strategies can be applied to improve the glass forming ability and thermal stability of binary Ge-Te glasses [2,3]. For example, by addition of Ga; compositions lying along the $GeTe_4$-$GaTe_3$ tie line are characterized by T_g around 150 °C and T_x (crystallization temperature) close to 250 °C. Besides having a better thermal stability, their shaping is also relatively simple allowing the preparation of long fibers, lenses or prisms as demonstrated in Fig. 1. Doping with iodine also results in a better glass forming ability and thermal stability. For instance, in the case of $Te_{73}Ge_{20}I_7$ T_g is also 150 °C and T_x is 274 °C [3]. Terminal iodine atoms are believed to split the Te-Te chains preventing tellurium from crystallizing. More recently, special attention has also been paid to Te rich alloys of the $GeSe_4$-$GeTe_4$ system. Among them, the $Te_{77}Ge_{20}Se_3$ composition appears to be the best compromise between thermal stability and optical transparency [4].

Table 1. Coordination numbers of Te obtained in various Te-Ge-X glasses (X=I, Se, Ga) [7].

Alloy	N_{TeTe}	N_{TeGe}	N_{TeX}	N_{Te}
$Te_{85}Ge_{15}$	1.41	0.70	–	2.11
TGI	1.00	1.02	0.03	2.08
TGS	1.07	0.93	0.09	2.09
TGG	1.36	0.57	0.43	2.36

The aim of our study was to gain insight into the structure of bulk glass formers $Te_{78}Ge_{11}Ga_{11}$, $Te_{70}Ge_{20}Se_{10}$ and $Te_{73}Ge_{20}I_7$ (denoted with TGG, TGS and TGI,

respectively) and understand how the third component builds in the host network. For this purpose, we have carried out neutron and X-ray diffraction measurements as well as extended X-ray absorption spectroscopy (EXAFS) experiments at Ga, Ge, Se, Te and I K-absorption edges. For each composition, the experimental datasets were fitted by the RMC simulation technique [5,6]. In this method, large scale atomic models compatible with experiments and physical constraints (e.g. density, coordination constraints) are generated. Coordination numbers of Te obtained by the RMC technique are listed in Table 1. For comparison we also give the corresponding values of $Te_{85}Ge_{15}$ glass. N_{Te}, the average coordination number is close to 2 in TGI, TGS as well as in the binary glass while it is significantly higher in TGG. It can also be observed that in TGG $N_{TeGe}+N_{TeTe}$ is very close to 2 suggesting that Ga participates in the 'third bond' of Te atoms. Thus, unlike Se or I, Ga does not build into the Ge-Te covalent network. Instead, it forms a covalent bond with the non bonding p electrons of Te, which results in an increase of the average Te coordination number. This is consistent with the expected role of Ga in the initial composition: catching the Te lone electron pairs to prevent tellurium from crystallizing. Fig. 2 shows a schematic model of TGG based upon the above results.
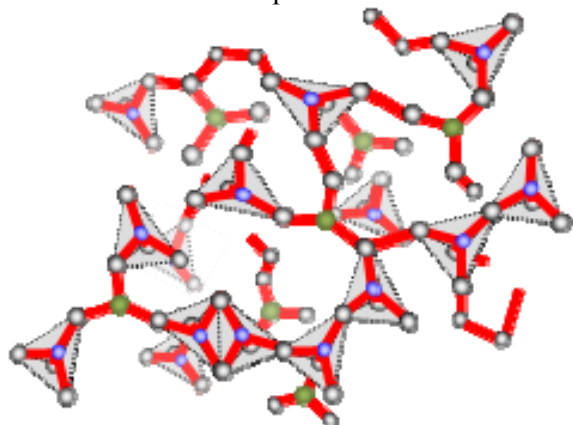

Fig. 2. A model structure of TGG with threefold coordinated Te atoms (Ge: blue, Ga: green, Te: gray).

Bond lengths are summarized in Table 2. Our results clearly show that the third component has strong influence on the average Te-Te distance. While the Ge-Te distance is essentially the same in all alloys investigated (2.60±0.02 Å), the Te-Te bond is significantly longer in TGG (2.80±0.02 Å) than either in

TGS (2.73±0.02 Å) or in TGI (2.70±0.02 Å). The Te-Te distance in $Te_{85}Ge_{15}$ (2.75±0.02 Å) is just half way between the corresponding values of TGI and TGG.

Table 2. Comparison of the r_{ij} bond lengths (in Å) found in glassy $Te_{85}Ge_{15}$, TGI, TGS and TGG.

Alloy	r_{TeTe}	r_{GeTe}	r_{XGe}	r_{XTe}
$Te_{85}Ge_{15}$	2.75	2.60	–	–
TGI	2.70	2.60	2.58	–
TGS	2.73	2.60	2.35	2.60
TGG	2.80	2.60	–	2.60

According to these observations, the strength of $GeTe_4$ (respectively $GeTe_3I$, $GeTe_3Se$) 'units' is very similar in $Te_{85}Ge_{15}$, TGG, TGI and TGS, but the connection between these units is different. Shorter Te-Te distances in TGS and TGI suggest that Te-Te bonding is stronger in these alloys than in TGG.

By combining different experimental techniques it was possible to determine short range order parameters in Te-Ge-based glasses. It was shown that the improvement of glass forming ability is achieved by entirely different strategies. While I and Se build in the covalent network making Te-Te bonding stronger, Ga increases the average coordination number of Te (and also network connectivity) but decreases Te-Te bond strength.

References

[1] E I. Kaban, E. Dost, W. Hoyer J. Alloys and Comp. **379** 166 (2004).
[2] S. Danto, P. Houizot, C. Boussard-Plédel, X. H. Zhang, F. Smektala, J. Lucas, Adv. Funct. Mat. **16** 1847 (2006).
[3] A. Wilhelm, C. Boussard-Plédel, Q. Coulombier, J. Lucas, B. Bureau, P. Lucas, Adv. Mat. **19** 3796 (2007)
[4] X. H. Zhang, B. Bureau, C. Boussard, H. L. Ma, J. Lucas, Chemistry **14** 432 (2008).
[5] R. L. McGreevy, L. Pusztai, Mol. Simul. **1** 359 (1998).
[6] O. Gereben, P. Jóvári, L. Temleitner, L. Pusztai, J. Optoelectron. Adv. Mater. **9** 3021 (2007)
[7] P. Jóvári, I. Kaban, B. Bureau, A. Wilhelm, P. Lucas, B. Beuneu, D. A. Zajac, J. Phys.: Condens. Matter **22** 404207 (2010)

DEFORMATION MECHANISMS OF A BCC STEEL UNDER UNIAXIAL LOADING STUDIED BY NEUTRON DIFFRACTION

V. Klosek[1], R. Dakhlaoui[2], L. Vincent[2], B. Marini[2], M.H. Mathon[1]

[1]CEA-CNRS, IRAMIS, Laboratoire Léon Brillouin, 91191 Gif-sur-Yvette Cedex, France
[2]CEA, DEN, SRMA, 91191 Gif-sur-Yvette Cedex, France

A polycrystalline material consists of a large number of crystallites belonging to one or more chemical phases and having various, more or less randomly distributed, orientations of the crystallographic lattice. Due to the anisotropic nature of single crystal, local mechanical behaviour of a grain within a polycrystalline aggregate depends strongly on its orientation and on its neighbourhood, and deformation incompatibilities are likely between grains. Polycrystalline materials are thus heterogeneous, from mechanical and physical points of view: a macroscopic external loading generates heterogeneous strains and stresses, and the macroscopic behaviour is generally very different from that of a single crystal. Of course, taking into account these heterogeneities is essential to develop truly predictive mechanical models.

At mesoscopic scale, polycrystalline materials can be described as multiphased materials if one defines a phase by all the grains with the same crystallographic orientation, and assumed to have the same mechanical behaviour, as it is generally done in homogenization-based micromechanical modelling. Neutron diffraction allows characterization of the behaviour of such crystallites families within the bulk of a massive sample, e.g. by associating texture determination and strains measurements. The obtained parameters are averaged values over all the grains with the same crystallographic orientation (i.e. over each "phase"). A statistically representative information can thus be obtained, which can be directly compared with results from micromechanical modelling, especially by means of homogenization methods. This methodology allows an intermediate approach between a "local", intragranular characterization (as obtained, e.g., by X-ray microdiffraction using synchrotron radiation) and a "global" characterization. The method applied here is an adaptation to neutron diffraction.on polycrystalline samples of the single crystal orientation analysis method originally developed by Ortner [1] for X-ray diffraction. It is deeply described in ref [2]. It was carried out to study the elastic and elastoplastic behaviours of a 16MnD5 bainitic steel (used for nuclear reactor vessels) under *in situ* uniaxial loading during neutron diffraction experiments.

Texture and strains were both determined using neutron diffraction on the 6T1 4-circles diffractometer at LLB (λ = 1.159 Å) [3]. For the *in situ* neutron diffraction measurements during the tensile tests, a compact uniaxial tensile machine adaptable on the Eulerian cradle was used. Additionally, the "modified" $sin^2\psi$ method [4] was applied to characterize the residual stresses after several plastic deformation steps. The G5.2 "stress scanner" at LLB [3] was then used to measure interplanar spacing of {110} reflections (λ = 2.86 Å)

Fig. 1: experimental setup on G5.2 with the tensile machine mounted on Eulerian cradle.

Five phases, corresponding to five grain orientations, have been selected in order to vary the loading direction with respect to the {110}<111> and {112}<111> slip systems of bcc steel. Fig. 2 reports comparison of $<\sigma_{11}^c>$ stress (tensile direction) for each grain orientation (from A to E) versus applied macroscopic strain. It appears that the five

selected phases exhibit very different mechanical responses and large plastic deformation heterogeneities are thus observed between these grains families (up to 400 MPa).

Plastic deformation heterogeneities have also been analyzed by applying the "modified" sin²ψ method [4] at several deformation steps, after having unloaded the sample. Results show the progressive appearance of undulations on the curves which are mainly due to plastic deformation incompatibilities between grains (Fig. 3). Quantitative interpretation of these results was performed by using self-consistent modelling.

*Fig. 3: sin²ψ curves obtained at two load levels. Linear (blue) and modified (red) fits are displayed. ψ is the angle between diffraction vector **k** and transverse direction: ϕ = 0° or 180° and ψ = 90° means **k** parallel to the load; ψ = 0° means **k** perpendicular to the load.*
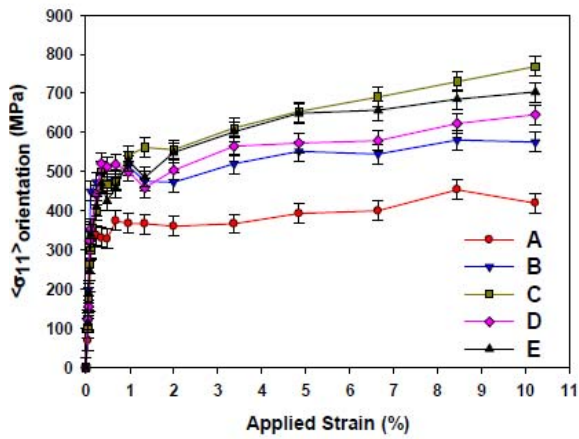
Fig. 2: σ₁₁ orientation stress comparison (A: Cube, B: {-110}<111>, C:{11-2}<111>, D:{-110}<112>, E:{111}<-211>)

16MnD5 bainitic steel is known to exhibit a transition between a brittle behaviour at low temperatures, leading to cleavage fracture, and a ductile behaviour which leads to a strong increase of toughness at higher temperature. The role in cleavage of crystalline plasticity mechanisms and of microstructure (grain size, misorientation) is always an open question. In that sense, the results obtained here consist of a rich and original data base which enabled: (i) to test and validate a crystalline model developed for the studied steel [5]; (ii) to better identify some material parameters required in this model using self-consistent homogenization (Fig. 4) or finite elements calculations (under progress).

Fig. 4: comparison between experimental results and self-consistent homogenization.

References

[1] B. Ortner, J. Appl. Cryst. **22** (1989) 216.
[2] R. Dakhlaoui, V. Klosek, M.H. Mathon, B. Marini, Acta Materialia **58** (2010) 499.
[3] http://www-llb.cea.fr
[4] S. Wroński, A. Baczmański, R. Dakhlaoui, C. Braham, K. Wierzbanowski, E.C.Oliver, Acta Materialia **55** (2007) 6219.
[5] M. Libert, PhD thesis, Ecole Centrale Paris (2006).

EFFECT OF THE Pb^{2+} LONE ELECTRON PAIR IN THE STRUCTURE AND PROPERTIES OF THE DOUBLE PEROVSKITES $Pb_2Sc(Ti_{0.5}Te_{0.5})O_6$ AND $Pb_2Sc(Sc_{0.33}Te_{0.66})O_6$: RELAXOR STATE DUE TO INTRINSIC PARTIAL DISORDER.

S.A. Larrégola[1], J.A. Alonso,[2*] M. Algueró[2], R. Jiménez[2], E. Suard[3], F. Porcher[4], J.C. Pedregosa[1]

[1] Área de Química General e Inorgánica, Departamento de Química, Facultad de Química, Bioquímica y Farmacia, Universidad Nacional de San Luis, Chacabuco y Pedernera, 5700 San Luis, Argentina.
[2] Instituto de Ciencia de Materiales de Madrid, C.S.I.C., Cantoblanco,28049 Madrid, Spain.
[3] Institut Max Von Laue Paul Langevin, F-38042 Grenoble, France.
[4] Laboratoire Leon Brillouin, CEA/Saclay, 91191 Gif Sur Ivette Cedex, France.

Lead perovskites are well known for their ferroic properties, typified by the paradigmatic example of $PbTiO_3$. The dielectric response in these materials is very sensitive to small changes in the chemical composition and order-disorder phenomena, which make these compounds very interesting from both the industrial and the academic points of view. For instance, Pb_2ScTaO_6 is ferroelectric in the ordered structure and a relaxor ferroelectric in the disordered phase while Pb_2YbNbO_6 is an antiferroelectric at room temperature and it undergoes, upon heating, an antiferroelectric-paraelectric phase transition at 578 K.

We have designed and prepared[1] two different compounds with intrinsic partial disordering over half of the perovskite B-positions; they have been characterized from a structural point of view in correlation with their dielectric properties. The two perovskites, $Pb_2Sc(Ti_{0.5}Te_{0.5})O_6$ (PSTTO) and $Pb_2Sc(Sc_{0.33}Te_{0.66})O_6$ or $Pb_3Sc_2TeO_9$ (PSTO), contain a random distribution at the B''-site of composition $(Ti_{0.5}Te_{0.5})$ and $(Sc_{0.33}Te_{0.66})$, respectively. PSTO and PSTTO were obtained by solid state reaction 950 °C for 12 h in air. NPD data were collected on the 3T2 high-resolution diffractometer (λ = 1.2252 Å) at the Laboratoire Léon Brillouin in Saclay (France) for PSTO and at the high-resolution powder diffractometer D2B (ILL, Grenoble, France) for PSTTO, where the high-flux mode was used, with a wavelength of 1.594 Å.

The structural refinements from the room-temperature high-resolution NPD data were performed in the $Fm\bar{3}m$ space group (N° 225), with unit-cell parameter related to the ideal cubic perovskite aristotype ($a_0 \approx 4$ Å) as a $\approx 2a_0$. In this model, Sc atoms were located at the $4a$ (0 0 0) site and (Sc, Te) or (Ti, Te) atoms were distributed at random at the $4b$ (½ 0 0) Wyckoff sites. O atoms are placed the $24e$ sites (x 0 0) and Pb atoms occupy the $32f$ (x x x) Wyckoff positions, presenting an off-centre displacement along the [1 1 1] direction. This is the elpasolite structure, commonly adopted by 1:1 long-range ordered double perovskites that contain untilted BO_6 octahedra.

The Rietveld plots after the NPD refinements are illustrated in Fig. 1 for PSTO.
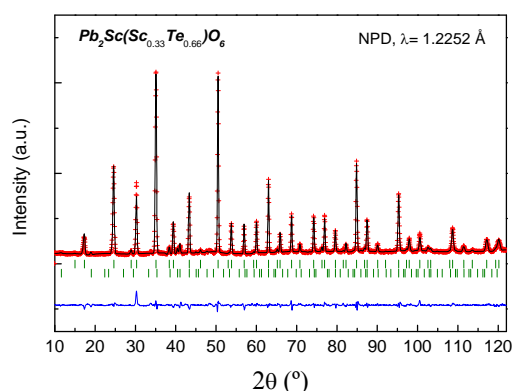
Fig. 1. Rietveld plot for PSSTO; data collected at 3T2 at RT.

Fig. 2 illustrates the geometrical environment of the lead atoms, which occupy the voids between eight octahedra exhibiting a 12-fold oxygen coordination and showing an off-centre displacement along the [1 1 1] cubic direction, towards an O3 face of one octahedron. The average distances <Pb-O> calculated for both compounds were 2.858 and 2.878 Å for PSTTO and PSTO, respectively, these distances are in

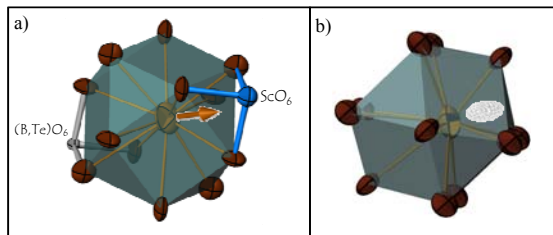agreement with the calculated from the ionic radii sums.

Fig. 2. a) A perspective view of the PbO_{12} polyhedron. The central ellipsoid represents the Pb atom which is shifted along the [1 1 1] direction (orange arrow) towards one face of the (B, Te)O_6 octahedra (plane of the three oxygen atoms). b) A lateral perspective of the PbO_{12} polyhedron where the three different Pb-O bond lengths and the schematic localization of Pb lone pair are shown.

The atomic displacement of lead atom has been reported several times in lead-containing compounds [2, 3], including the former report of the crystal structure of PSTTO.[4] This displacement can be understood as a result of the electrostatic repulsion undergone by the $6s^2$
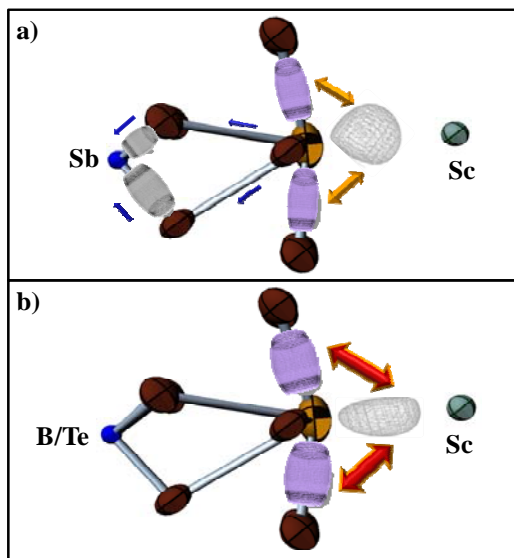
Fig. 3. Schematic representation of the effect of different B'' atoms in the displacement pattern of the lead atoms (orange ellipsoid). a) The covalent character of Sb-O bonds reduces the electronic density at the Pb-O bonds of the equatorial plane. Orange arrows describe the repulsive interactions between Pb-O bonds and the $6s^2$ lone pair (gray cloud), blue arrows describe the inductive effect from Sb^{5+} to the Pb-O bonds. b) The smaller proportion of a p-block element at the B'' site decrease the covalent character of the (B,Te)-O bond, which enhances the repulsion between the equatorial Pb-O bonds and the lone pair.

lone pair of the lead atom mainly with the three shorter Pb-O bonds, and in second term with the six equatorial Pb-O bonds, shifting the lead atom from the centre of the polyhedra along the [1 1 1] direction, in order to reduce this destabilizing interaction (see Fig. 3). The magnitude of the displacements for both compounds, calculated from x(Pb), are 0.249 and 0.242 Å for PSTTO and PSTO, respect.

Permittivity measurements indicate that both compounds present a relaxor state below RT, with freezing temperatures of 99 and 156 K for PSTO and PSTTO, respectively obtained from the fit of the maximum in permittivity vs. frequency data to the Vogel-Fulcher's equation. In this work[1] we have demonstrated that relaxor states can be induced by the selective introduction of chemical disorder in only one of the B sites of a double perovskite. The freezing temperatures below RT indicate weaker correlations among polar nano-regions as compared with the case of general B site disorder, and it might be a characteristic of the confinement of disorder in a specific B site.
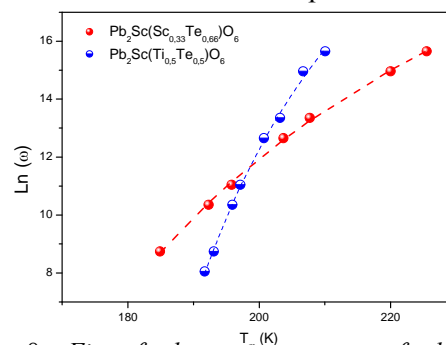
Fig. 8. Fit of the temperatures of the real permittivity maxima to a Vogel-Fulcher relation for PSTO and PSTTO.

References

[1] S.A. Larregola, J.A. Alonso, M. Alguero, R. Jimenez, E. Suard, F. Porcher, J.C. Pedregosa, Dalton Trans. 2010, **39**, 5159.

[2] G. Baldinozzi, Ph. Sciau, J. Moret, P.A. Buffat, Solid State Comm. 1994, **89**, 441.

[3] Y. Park and K. Cho, J. Am. Ceram. Soc. 2000, **83**, 135.

[4] J.A. Alonso, I. *J.* Rasines Phys. Chem. Solids 1988, **49**, 385.

GIANT MAGNETIC HARDNESS IN THE SYNTHETIC MINERAL FERRIMAGNET $K_2Co_3^{II}(OH)_2(SO_4)_3(H_2O)_2$

S. Vilminot[1], P. J. Baker[2], S. J. Blundell[2], T. Sugano[3], G. André[4], M. Kurmoo[5]

[1] CNRS, Université de Strasbourg, IPCMS, 23 rue du Loess, BP 43, 67034 Strasbourg, France
[2] Oxford University, Clarendon Laboratory, Parks Road, OX1 3PU, United Kingdom
[3] Meiji Gakuin University, Department of Chemistry, Yokohama 244-8539, Japan
[4] CEA, IRAMIS, 91191 Gif-sur-Yvette, France
[5] CNRS, Université de Strasbourg, DECOMET, 4 rue B. Pascal, 67081 Strasbourg, France

The three most important parameters defining a magnet are the Curie temperature (T_C), remanent field (B, related to magnetization M_{REM}) and coercive field (H_{COER}). The last two parameters define the strength or power of a magnet, *i.e.* the energy product (BH) is related to the amount of energy absorbed upon magnetization. To enhance BH, one usually chooses carriers with high moments and fragments the sample to almost the size of single domains to amplify M_{REM}. However, although much is known about what is required to obtain a wide H_{COER}, far less is known about controlling it at the synthetic level. The common element for high coercive magnet is a high magneto-crystalline anisotropy energy, which in many cases is obtained by use of carriers with orbital contribution through spin-orbit coupling. Several high coercive magnets have been obtained recently including oxides such as $CoFe_2O_4$ [1] and ε-Fe_2O_3 [2] and metal-organic networks [3]. We present the first example of a synthetic mineral $K_2Co_3^{II}(OH)_2(SO_4)_3(H_2O)_2$, displaying a considerable variation of coercivity from soft (few Oe) to hard (> 70 kOe) as a function of temperature [4].

$K_2Co_3^{II}(OH)_2(SO_4)_3(H_2O)_2$ is obtained by hydrothermal treatment at 200°C for 48 h of a suspension prepared from $CoSO_4.7H_2O$, KOH and K_2SO_4 in the molar ratio 2:1:1. The crystal structure reveals the presence of zig-zag chains (*Fig. 1*) of CoO_6 octahedra, from two independent Co1 and Co2 atoms, parallel to the *a*-axis connected by SO_4 groups and K polyhedra.
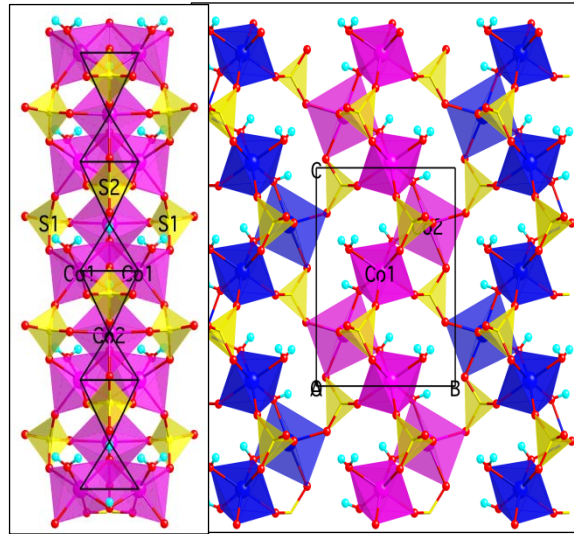
Fig. 1. Polyhedral view of a single $Co_3(OH)_2$ chain (left) and of the sulfate bridged connections of the chains into layers (right).

The ZFC-FC M/H data and those of the ac-susceptibilities as a function of frequency are shown in *Fig. 2* for a polycrystalline sample. Spontaneous magnetization is observed at 30 K. This long-range magnetic ordering is accompanied by a very sharp lambda-peak in the heat capacity (*Fig. 3*). There is an additional anomaly in the magnetization data around 10 K, which is absent in the heat capacity measurement, where the ZFC and FC magnetizations diverge and it is accompanied by a decrease of χ' and a peak of χ''. In contrast to the ZFC and FC magnetizations weak frequency dependence, the ac-susceptibilities display a considerable shift with frequency.
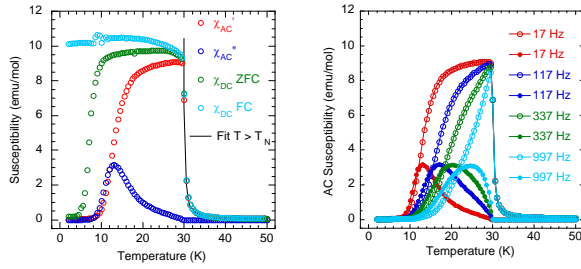
Fig. 2. Temperature dependence of the dc and ac magnetic susceptibilities of a polycrystalline sample (left) and the frequency dependence of χ' and χ'' (right).
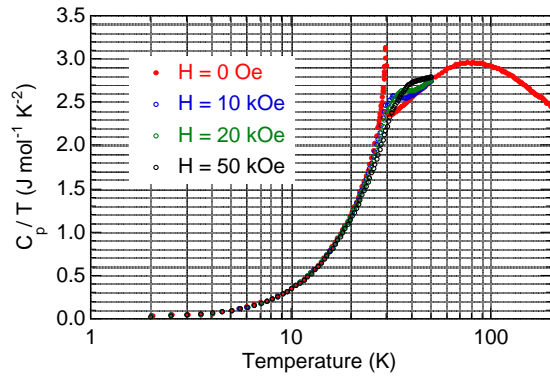
Fig. 3. Temperature-normalized molar heat capacity at different applied magnetic fields.
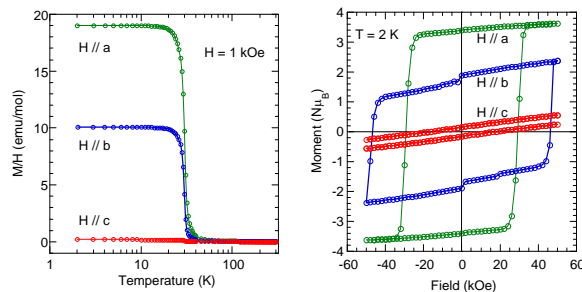
Fig. 4. Temperature dependence of dc magnetization in a field of 1 kOe (left) and isothermal magnetizations at 1.8 K (right) along the three crystallographic axes of a single crystal.

Data from a single crystal (*Fig. 4*), with magnetizations studied as a function of field and temperature, reveal that the *a*-, *b*-, and *c*-axis correspond to the easy, intermediate and hard axis of the magnet, respectively. The isothermal magnetizations at 2 K display a magnetic hardness that is among the highest recorded.

A comparison of the neutron powder patterns of a deuterated sample recorded at 1.6 and 40 K (T_C = 29.7 K) reveals an increase of the

intensity of numerous Bragg reflections as expected for ferromagnetic ordering. Moreover, a broad bump in the background has been attributed to the concomitant presence of a short-range-order structure. The best fit between observed and calculated profiles is obtained with ferromagnetic order along the *a*-axis, with a small AF component along the *b*-axis. *Fig. 5* shows the magnetic structure observed at all temperatures below T_C.

Moreover, the M_x components for Co1 and Co2 are antiparallel.
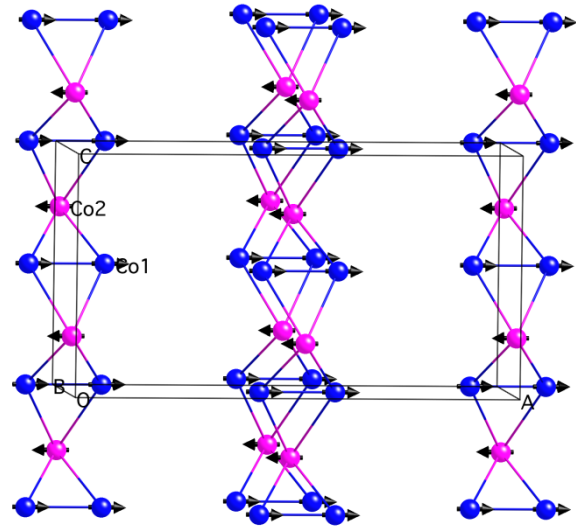
Fig. 5. Magnetic structure at 1.6 K. Blue atoms are Co1, pink atoms are Co2.

In conclusion, the magnetic structure determined by neutron is consistent with the ferromagnetic long-range order observed by magnetization and heat capacity measurements.

References

[1] A. Hutlova *et al*. Adv. Mater. **15**, 1622, (2003).
[2] M. Kurmoo *et al*. Chem. Mater., **17**, 1106, (2005).
[3] M. Kurmoo *et al*. New J. Chem., 1525 (1998)
[4] S. Vilminot *et al*. Chem. Mater., **22**, 4090, (2010).

THE ISOTOPE EFFECT IN HYDRATION OF CEMENT

S. Mazumder[1], D. Sen[1], J. Bahadur[1], J. Klepp[2], H. Rauch[3], J. Teixeira[4]

[1]Solid State Physics Division, Bhabha Atomic Research Centre, Mumbai 400085, India
[2] Fakultät für Physik, Universität Wien, Boltzmanngasse 5, A-1090 Wien, Austria
[3] Atominstitut der Österreichischen Universitäten, A-1020 Wien, Austria and Institut LaueLangevin, BP 156, 38042 Grenoble Cedex 9, France
[4] Laboratoire Léon Brillouin (CEA-/CNRS), Saclay 91191 Gif-sur-Yvette Cedex, France

Concrete, the most utilized material (the world's annual production exceeds 3 billion tons) by man, is the result of a sol-gel process due to the hydration of cement. Is there any significant isotope effect during hydration process by use of light or heavy water? This issue is not only of academic interest but also can yield a better understanding of a hydration process vis-à-vis, the evolution of compressive strength that takes place on a long time scale (several days to weeks) and is still inadequately understood.

The sol-gel process during cement hydration can be described succinctly by the reaction: Hydration of $C_3S \rightarrow$ C-S-H + Ca $(OH)_2$ where, in abbreviated form, C_3S (tri-calcium silicate) is the cement powder, the C-S-H gel, a chemical composite with constituents like calcium oxide, silicon oxide and water, and Ca $(OH)_2$ - a crystalline phase. This reaction takes place over days to weeks. Under ideal conditions, whole cement powder reacts with water and the C-S-H gel, at the end of hydration reaction, represents 70 to 80% in volume of the final product. It gives the concrete qualities of a long-lived material with high compressive strength.

With neutron scattering, we followed the hydration of C_3S over several days, by analyzing both the scattered intensity at zero angle versus time (using ultra small angle scattering (USANS) S18 at ILL) and also by SANS, i.e. the scattered intensity as a function of the momentum exchange, Q, and reaction time. In the latter case, knowledge of the density of coherent scattering of each phase, present in the samples during the hydration process, indicates a plausible scenario for the temporal evolution obtained by the first technique. The results are distinctly different depending on whether the hydration is achieved with H_2O or with D_2O. In the case of the H_2O

hydration, the gel (C-S-H) begins by forming a thin layer that retards the reaction of water with the powder (C_3S). But the water dynamics is fast enough to cross this layer and the reaction proceeds slowly but forming at the end a significant amount of gel and a small amount of crystalline phase. In contrast, in the case of D_2O, the less rapid dynamic of the water hinders the penetration of the layer and ultimately the reaction stops. The final result is a minority gel phase and a large amount of crystalline phase, in addition to an excess of unhydrated cement. Fig. 1 represents schematically the beginning of the reaction and the resulting material at the end in both the cases. These processes have been reconstructed from the analysis of small-angle scattering intensities measured as a function of time for tens of hours (~ 50 hours).

USANS experiments also show the non-monotonic character of the scattered intensity at zero angle, $S (Q = 0)$, plotted against the reaction time, in the case of H_2O. Indeed, oscillations of $S(Q = 0)$ are visible in the case of H_2O, while they are absent for D_2O. The maxima, visible in the case of H_2O, correspond to successive sol-gel transitions. Finally, SANS measurements provide information about the interfaces of the gel.

If we represent the scattered intensity by a power law suitable for fractal surfaces,
$$S(Q) \propto Q^{-\eta(t)},$$
$\eta(t)$ is greater than 4 for a diffuse interface, signature of the process of hydration, becomes equal to 4 for sharp interface or becomes less than 4 for a, possibly rough surface. Fig. 2 shows the evolution of $\eta(t)$ in the case of D_2O, and two inserts depict the monotonic evolution of $\eta(t)$ in the case of H_2O (for two different hydration levels). Although isotope effects of hydration water are known, especially regarding

the different affinity of the light water and heavy water for hydrophilic surfaces, this experiment demonstrates the resulting consequences for the hydration of cement.
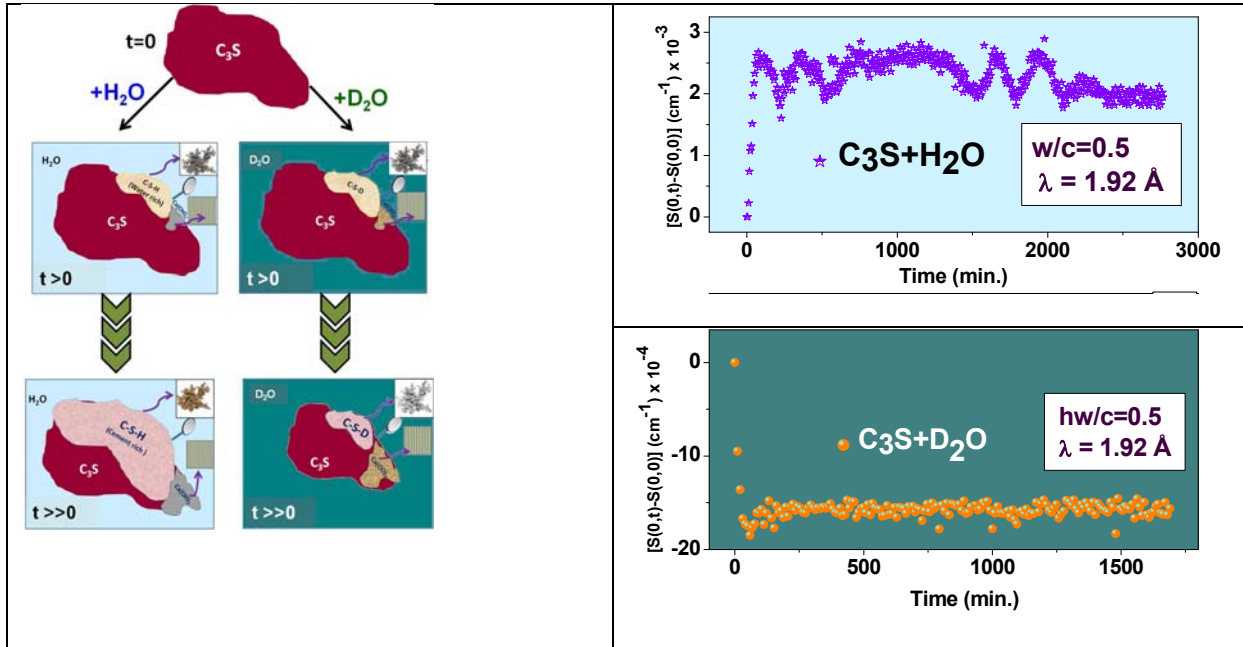
Fig. 1: Schematic representation of the structural evolution of cement hydrating with light and heavy water (left and right panels, respectively). The typical length scale of the Fig.s is of the order of 1 000 nm. At the outset a volume of cement (C₃S) is put in contact with water at time t = 0. The second row represents the first states of the hydration reaction forming the water-rich C-S-H sol and crystalline Ca (OH)₂. The isotope effects are not apparent at this initial state. The next row shows the latest states of the phase transformation. In the case of H₂O, the largest part of the volume is the cement rich phase C-S-H while the crystalline part is a minority phase. Peaks in S(0,t) represents sol-gel transformations. Conversely, for the case of hydration by D₂O, the relative volume of the gel phase is much smaller. The last row shows the temporal evolution of the zero-angle scattering as a function of time. w/c is the level of hydration. Note the oscillations that are apparent only in the case of hydration by H₂O.
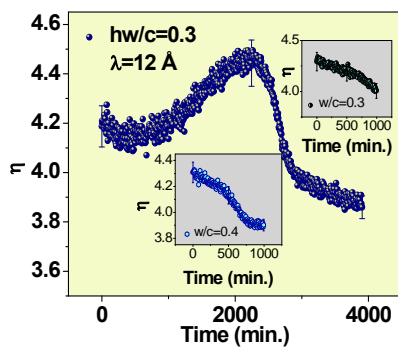
Fig. 2: Temporal evolution of η(t) associated with power-law scattering, for D₂O and for H₂O (inserts) at different hydrating levels.

References

[1] S. Mazumder, D. Sen, J. Bahadur, J. Klepp, H. Rauch and J. Teixeira, Nonlinearity and isotope effect in temporal evolution of mesoscopic structure during hydration of cement, Phys. Rev B **82**, 064203 (2010).

35

AXE 3
Soft Matter and Biophysics

The third scientific axis concerns soft matter and biophysics. Flourishing of many new systems, combining different components, many involving nanoscales (1-100 nm) has become a major current trend in soft mater. At LLB, researchers have developed in similar directions keeping some of the historical specificities of the lab: involving polymers is one of the components illustrating the advantages of neutron scattering, *i.e.* labelling and contrast matching, while we often marry the reciprocal space (SANS but also SAXS) with other techniques, in real space or at macroscopic scales. The following topics are investigated: nanoparticles and hybrid systems; organic systems and self-organization; polymer dynamics; electrostatics complexes. The research at the interface of physics and biology is based on three main topics: 1) Proteins in complex media viewed as model systems for living environments. Experiments are concerned with macro- or supra-molecular scales and their analysis is strongly influenced by our background in polymer physics, statistical physics and phase transition physics; 2) Local dynamics of proteins and hydration water in relation with the dynamical transition of proteins and their enzymatic activity. Neutron scattering techniques, that are very sensitive to protons, are particularly suitable for these studies; 3) Water and its specific properties are fundamentally related to life and to the very peculiar properties of some biological molecules like proteins. Here, water properties are studied in relation with the dynamics of hydrogen bonds network, the notions of hydrophobicity and confinement.

- **HOW MUCH ANESTHETICS EFFECTS DEPEND ON THE LENGTH OF ALCOHOL CHAINS?**
  M. Klacsová, N. Kuèerka, D. Uhríková, J. Teixeira and P. Balgavý

- **MULTIPLE SCALE REORGANIZATION OF ELECTROSTATIC COMPLEXES OF POLY(STYRENESULFONATE) AND LYSOZYME**
  F. Cousin, J. Gummel, F. Boué

- **EFFICIENT APPROACHES FOR THE SURFACE MODIFICATION OF PLATINUM NANOPARTICLES VIA CLICK CHEMISTRY**
  E. Drockenmuller, I. Colinet, F. Gal, D. Damiron, H. Perez, G. Carrot

- **A CHEMICAL PATH TO TURN FROZEN AGGREGATES BASED ON AMPHIPHILIC DIBLOCK COPOLYMERS INTO DYNAMIC MICELLES EVIDENCED THROUGH SANS EXPERIMENTS**
  E. Lejeune, J. Jestin, C. Chassenieux, O. Colombani

- **HIERARCHICAL STRUCTURES BASED ON SELF-ASSEMBLED DIBLOCK COPOLYMERS WITHIN HONEYCOMB MICRO-STRUCTURED POROUS FILMS**
  P. Escale, M. Save, A. Lapp, L. Rubatat, L. Billon

- **GLYCODYNAMERS : DYNAMIC POLYMERS BEARING OLIGOSACCHARIDES RESIDUES – GENERATION, STRUCTURE, PHYSICOCHEMICAL, COMPONENT EXCHANGE AND LECTIN BINDING PROPERTIES**
  Y. Ruff , E. Buhler , S-J. Candau, E. Kesselman , Y. Talmon, J-M. Lehn

HOW MUCH ANESTHETICS EFFECTS DEPEND ON THE LENGTH OF ALCOHOL CHAINS?

M. Klacsová[1], N. Kučerka[1,2], D. Uhríková[1], J. Teixeira[3] and P. Balgavý[1]

[1] Faculty of Pharmacy, Comenius University, 832 32 Bratislava, Slovakia
[2] Canadian Neutron Beam Centre, NRC, Chalk River, Ontario K0J 1P0, Canada
[3] Laboratoire Léon Brillouin, CNRS-CEA, 91191 Gif-sur-Yvette, France

The rule of Meyer-Overton that establishes a correlation between lipophility and potency of anesthetics is generally accepted. Exceptions were first observed for n-alcohols, C_nOH: the anesthetic potency reaches a maximum for $C_{11}OH$ and the compounds with $n>13$ are non-anesthetic [1]. This problem can be studied at the molecular level by dissolving long alcohols (C_8OH to $C_{18}OH$) in the lipid part of biomembranes [1]. In this work we analyse the structural changes of fluid PCPS bilayers, composed of dioleoylphosphatidylcholine (DOPC, 96 mol %) + dioleoylphosphatidylserine (DOPS, 4 mol %), in unilamellar vesicles (ULVs) prepared by extrusion. Indeed, unsaturated phospoholipids are important constituents of biomembranes and due to their low gel-liquid crystal phase transition temperature they are currently accepted as models of fluid bilayers in biological membranes, and ULVs are topologically similar to cell membranes. The small amount of DOPS in DOPC charges the bilayer surface negatively and thus prevents ULV aggregation after extrusion. We measure the bilayer thickness, D, and the lateral area of the unit cell consisting of a phospholipid molecule and a particular fraction of the alcohol at the bilayer –aqueous phase interface, A_{UC}.

Solid DOPC+DOPS+C_nOH mixtures were dispersed in 100, 90, 80, 70, 60 and 50 % D_2O in H_2O mixtures (outer contrasts) at 10 mg/ml concentration and extruded through 50 nm pores in 2 stacked carbohydrate filters as described in [2]. SANS spectra were measured on PAXE (sample to detector distance 1.3 m and 5.05 m, λ=0.6 nm) at 25 ºC. It is supposed that extruded ULVs are polydisperse hollow spheres with a single bilayer separating the inside and outside aqueous compartments, and that the bilayer can be divided into three strips corresponding to two polar headgroup regions and the bilayer center spanning hydrocarbon region. The normalized SANS intensity $I_{exp}(q)$ as a function of the scattering vector modulus q can be than fitted by

$$I_{\exp}(q) = N_P \int_{q'} T(q') \int_R G(R) I(R, q-q') dR dq'$$

where N_P is the number density of particles, $T(q)$ is the PAXE resolution function, $I(R,q)$ the structure factor of the ULV with radius R, and the ULVs polydispersity is described by the Schulz function $G(R)$. The scattering length densities of polar and hydrophobic regions were calculated using the known scattering lengths and component volumes of DOPC, DOPS and C_nOH measured in [3]. Details of the model and fitting procedure were described earlier [4].

Selected D results as a function of C_nOH:PCPS molar ratio (Fig 1) and as a function of C_nOH chain length n at fixed C_nOH:PCPS=0.4 molar ratio (Fig. 2) are shown and compared with control value of D (dashed line) obtained for the pure lipid. As expected, the thickness D decreases due to mismatch of the lengths of the two chains, the effect being smaller with longer alcohols. The lateral area A_{UC} increases due to C_nOH intercalation between lipid molecules (Fig. 1), particularly for large chain alcohols. The resulting partial area at the interface, A_{CnOH}, (Fig. 2) is anomalously small for anesthetically active alcohols ($n<12$), even smaller than the area of the chain cross-section in solid rotator phases of n-alkanes, which is of the order of 20 Å^2 (dashed line). We suppose that this is due to the lipid head group: its interface area A_{PCPS} is equal or larger than the sum of the areas of the hydrocarbon chains cross-sections, so that a small OH group of C_nOH is located underneath at the lipid glycerol fragment. Our experimental results are reproduced by molecular dynamics simulations of DOPC+C_nOH bilayers carried

out with the GROMACS molecular dynamics package, using the MARTINI coarse-grained force field (M. Bulacu and S.-J. Marrink, personal communication).
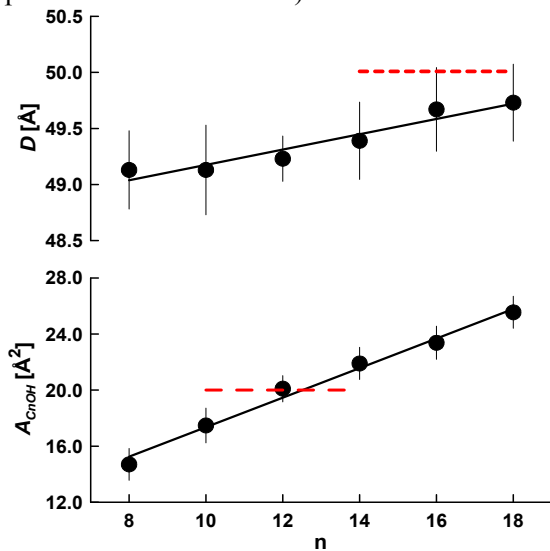
Fig. 1. Bilayer structural parameters as a function of C_nOH:PCPS molar ratio.
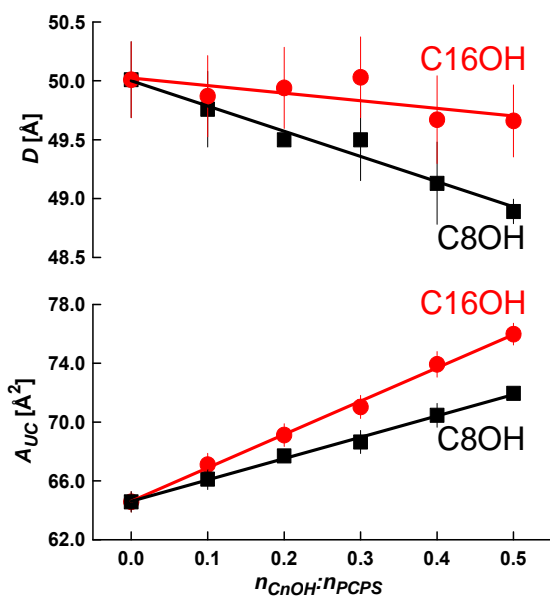
Fig. 2. Bilayer structural parameters as a function of C_nOH chain length for C_nOH:PCPS=0.4 molar ratio

References

[1] R.S. Cantor, Biophys. J. 80 (2001) 2284
[2] N. Kučerka, J. Gallová, D. Uhríková, P. Balgavý, M. Bulacu, S.-J. Marrink and J. Katsaras, Biophys. J. 97 (2009) 1926
[3] M. Klacsová, P. Westh and P. Balgavý, Chem. Phys. Lipids 163 (2010) 498
[4] N. Kučerka, J.F. Nagle, S.E. Feller and P. Balgavý, Phys. Rev. E 69 (2004) 051903

Contact: balgavy@fpharm.uniba.sk

MULTIPLE SCALE REORGANIZATION OF ELECTROSTATIC COMPLEXES

OF POLY(STYRENESULFONATE) AND LYSOZYME

F. Cousin[1], J. Gummel[1], F. Boué[1]

[1] CEA–CNRS, IRAMIS, Laboratoire Léon Brillouin, 91191 Gif-sur-Yvette Cedex, France

Polyelectrolyte-protein complexes of opposite charge are now attracting growing interest, especially for protein-polysaccharide complexes, given the potential application of these systems for the food or pharmaceutical industries (drug release, biochips, fractionation, stabilization of emulsions, etc). These systems generally display a multi-scale structure. Rearrangement processes can thus occur in systems and involve various dynamics over a wide range of times, long ones being characteristic of intrinsically large objects. This can dramatically limit the applications if some primordial properties are altered during reorganization, e.g. the colloidal stability of the complexes or the activity of the proteins. Alternately, since soft matter systems are extremely sensitive to low fields, small external changes can trigger reorganization processes. It is then worth identifying the key parameters in this case, for further applications. It is important, to obtain a detailed description of the mechanisms involved during their initial formation and during their kinetic evolution, in terms of both the physicochemical parameters and length scales.

To address this problem, we have decided to probe the reorganizations processes in a model system made of positively charge protein (lysozyme) and a negatively charged polyelectrolyte (PSS). This system enables to tune all the parameters that may act on the structure of the complexes (charge densities and concentration of the species, partial hydrophobicity of the polyion chain, ionic strength). Moreover it offers extended possibilities of contrast variation for neutron scattering, to make a full determination of the structures on a scale range lying from 10Å to 1000Å by Small-Angle Neutron Scattering. When PSS chains are in a semi-dilute regime they are crosslinked by proteins into a gel [1,2]. When in dilute regime, they form dense globular primary complexes of radius of a few

hundreds Å, with an electrically neutral core, and organized at a higher scale in a fractal way with a dimension 2.1 [3,4]. Specific to PS, at very high PSS content, the native protein is unfolded [1].

Prior to the study of the reorganization process, we need to answer the still pending question: *what tunes the finite size of the primary complexes?* For this, we have measured by SANS the sizes of primary complexes in various conditions.
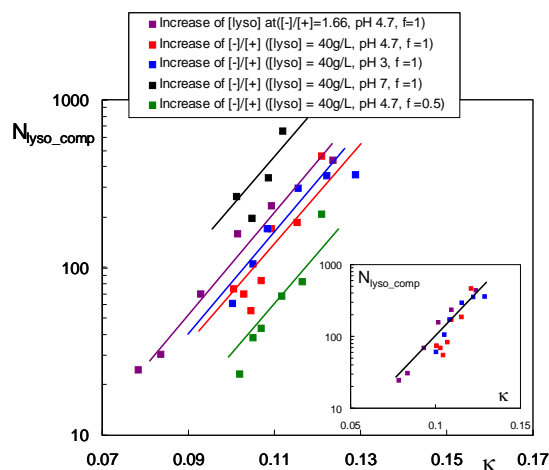
Fig. 1: Influence of k^{-1} *on mean aggregation per primary complexes* $N_{lyso\_comp.}$ *in systems at different pH (3, 4.7 and 7) or sulfonation rate (f = 1 and 0.5), which enable to vary the strength of the electrostatic interactions.*

We find that in all conditions, the same structure is found, based on the formation of dense globules of $\sim$ 100Å with a neutral core and a volume fraction of organic species (compacity) of $\sim$ 0.3. At higher scale, the globules are arranged in fractal aggregates. Globular complexes have a total positive charge when $[-]/[+]_{intro} > 1$ and a total negative charge when $[-]/[+]_{intro} < 1$. This comes from the presence of excess charged species at the surface of the globules. We also find that the globule finite size is determined by the Debye

length κ^{-1} as long as chain-protein interactions are of simple electrostatics nature [5]. Also, the mean number of proteins per primary complex N_{lyso_comp} grows exponentially with κ as seen on the master curve (*Fig. 1*). This yields a picture of the formation of the complexes. There is a first stage where the growth of the complexes is only driven by attractions between opposite species and counterion release [6]. During the growth of the complexes, the charge of globules progressively increases due to excess charges, which makes them repel themselves by electrostatic repulsion When repulsion dominates attraction, which occurs at long distance, globules stop growing; however attraction can stay strong at short distance, and they can undergo a Reaction Limited Aggregation (RLCA) process, which leads to fractal aggregates of dimension Df 2.1.
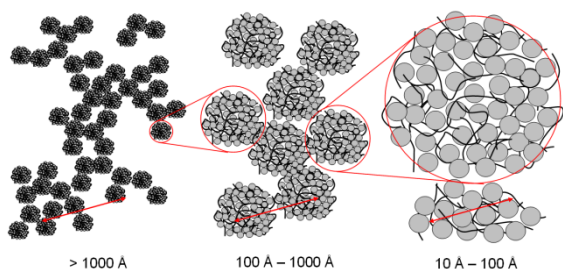
Fig. 2: Sketch of the PSS-lysozyme system in the globular regime at the 3 different scales

The system in the dilute regime appears particularly suitable for thestudy of reorga nization processes at the 3 scales of *Fig. 2*.
 - at large scales (> 1000 Å), we investigate the reorganization between fractal aggregates To probe them, we simply diluted the solution of complexes, all other parameters kept fixed. This induced a macroscopic destabilization of the solutions but did not modify the structure of the complexes at submicronic scales *(Fig. 3)*. This suggests that the colloidal stability of the mixtures is due the interlocking of the fractal aggregates into a scaffold. At high concentration, dilution does not break the local aggregate structure but the scaffold disappears, modifying its colloidal stability and viscosity.
- at intermediate scales (100 Å – 1000 Å) we look at the outer characteristics of the primary complexes (size, charge, specific area); important in the control of properties such as enzymatic activity. To probe them, we added salt in solution to *in situ* change κ^{-1}. This did not change the almost frozen inner structure of the cores of the primary complexes, while salt

screening did screen the electrostatic repulsions between two primary complexes, which coalesce into larger globules, and then in fractals of dimension 2.1 *(Fig. 3)*.
- at local scales (10 Å – 100 Å), we examine the inner organization of primary complexes for information on protein conformation, the direct interactions between components and the compactness of globules [7]. To probe the local scale, we added PSS chains in solution *after* the formation of the primary complex (made with a $[-]/[+]_{intro}$ close to 1) up to $[-]/[+]intro \sim 20$, a ratio for which the proteins are unfolded when the mixture is achieved in one step. There were here only slightly inner structural changes: the native conformation of the proteins is preserved inside the frozen core *(Fig. 3)*.
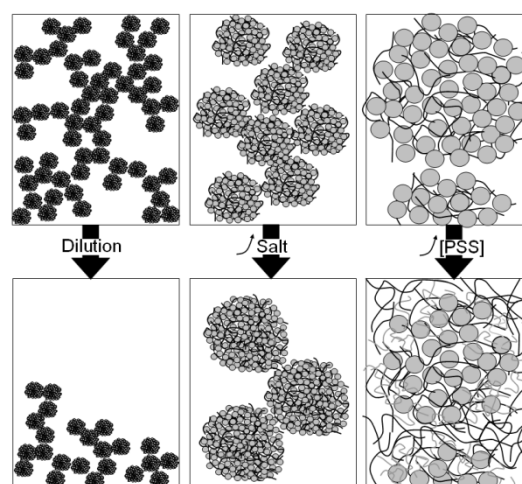
Fig. 3: Representations of the 3 kinds of reorganization at the related scale.

The clear correlation seen here between structural reorganization and physicochemical parameters and length scale opens the way to applications such as carriers for drug delivery.

References

[1] F. Cousin *et al,* Langmuir **21(21),** 9675-9688, (2005).
[2] J. Gummel *et al.* Macromol. **41(8)**, 2898-2907, (2008).
[3] J. Gummel *et al.* J. Phys. Chem. B **110(49)**, 24837-24846, (2006).
[4] J. Gummel *et al.* J. Phys. Chem. B **111**, 8540-8546, (2007).
[5] J. Gummel *et al.* Soft Matter **4**, 1653-1664, (2008).
[6] J. Gummel *et al.* J. Am. Chem. Soc. **129(18)**, 5806-5807, (2007).
[7] F. Cousin *et al.* Langmuir **26(10),** 7078-7078, (2010).

A CHEMICAL PATH TO TURN FROZEN AGGREGATES BASED ON AMPHIPHILIC DIBLOCK COPOLYMERS INTO DYNAMIC MICELLES EVIDENCED THROUGH SANS EXPERIMENTS

E. Lejeune[1], J. Jestin[2], C. Chassenieux[1], O. Colombani[1]

[1] LUNAM Université, Polymères, Colloïdes et Interfaces, UMR CNRS 6120 - Université du Maine, av. O. Messiaen, 72085 Le Mans cedex 09, France
[2] CEA–CNRS, IRAMIS, Laboratoire Léon Brillouin, 91191 Gif-sur-Yvette Cedex, France

Despite their chemical similarity with molecular surfactants, amphiphilic diblock copolymers behave differently in aqueous solution. Indeed, most amphiphilic diblock copolymers self assemble within "frozen" aggregates[1] in aqueous solution; that is out-of-equilibrium structures unable to exchange "unimers" within the experimental time-window. Literature claims that the glassy nature of the core in the case of poly(styrene)-block-poly(acrylic acid) PS-b-PAA diblock copolymers accounts for such a behavior ($T_g(PS)\sim100°C$). However, when this glassy hydrophobic block is replaced by a soft one, such as poly(n-butyl acrylate) ($T_g\sim-55°C$ for PnBA), the aggregates remain frozen[2,3]. Both facts can actually be reconciled by considering the interfacial tension of the hydrophobic block with respect to the solvent[1,4] as the key parameter. Indeed, exchange of unimers between aggregates requires the hydrophobic block to go through the hydrophilic corona and then in the aqueous solution.

To decrease this interfacial tension, we have incorporated hydrophilic AA units into the hydrophobic block of a PnBA-b-PAA diblock copolymer. This has been done in a controlled manner by the use of Atom Transfer Radical Polymerization (ATRP). A diblock copolymer with a tempered hydrophobic block denoted P(nBA$_{50\%}$-$stat$-AA$_{50\%}$)$_{100}$-b-PAA$_{100}$ was then prepared with a very good control over the chemical composition and molecular weight of both blocks ($M_w/M_n \sim 1.1$). Both blocks had a degree of polymerization equal to 100. The hydrophilic block consisted of a pure PAA block, whereas the "moderately hydrophobic" block contained randomly distributed nBA and AA units (50/50 %mol).

P(nBA$_{50\%}$-$stat$-AA$_{50\%}$)$_{100}$-b-PAA$_{100}$ was dispersed in D$_2$O with 0.3M NaCl. Small angle neutron scattering (SANS) experiments reveal that the characteristics of the self-assemblies strongly depend on the value of the ionization degree of the AA units α, and thus on the pH (Fig. 1). With increasing α, the scattering curves clearly shift towards higher q values accounting for a decrease in the size of the scattering objects. Simultaneously, the scattered intensity in the intermediate q region strongly decreases indicating a decrease of the molecular weight of the aggregates. Note the upturn of the intensity observed in the low-q region. It has been attributed to the presence of a very small amount of large spurious aggregates whose contribution can be neglected at larger q where the form factor of the objects P(q) dominates the scattered signal.
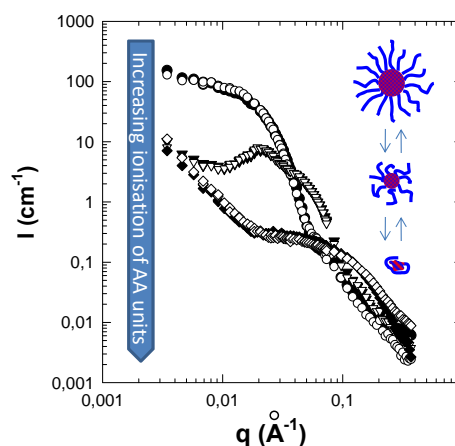
Fig. 1: Scattering curves for P(nBA$_{50\%}$-stat-AA$_{50\%}$)$_{100}$-b-PAA$_{100}$ at 20 g/L with 0.3M NaCl at 10% ionization (polymer directly dispersed ●, polymer first dispersed at α = 50% followed by addition of DCl ○), 50% ionization (from α = 30% ▼, from α = 90% ▽), 90% ionization (from a solution prepared at α = 10% brought to 90% in 3 steps ◆, from another solution pre-pared at α = 10% brought to 90% in 2 steps ◇). SANS experiments were performed at LLB on PACE spectrometer.

We have fitted the data with the form factor of polydisperse hard spheres displaying a log normal distribution of their radii (Fig. 2). The

radii extracted from the fits correspond to the size of the core of the aggregates and are of the same order of magnitude than the core size of frozen aggregates based on the pure diblock homologue $PnBA_{90}$-b-PAA_{100}[3]. However, in the latter case the core radius of the frozen aggregates is not affected by α which is very different from the behavior encountered here with the "moderately hydrophobic" diblock copolymer (inset Fig. 2). It should be mentioned that at the highest α investigated, the scattering objects rather correspond to a Gaussian coil which means that the tempered diblock is no more aggregated as independently revealed by light scattering experiments.
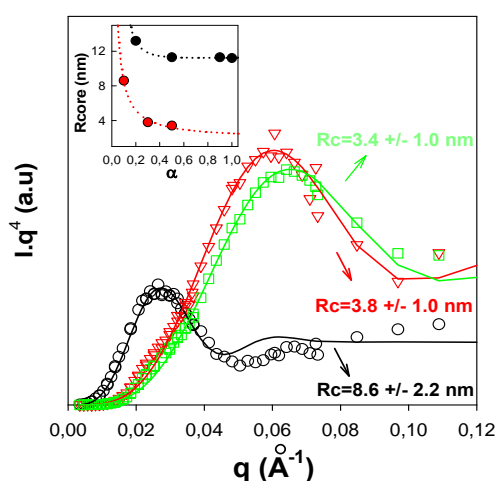
Fig. 2: Porod representation of SANS data for $P(nBA_{50\%}$-$stat$-$AA_{50\%})_{100}$-b-PAA_{100} in the presence of 0.3M NaCl at 10% ionization (○), 30% ionization (▽), 50% ionization (□). Solid lines represent fits. Inset: Variation of the radius of the core of the aggregates with α for pure diblock copolymer (●) and their tempered homologues (●).

The SANS experiments indicate qualitatively that the system is able to decrease its aggregation number upon increasing the ionisation of AA units. A remarkable feature is that this pH-sensitivity of the aggregation is fully reversible. Indeed, if α comes back to its initial value right after being increased, the characteristics of the self assemblies in terms of size, molecular weight and topology also go back to their initial value as seen in Fig. 1 from the perfect superimposition of curves obtained at the same ionization α but following different paths.

As a conclusion, we demonstrated that whereas pure diblock copolymers form frozen aggregates whose organization is preparation

dependent and not sensitive to external stimuli[2,3], controlled incorporation of AA units in the hydrophobic block in a statistic manner leads to a copolymer undergoing dramatic and reversible reorganization upon changes of the ionization degree of the AA units. The reversibility of the pH-controlled aggregation is strongly hinting at a dynamic behavior where aggregates are able to exchange unimers to reach thermodynamic equilibrium no matter the preparation conditions. We believe this chemical approach to be highly relevant to tune the dynamics of self-association of amphiphilic block copolymers. Indeed, it can be applied to any system and allows controlling the dynamics of the aggregates directly via their chemistry.

References

[1] Nicolai, T.; Colombani, O.; Chassenieux, C. Soft Matter 2010, **6**, 3111-3118.
[2] Jacquin, M.; Muller, P.; Talingting-Pabalan, R.; Cottet, H.; Berret, J.-F.; Futterer, T.; Théodoly, O. J. Colloid Interface Sci. 2007, **316**, 897-911.
[3] Colombani, O.; Burkhardt, M.; Drechsler, M.; Ruppel, M.; Schumacher, M.; Gradzielski, M.; Schweins, R.; Müller, A. H. E. Macromolecules 2007, **40**, 4351-4362.
[4] Lund, R.; Willner, L.; Richter, D.; Dormidontova, E. E. Macromolecules 2006, 39, 4566-4575. Nose, T.; Iyama, K. Comp. Theo. Polym. Sci. 2000, **10**, 249-257. Lund, R.; Willner, L.; Monkenbusch, M.; Panine, P.; Narayanan, T.; Colmenero, J.; Richter, D. Phys. Rev. Lett. 2009, **102**, 188301. Abbas, S.; Li, Z.; Hassan, H.; Lodge, T. P. Macromolecules 2007, **40**, 4048-4052. Dormidontova, E. E. Macromolecules 1999, 32, 7630-7644. Haliloglu, T.; Bahar, I.; Erman, B.; Mattice, W. L. Macromolecules 1996, **29**, 4764-4771. Lund, R.; Willner, L.; Stellbrink, J.; Radulescu, A.; Richter, D. Physica B 2004, **350**, e909-e912.

HIERARCHICAL STRUCTURES BASED ON SELF-ASSEMBLED DIBLOCK COPOLYMERS WITHIN HONEYCOMB MICRO-STRUCTURED POROUS FILMS

P. Escale[1], M. Save[1], A. Lapp[2], L. Rubatat[1], L. Billon[1]

[1] IPREM Equipe de Physique et Chimie des Polymères, UMR 5254 CNRS, Université de Pau et des Pays de l'Adour, 64053 Pau Cedex, France
[2] CEA–CNRS, Laboratoire Léon Brillouin, 91191 Gif-sur-Yvette Cedex, France

The so-called breath Fig. approach has received considerable interest due to the simple, inexpensive, and robust mechanism of pattern formation.[1] Breath Fig.s occur when vapor condenses onto either a cold solid or a cold liquid surfaces. When using the appropriate polymer solution, breath Fig. can be fixed in the polymer matrix creating a hexagonally ordered porosity named Honeycomb (HC) (Cf. Fig. 1).[2,3] The aim of the present study is to prepare and investigate hierarchical polymeric films. The first level of structuring is a micrometer honeycomb morphology obtained by a controlled solvent evaporation method under humid atmosphere. The second level of structuring is achieved via the self-assembly of the diblock copolymers at the nanometer length scale. Crucially, the nanostructuration of the copolymer has to occur within the temperature and time scales of the HC formation, *i.e.* less than 2 minutes. Thus, the challenge of the present study relies on appropriately designing the diblock copolymers that will form ordered HC films and concomitantly will arrange into self-assembled nanostructures through fast solvent evaporation. In the present paper only one copolymer will be discussed, namely poly(n-butyl acrylate)- block-polystyrene (PnBA-b-PS); the data obtained on the other copolymers are discussed in the paper of P. Escalé *et al.* Soft Matter 2010.[4]

Copolymer synthesis. Well-defined high molecular weight PS-based diblock copolymers associated to acrylate blocks were synthesized via nitroxide-mediated controlled free-radical polymerization.[5] PnBA first block was synthesized using BlocBuilder® alkoxyamine acting as both initiator and controlling agent via the SG1 nitroxide produced by thermal homolytic cleavage (see Scheme 1).

BlockBuilder   **SG1**

Diblock copolymer
P*n*BA-*b*-PS (R = (CH$_2$)$_3$CH$_3$) or **P*t*BA-*b*-PS** (R = C(CH$_3$)$_3$)
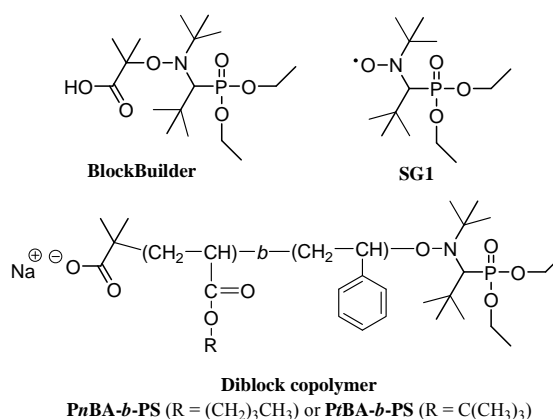
Scheme 1: Structures of the BlocBuilder® alkoxyamine, the SG1 nitroxide and the synthesized poly(butyl acrylate)-b-(polystyrene) diblock copolymers.

Micrometer Length Scale Morphology. Optical microscopy was used to examine the quality of the films in regard to the pore size and the characteristic length scale of the ordered hexagonal porous lattice. The pore-to-pore distances is 2 µm in average and the order is preserved over the whole images (170 × 170 µm^2) since the 2D FFT presents discrete orders, characteristic of a well-ordered hexagonal arrangement.

50 µm
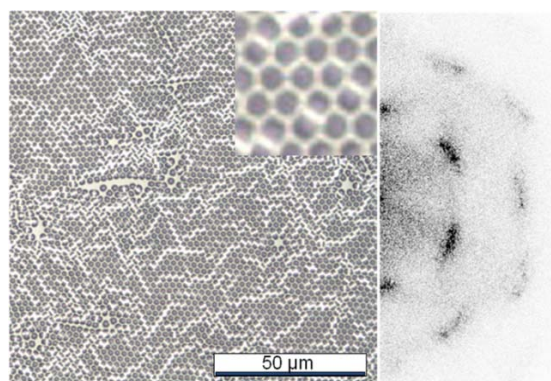
Fig. 1: Optical microscopy pictures with a blow-up in the inset and the corresponding 2D Fast Fourier Transform.

Diblock Copolymer Nanostructuration. The investigated continuous (*i.e.* regular solvent cast

films) and honeycomb block copolymer films exhibit a phase separation at the nanometer length scale as shown by Small Angle Neutron Scattering (SANS) and Atomic Force Microscopy (AFM). After a thermal annealing at 120ºC of the continuous film, the nature of the copolymer arrangement is unambiguously the thermodynamically stable hexagonal cylinders packing (*hcp*) since three orders are present at q^*, $\sqrt{4}\,q^*$ and $\sqrt{7}\,q^*$ (Cf. Fig. 2), leading to cylinder-to-cylinder distance of 55 nm. The SANS curve of the non annealed continuous film shows only a first order peak and a broad shoulder at larger q located in the vicinity of *2q**, indicating the presence of a phase-segregation in the film but with a weak ordering. The scattering curve measured on the HC film (Cf. Fig. 2) shows also a single peak, that can be interpreted as a liquid-like order of PS rich domains in the PnBA matrix. It points out that the copolymer did not fully reach its thermodynamical equilibrium. Furthermore, the Porod regime (q^{-4} slope) at large q indicates a sharp interface between both segregated domains.
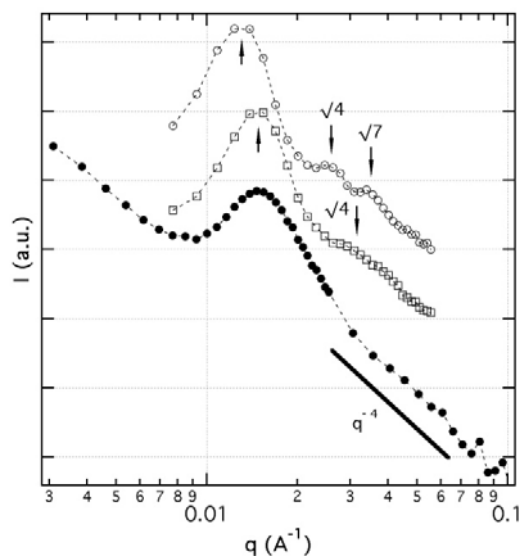
Fig. 2: SANS curves of PnBA-b-PS diblock copolymer films: (i) solvent cast film (open square), (ii) the thermally annealed solvent cast film (open circle) and (iii) the honeycomb film (solid circle). Upward arrows are showing the first order peak and the downward ones the expected higher order peaks.

Nevertheless, the AFM phase image scanned on the HC film surface (Cf. Fig. 3) is in good agreement with the SANS results. Indeed, the *hcp* structure was confirmed on the HC film and also on the continuous film (the AFM picture is not presented in here).
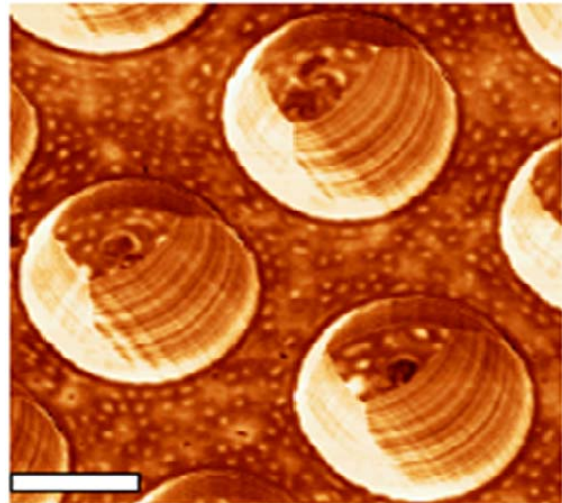
Fig. 3: AFM phase image of PnBA-b-PS diblock copolymer honeycomb film (scale bar represents 500 nm).

The present study has shown that both, the micrometric pore organization and the internal nanoscale morphology of the diblock copolymer self-assembly can be spontaneously achieved by tuning the copolymer features, *i.e.* interaction parameter, monomer weight fraction and molecular weight. A complete understanding of the effect of each parameter is the object of an on going research. Furthermore, adhesion and wettability properties, using HC films as model substrates, are currently investigated.

Acknowledgements:

References

[1] U. Bunz, Adv. Mater., 2006, **18**, 973
[2] G. Widawski *et al.* Nature, 1994, **369**, 387
[3] B. Francois *et al.* Adv. Mater., 1995, **7**, 1041
[4] P. Escalé *et al.* Soft Matter, 2010, **6**, 3202
[5] C. Hawker *et al.* Chem. Rev., 2001, **101**, 366

GLYCODYNAMERS : DYNAMIC POLYMERS BEARING OLIGOSACCHARIDES RESIDUES – GENERATION, STRUCTURE, PHYSICOCHEMICAL, COMPONENT EXCHANGE AND LECTIN BINDING PROPERTIES

Y. Ruff [1], E. Buhler [2,3], S-J. Candau [1], E. Kesselman [4], Y. Talmon [4], and J-M. Lehn[*,1]

[1] Laboratoire de Chimie Supramoléculaire, ISIS, Université de Strasbourg, Allée Gaspard Monge, 67000 Strasbourg, France
[2] Laboratoire Matière et Systèmes Complexes (MSC), UMR CNRS 7057, Bâtiment Condorcet, Université Paris Diderot-Paris 7, 75205 Paris Cedex 13, France
[3] Laboratoire Léon Brillouin, IRAMIS, CEA Saclay, 91191 Gif-Sur-Yvette Cedex, France
[4] Department of Chemical Engineering, Technion-Israel Institute of Technology, Haifa 32000, Israel

Dynamic glycopolymers have been generated by polycondensation through acylhydrazone formation between components bearing lateral bioactive oligosaccharide chains. They have been characterized as bottlebrush type by cryo-TEM and SANS studies. They present remarkable fluorescence properties whose emission wavelengths depend on the constitution of the polymer and are tunable by constitutional modification through exchange/incorporation of components, thus also demonstrating their dynamic character (see following scheme). Constitution dependent binding of these glycodynamers to a lectin, peanut agglutinin, has been demonstrated.[1]
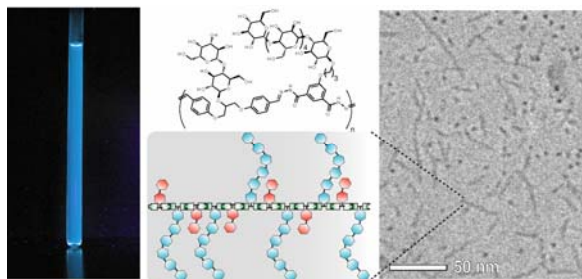
Constitutional Dynamic Chemistry (CDC)[2] rests on the implementation of reversible chemical connections of either covalent or non-covalent nature linking the components of a molecular or supramolecular entity. As a consequence, constitutionally dynamic entities are able to continuously modify their constitution by assembly-disassembly of their building blocks, thus generating a mixture of interconvertible species, a dynamic set of constituents, a constitutional dynamic library[2] (CDL).

A CDL is also combinatorial, as all possible combinations of the initial building blocks may form, in proportions specific to the thermodynamic equilibrium of the system.[3] Disruption of this equilibrium by physical or chemical factors, may lead to adaptation through amplification of one or more constituents of the library by rearrangement of its components. This approach was used successfully, for example for the discovery of biologically active substances selected by the biological target itself under the pressure of recognition.[4]

The implementation of CDC in material science, in particular in polymer chemistry, led to the introduction of the notion of dynamic polymers, dynamers that result from the reversible connection of monomers via either covalent or non-covalent linkages.[5,6] Such equilibrium polymers present the ability to undergo changes in their constitution, length, and sequence even after polymerization. These modifications can be triggered by physical stimuli or chemical effectors like temperature, or addition of protons or of metal cations. Dynamers are thus smart, adaptive materials. Moreover, changes in the molecular constitution of the polymer can induce a modification of the properties (such as mechanical or optical) of the material.

Dynamers based on components of biological nature may generate dynamic analogs of natural polymers, *biodynamers*, that offer the possibility to combine the functional properties (recognition, catalysis) of naturally occurring polymers with the adaptive behavior of constitutional dynamic systems. Therefore, in view of the prospects offered, the incorporation of biologically relevant moieties into dynamic polymers deserves close scrutiny.

In addition to proteins and nucleic acids, polysaccharides represent a third class of biopolymers. Oligo- and polysaccharides are involved in a wide range of biological or pathological events like immune response, inflammation, cancer, cell adhesion or cell-cell recognition. These recognition processes involve in particular carbohydrate-protein interactions. As the interaction of a single saccharide with its receptor is generally weak, biology uses multivalency to enhance the binding efficiency. The oligosaccharides involved in recognition processes are generally clustered, displayed in a multivalent fashion, at the surface of cells or bacteria. It is therefore of much interest to design synthetic analogs of these natural multivalent assemblies in order to mimic, or even improve over, their native properties.

Extending our work on dynamers[5,6] to the biopolymer area, we were interested in designing dynamic analogs of glycopolymers, *glycodynamers*.[1,7] Such dynamic or equilibrium polymers could provide, in addition to potential biorecognition properties, an adaptive character that would enable them to reorganize their sequence or constitution so as to select the preferential/optimal sequence, nature and proportion of the bioactive monomeric subunits, in response to external physical stimuli or chemical effectors (temperature, pH, etc.), or to the presence of a (bio)chemical target template.

Such biodynamers may be of three types: 1) main-chain, resulting from polycondensation of saccharide residues through reversible reactions; 2) side- chain, where the saccharide residues are either (a) appended on a dynamic main chain, or (b) reversibly grafted on a non-dynamic main chain; 3)"doubly-dynamic", incorporating both main-chain and side-chain dynamics.

We present here our results on the generation of glycodynamers (non-glycosydic dynamic main-chain bearing lateral carbohydrate residues). The structure of these dynamic glycodynamers was characterized in detail by SANS.[1] Analysis of the scattering data agrees with it having a rigid rodlike structure. For the example presented in Fig. 1, we found a radius of gyration of 187 Å and an average contour length of 650 Å. Its average molecular weight was about 511K, which corresponds to 275 monomeric units for an initial concentration of 5mM at pD=4. In the intermediate q^{-1} regime, the data can be fitted by a rigidrod model giving a linear mass density M_L=744g/mol/Å.[1] The high-q data can be fitted by a Guinier expression for the form factor of the polymer cross-section.[1] From the fit of Fig. 1, we obtain a section area of 1300 Å^2 and a section radius of gyration R_c=17.3 Å. As the polymer may be considered a solid cylinder, $d=\sqrt{8}R_c$, which gives a section diameter of 48.9 Å.
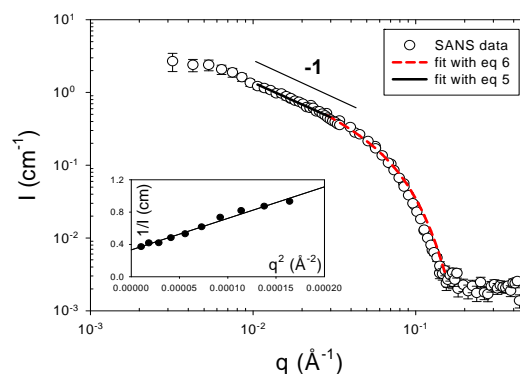
Fig. 1: SANS spectra obtained for a 5mM solution in D_2O at T=57°C and pD= 4. The black line represents the fit of the data in the intermediate regime with a rigidrod model, and the dashed red line represents the fit of the high-q data by a Guinier expression for the form factor of the section.

These dimensions are in agreement with the expected diameter of a single polymer chain with bottlebrush-like shape. Such shape confers interesting biorecognition properties to the resulting glycopolymer that has the potential to bind lectin.[1]

References

[1] Ruff, Y.; Buhler, E.; Candau, S. J.; Kesselman, E.; Talmon , Y.; Lehn, J.-M. J. Am. Chem. Soc. 2010, **132**, 2573-2584.
[2] Lehn, J.-M. Chem. Soc. Rev. 2007, **36**, 151-160.
[3] Lehn, J.-M. Chem. Eur. J. 1999, **5**, 2455-2463.
[4] Ramström, O.; Lehn, J.-M. Nat. Rev. Drug. Discovery 2002, **1**, 26-36.
[5] Lehn, J.-M. Prog. Polym. Sci. 2005, **30**, 814-831.
[6] Lehn, J.-M. Polym. Int. 2002, **51**, 825-839.
[7] Ruff, Y.; Lehn, J.-M. Angew. Chem. Int. Ed. 2008, **47**, 3556-3559.

Publications
2010

Publications

1) *pH and Temperature Responsive Polymeric Micelles and Polymersomes by Self-Assembly of Poly 2-(dimethylamino)ethyl methacrylate -b-Poly(glutamic acid) Double Hydrophilic Block Copolymers*. Agut W., Brulet A., Schatz C., Taton D. and Lecommandoux S. **Langmuir**, vol. 26(13), pp. 10546-10554, (2010)

2) *Photo-Crosslinked Fluorinated Thin Films from Azido-Functionalized Random Copolymers*. Al Akhrass S., Damiron D., Carrot G. and Drockenmuller E. **Journal of Polymer Science Part a-Polymer Chemistry**, vol. 48(17), pp. 3888-3895, (2010)

3) *Interplay between magnetism and superconductivity in HoNi2B2C revisited*. Alleno E., Singh S., Dhar S. K. and Andre G. **New Journal of Physics**, vol. 12, pp., (2010)

4) *From antiferromagnetic to ferromagnetic ordering induced by hydrogenation of the compounds NdCoSi and NdCoGe*. B C. and S Tencé[1,] G André[2], S F Matar[1] and E Gaudin1. **journal physics; conf series**, vol. 200, pp. 032012, (2010)

5) *Formation of Rodlike Silica Aggregates Directed by Adsorbed Thermoresponsive Polymer Chains*. Babayan D., Chassenieux C., Lafuma F., Ventelon L. and Hernandez J. **Langmuir**, vol. 26(4), pp. 2279-2287, (2010)

6) *Hydrogen bonded network properties in liquid formamide*. Bako I., Megyes T., Balint S., Chihaia V., Bellissent-Funel M. C., Krienke H., Kopf A. and Suh S. H. **Journal of Chemical Physics**, vol. 132(1), pp., (2010)

7) *Two-Dimensional Orbital-Like Magnetic Order in the High-Temperature La2-xSrxCuO4 Superconductor*. Baledent V., Fauque B., Sidis Y., Christensen N. B., Pailhes S., Conder K., Pomjakushina E., Mesot J. and Bourges P. **Physical Review Letters**, vol. 105(2), pp., (2010)

8) *Effects Of Pressure On Stability Of Biomolecules In Solutions Studied By Neutron Scattering*. Bellissent-Funel M. C., Appavou M. S. and Gibrat G., Metastable Systems under Pressure. Rzoska, S., Rzoska, A. D. and Mazur, V.**:** pp. 377-388, (2010)

9) *Structural, static and dynamic magnetic properties of Co2MnGe thin films on a sapphire a-plane substrate*. Belmeguenai M., Zighem F., Chauveau T., Faurie D., Roussigne Y., Cherif S. M., Moch P., Westerholt K. and Monod P. **Journal of Applied Physics**, vol. 108(6), pp., (2010)

10) *Network swelling competing with translational entropy in autophobic polymer dewetting*. Beziel W., Reiter G., Drockenmuller E., Ostaci R. V., Al Akhrass S., Cousin F. and Sferrazza M. **Epl**, vol. 90(2), pp., (2010)

11) *Dynamic study of N ' N-dimethylparanitroaniline encapsulated in silicalite-1 matrix using neutron spin-echo spectroscopy*. Bhange D. S., Dejoie C., Porcher F., Malikova N., Martinetto P., Dooryhee E. and Anne M. **European Physical Journal-Special Topics**, vol. 189(1), pp. 279-284, (2010)

12) *Identification of a protein required for recovery of full antenna capacity in OCP-related photoprotective mechanism in cyanobacteria*. Boulay C., Wilson A., D'Haene S. and Kirilovsky D. **Proceedings of the National Academy of Sciences of the United States of America**, vol. 107(25), pp. 11620-11625, (2010)

13) *Influence of FSSW parameters on fracture mechanisms of 5182 aluminium welds*. Bozzi S., Helbert-Etter A. L., Baudin T., Klosek V., Kerbiguet J. G. and Criqui B. **Journal of Materials Processing Technology**, vol. 210(11), pp. 1429-1435, (2010)

14) *The key to control Cu II loading in silica based mesoporous materials*. Brodie-Linder N., Besse R., Audonnet F., LeCaer S., Deschamps J., Imperor-Clerc M. and Alba-Simionesco C. **Microporous and Mesoporous Materials**, vol. 132(3), pp. 518-525, (2010)

15) *H-2 formation by electron irradiation of SBA-15 materials and the effect of Cu-II grafting*. Brodie-Linder N., Le Caer S., Alam M. S., Renault J. P. and Alba-Simionesco C. **Physical Chemistry Chemical Physics**, vol. 12(42), pp. 14188-14195, (2010)

16) *Study of the heating effect contribution to the nonlinear dielectric response of a supercooled liquid*. Brun C., Crauste-Thibierge C., Ladieu F. and L'Hote D. **Journal of Chemical Physics**, vol. 133(23), pp., (2010)

17) *Field evolution of the magnetic structures in Er2Ti2O7 through the critical point*. Cao H. B., Mirebeau I., Gukasov A., Bonville P. and Decorse C. **Physical Review B**, vol. 82(10), pp., (2010)

18) *Self-assembly of an amyloid peptide fragment-PEG conjugate: lyotropic phase formation and influence of PEG crystallization*. Castelletto V., Newby G. E., Merino D. H., Hamley I. W., Liu D. and Noirez L. **Polymer Chemistry**, vol. 1(4), pp. 453-459, (2010)

19) *Self-Assembly of PEGylated Peptide Conjugates Containing a Modified Amyloid beta-Peptide Fragment*. Castelletto V., Newby G. E., Zhu Z., Hamley I. W. and Noirez L. **Langmuir**, vol. 26(12), pp. 9986-9996, (2010)

20) *Small-Angle Neutron Scattering Study of Solubilization of Tributyl Phosphate in Aqueous Solutions of L64 Pluronic Triblock Copolymers*. Causse J., Oberdisse J., Jestin J. and Lagerge S. **Langmuir**, vol. 26(20), pp. 15745-15753, (2010)

21) *Elaboration of Spin-Coated Cellulose-Xyloglucan Multilayered Thin Films*. Cerclier C., Cousin F., Bizot H., Moreau C. and Cathala B. **Langmuir**, vol. 26(22), pp. 17248-17255, (2010)

22) *Collective molecular reorientation of a calamitic liquid crystal (12CB) confined in alumina nanochannels*. Chahine G., Kityk A. V., Demarest

N., Jean F., Knorr K., Huber P., Lefort R., Zanotti J. M. and Morineau D. **Physical Review E**, vol. 82(1), pp., (2010)

23) *Criticality of an isotropic-to-smectic transition induced by anisotropic quenched disorder*. Chahine G., Kityk A. V., Knorr K., Lefort R., Guendouz M., Morineau D. and Huber P. **Physical Review E**, vol. 81(3), pp., (2010)

24) *"Wet-to-Dry" Conformational Transition of Polymer Layers Grafted to Nanoparticles in Nanocomposite*. Chevigny C., Jestin J., Gigmes D., Schweins R., Di-Cola E., Dalmas F., Bertin D. and Boue F. **Macromolecules**, vol. 43(11), pp. 4833-4837, (2010)

25) *Can multistate dark matter annihilation explain the high-energy cosmic ray lepton anomalies?* Cirelli M. and Cline J. M. **Physical Review D**, vol. 82(2), pp., (2010)

26) *Small-angle scattering and the structure of ambient liquid water*. Clark G. N. I., Hura G. L., Teixeira J., Soper A. K. and Head-Gordon T. **Proceedings of the National Academy of Sciences of the United States of America**, vol. 107(32), pp. 14003-14007, (2010)

27) *Proton Dynamics and Structural Modifications in the Protonic Conductor Perovskites*. Colomban Philippe and Aneta Slodczyk D. L., Gilles Andre, Oumaya Zaafrani, Olivier Lacroix, Stephanie Willemin, and Beatrice Sala. **journal of the physical society of japan**, vol. 79(SUP A), pp. 1-6, (2010)

28) *Multiple Scale Reorganization of Electrostatic Complexes of Poly(styrenesulfonate) and Lysozyme*. Cousin F., Gummel J., Clemens D., Grillo I. and Boue F. **Langmuir**, vol. 26(10), pp. 7078-7085, (2010)

29) *Phonon dispersion and low-energy anomaly in CaC6 from inelastic neutron and x-ray scattering experiments*. d'Astuto M., Calandra M., Bendiab N., Loupias G., Mauri F., Zhou S. Y., Graf J., Lanzara A., Emery N., Herold C., Lagrange P., Petitgrand D. and Hoesch M. **Physical Review B**, vol. 81(10), pp., (2010)

30) *Orientation stress field analysis in polycrystalline bcc steel using neutron diffraction*. Dakhlaoui R., Klosek V., Mathon M. H. and Marini B. **Acta Materialia**, vol. 58(2), pp. 499-509, (2010)

31) *The Role of Chain Length in Nonergodicity Factor and Fragility of Polymers*. Dalle-Ferrier C., Niss K., Sokolov A. P., Frick B., Serrano J. and Alba-Simionesco C. **Macromolecules**, vol. 43(21), pp. 8977-8984, (2010)

32) *Zigzag ladders with staggered magnetic chirality in the S=3/2 compound beta-CaCr2O4*. Damay F., Martin C., Hardy V., Maignan A., Andre G., Knight K., Giblin S. R. and Chapon L. C. **Physical Review B**, vol. 81(21), pp., (2010)

33) *Investigations for the growth of large underdoped Bi2Sr2CaCu2O8+delta single crystals*. De Almeida-Didry S., Giovannelli F., Monot-Laffez I., Sidis Y., Bourges P., Sohoenstein F., Pruvost S. and Pignon B. **Journal of Crystal Growth**, vol. 312(3), pp. 466-470, (2010)

34) *An investigation of the polytypical structure of Sr0.2Ba0.8CoO3-delta by neutron powder diffraction*. de la Calle C., Alonso J. A., Aguadero A., Fernandez-Diaz M. T. and Porcher F. **Zeitschrift Fur Kristallographie**, vol. 225(5), pp. 209-215, (2010)

35) *Indigo@Silicalite: a New Organic Inorganic Hybrid Pigment*. Dejoie C., Martinetto P., Dooryhee E., Strobel P., Blanc S., Bordat P., Brown R., Porcher F., del Rio M. S. and Anne M. **Acs Applied Materials & Interfaces**, vol. 2(8), pp. 2308-2316, (2010)

36) *Association of Indigo with Zeolites for Improved Color Stabilization*. Dejoie C., Martinetto P., Dooryhee E., Van Elslande E., Blanc S., Bordat P., Brown R., Porcher F. and Anne M. **Applied Spectroscopy**, vol. 64(10), pp. 1131-1138, (2010)

37) *A thermodynamic limit of the melting/freezing processes of water under strongly hydrophobic nanoscopic confinement*. Deschamps J., Audonnet F., Brodie-Linder N., Schoeffel M. and Alba-Simionesco C. **Physical Chemistry Chemical Physics**, vol. 12(7), pp. 1440-1443, (2010)

38) *Self assembly of anastomosis-like superstructures in fatty acid/guanidine hydrochloride aqueous dispersions*. Douliez J. P., Houinsou-Houssou B., Fameau A. L., Novales B. and Gaillard C. **Journal of Colloid and Interface Science**, vol. 341(2), pp. 386-389, (2010)

39) *Chemistry*. Drockenmuller E., Colinet I., Damiron D., Gal F., Perez H. and Carrot G. **Macromolecules**, vol. 43(22), pp. 9371-9375, (2010)

40) *Hierarchical structures based on self-assembled diblock copolymers within honeycomb micro-structured porous films*. Escale P., Save M., Lapp A., Rubatat L. and Billon L. **Soft Matter**, vol. 6(14), pp. 3202-3210, (2010)

41) *12-Hydroxystearic acid lipid tubes under various experimental conditions*. Fameau A. L., Houinsou-Houssou B., Novales B., Navailles L., Nallet F. and Douliez J. P. **Journal of Colloid and Interface Science**, vol. 341(1), pp. 38-47, (2010)

42) *Neutron diffraction study of magnetic structures in single crystal Ho$_2$PdSi$_3$ in magnetic fields up to 5 T*. Fei T. and Fei Tang1 P. L., Matthias Frontze[k]1, Jean-Michel Migno[t]3, Jens-Uwe Hoffma[n]4, Wolfgang Löse[r]5 and Michael Loewenhaup[t]1. **journal physics conf series**, vol. 2010, pp. 012017, (2010)

43) *Evidence of macroscopically entangled protons in a mixed isotope crystal of KHpD1-pCO3*. Fillaux F., Cousson A. and Gutmann M. J. **Journal of Physics-Condensed Matter**, vol. 22(4), pp., (2010)

44) *Neutron scattering evidence for a lattice displacement at the charge ordering transition of*

Publications

(TMTTF)(2)PF6. Foury-Leylekian P., Petit S., Andre G., Moradpour A. and Pouget J. P. **Physica B-Condensed Matter**, vol. 405(11), pp. S95-S97, (2010)

45) *Correlation between crystallographic superstructure and magnetic structures in finite magnetic fields: A neutron study on a single crystal of Ho2PdSi3*. Frontzek M., Tang F., Link P., Schneidewind A., Hoffman J. U., Mignot J. M. and Loewenhaupt M. **Physical Review B**, vol. 82(17), pp., (2010)

46) *Two-dimensional neutron scattering in a floating heavy water bridge*. Fuchs E. C., Baroni P., Bitschnau B. and Noirez L. **Journal of Physics D-Applied Physics**, vol. 43(10), pp., (2010)

47) *Partial area of cholesterol in monounsaturated diacylphosphatidylcholine bilayers*. Gallova J., Uhrikova D., Kucerka N., Teixeira J. and Balgavy P. **Chemistry and Physics of Lipids**, vol. 163(8), pp. 765-770, (2010)

48) *Polar clusters in impurity-doped quantum paraelectric K1-xLixTaO(3)*. Geneste G., Kiat J. M., Yokota H., Uesu Y. and Porcher F. **Physical Review B**, vol. 81(14), pp., (2010)

49) *Cubic to Hexagonal Phase Transition Induced by Electric Field*. Giacomelli F. C., da Silveira N. P., Nallet F., Cernoch P., Steinhart M. and Stepanek P. **Macromolecules**, vol. 43(9), pp. 4261-4267, (2010)

50) *Size-dependent magnetic behavior and spin-wave gap in MnF2 epitaxial films with orthorhombic crystal structure*. Golosovsky I. V., Sokolov N. S., Gukasov A., Bataille A., Boehm M. and Nogues J. **Journal of Magnetism and Magnetic Materials**, vol. 322(6), pp. 664-667, (2010)

51) *Effects of flow fluctuations and partial thermalization on v(4)*. Gombeaud C. and Ollitrault J. Y. **Physical Review C**, vol. 81(1), pp., (2010)

52) *On the relation between the microscopic structure and the sound velocity anomaly in elemental melts of groups IV, V, and VI*. Greenberg Y., Yahel E., Caspi E. N., Beuneu B., Dariel M. P. and Makov G. **Journal of Chemical Physics**, vol. 133(9), pp., (2010)

53) *Interplay between crystalline chirality and magnetic structure in Mn1-xFexSi*. Grigoriev S. V., Chernyshov D., Dyadkin V. A., Dmitriev V., Moskvin E. V., Lamago D., Wolf T., Menzel D., Schoenes J., Maleyev S. V. and Eckerlebe H. **Physical Review B**, vol. 81(1), pp., (2010)

54) *Noncentrosymmetric cubic helical ferromagnets Mn1-y Fe (y) Si and Fe1-x Co (x) Si*. Grigoriev S. V., Dyadkin V. A., Maleyev S. V., Menzel D., Schoenes J., Lamago D., Moskvin E. V. and Eckerlebe H. **Physics of the Solid State**, vol. 52(5), pp. 907-913, (2010)

55) *Synthesis of thermally responsive cylindrical molecular brushes via a combination of nitroxide-mediated radical polymerization and "grafting onto" strategy*. Gromadzki D., Jigounov A., Stepanek P. and Makuska R. **European Polymer Journal**, vol. 46(4), pp. 804-813, (2010)

56) *Rearrangement of the structure during nucleation of a cordierite glass doped with TiO2*. Guignard M., Cormier L., Montouillout V., Menguy N., Massiot D., Hannon A. C. and Beuneu B. **Journal of Physics-Condensed Matter**, vol. 22(18), pp., (2010)

57) *Determination of atomic site susceptibility tensors from neutron diffraction data on polycrystalline samples*. Gukasov A. and Brown P. J. **Journal of Physics-Condensed Matter**, vol. 22(50), pp., (2010)

58) *Neutron scattering study of the magnetic phase diagram of underdoped YBa2Cu3O6+x*. Haug D., Hinkov V., Sidis Y., Bourges P., Christensen N. B., Ivanov A., Keller T., Lin C. T. and Keimer B. **New Journal of Physics**, vol. 12, pp., (2010)

59) *Superconductivity and electronic liquid-crystal states in twin-free YBa2Cu3O6+x studied by neutron scattering*. Hinkov V., Lin C. T., Raichle M., Keimer B., Sidis Y., Bourges P., Pailhes S. and Ivanov A. **European Physical Journal-Special Topics**, vol. 188(1), pp. 113-129, (2010)

60) *Growth and Branching of Charged Wormlike Micelles as Revealed by Dilution Laws*. In M., Bendjeriou B., Noirez L. and Grillo I. **Langmuir**, vol. 26(13), pp. 10411-10414, (2010)

61) *Bridging Multiferroic Phase Transitions by Epitaxial Strain in BiFeO3*. Infante I. C., Lisenkov S., Dupe B., Bibes M., Fusil S., Jacquet E., Geneste G., Petit S., Courtial A., Juraszek J., Bellaiche L., Barthelemy A. and Dkhil B. **Physical Review Letters**, vol. 105(5), pp., (2010)

62) *Normal-state spin dynamics and temperature-dependent spin-resonance energy in optimally doped BaFe1.85Co0.15As2*. Inosov D. S., Park J. T., Bourges P., Sun D. L., Sidis Y., Schneidewind A., Hradil K., Haug D., Lin C. T., Keimer B. and Hinkov V. **Nature Physics**, vol. 6(3), pp. 178-181, (2010)

63) *Chirality in Dynamic Supramolecular Nanotubes Induced by a Chiral Solvent*. Isare B., Linares M., Zargarian L., Fermandjian S., Miura M., Motohashi S., Vanthuyne N., Lazzaroni R. and Bouteiller L. **Chemistry-a European Journal**, vol. 16(1), pp. 173-177, (2010)

64) *Studies of water and ice in hydrophilic and hydrophobic mesoporous silicas: pore characterisation and phase transformations*. Jelassi J., Castricum H. L., Bellissent-Funel M. C., Dore J., Webber J. B. W. and Sridi-Dorbez R. **Physical Chemistry Chemical Physics**, vol. 12(12), pp. 2838-2849, (2010)

65) *KAM tori in 1D random discrete nonlinear Schrodinger model?* Johansson M., Kopidakis G. and Aubry S. **Epl**, vol. 91(5), pp., (2010)

66) *Direct small-angle-neutron-scattering observation of stretched chain conformation in*

nanocomposites: More insight on polymer contributions in mechanical reinforcement. Jouault N., Dalmas F., Said S., Di Cola E., Schweins R., Jestin J. and Boue F. **Physical Review E**, vol. 82(3), pp., (2010)

67) *Direct Measurement of Polymer Chain Conformation in Well-Controlled Model Nanocomposites by Combining SANS and SAXS.* Jouault N., Dalmas F., Said S., Di Cola E., Schweins R., Jestin J. and Boue F. **Macromolecules**, vol. 43(23), pp. 9881-9891, (2010)

68) *Structure of Te-rich Te-Ge-X (X = I, Se, Ga) glasses.* Jovari P., Kaban I., Bureau B., Wilhelm A., Lucas P., Beuneu B. and Zajac D. A. **Journal of Physics-Condensed Matter**, vol. 22(40), pp., (2010)

69) *Neutron diffraction study of the high magnetic field phase diagram of La-doped PrB_6.* Julien R. and Julien Robert1 J.-M. M., M Se^ra2 and F Iga2. **journal physics ; conf series**, vol. 200, pp. 012166, (2010)

70) ***Neutron Diffraction Investigation of $Pb_{0.5}La0.5_FeO3$.*** K K. and S. Kovachev [a.] D. K., [b] E. Svab,[c] G. Andre,[d] and F. Porcherd. **AIP conf proc**, (2010)

71) *Structure of GeSe4-In and GeSe5-In glasses.* Kaban I., Jovari P., Petkova T., Petkov P., Stoilova A., Hoyer W. and Beuneu B. **Journal of Physics-Condensed Matter**, vol. 22(40), pp., (2010)

72) *On the atomic structure of Zr60Cu20Fe20 metallic glass.* Kaban I., Jovari P., Stoica M., Mattern N., Eckert J., Hoyer W. and Beuneu B. **Journal of Physics-Condensed Matter**, vol. 22(40), pp., (2010)

73) *Composition, structural parameters, and color of langatate.* Kaurova I. A., Kuz'micheva G. M., Rybakov V. B., Dubovskii A. B. and Cousson A. **Inorganic Materials**, vol. 46(9), pp. 988-993, (2010)

74) *Low-symmetry phases and loss of relaxation in nanosized lead scandium niobate.* Kiat J. M., Bogicevic C., Karolak F., Dezanneau G., Guiblin N., Ren W., Bellaiche L. and Haumont R. **Physical Review B**, vol. 81(14), pp., (2010)

75) *Development and application of setup for ac magnetic field in neutron scattering experiments.* Klimko S., Zhernenkov K., Toperverg B. P. and Zabel H. **Review of Scientific Instruments**, vol. 81(10), pp., (2010)

76) *Representation of data on off-specular neutron scattering.* Kozhevnikov S. V. and Ott F. **Physics of the Solid State**, vol. 52(8), pp. 1561-1570, (2010)

77) *Competition between ferromagnetic and antiferromagnetic ground states in multiferroic BiMnO3 at high pressures.* Kozlenko D. P., Belik A. A., Kichanov S. E., Mirebeau I., Sheptyakov D. V., Strassle T., Makarova O. L., Belushkin A. V.,

Savenko B. N. and Takayama-Muromachi E. **Physical Review B**, vol. 82(1), pp., (2010)

78) *Neutron Diffraction Investigation of Langanite Crystals.* Kuz'micheva G. M., Kaurova I. A., Rybakov V. B., Dubovsky A. B., Cousson A. and Zaharko O. **Crystallography Reports**, vol. 55(6), pp. 1067-1073, (2010)

79) *Dynamical behavior of a single polymer chain under nanometric confinement.* Lagrene K., Zanotti J. M., Daoud M., Farago B. and Judeinstein P. **European Physical Journal-Special Topics**, vol. 189(1), pp. 231-237, (2010)

80) *Large-scale dynamics of a single polymer chain under severe confinement.* Lagrene K., Zanotti J. M., Daoud M., Farago B. and Judeinstein P. **Physical Review E**, vol. 81(6), pp., (2010)

81) *Lattice dynamics in the itinerant helical magnet MnSi.* Lamago D., Clementyev E. S., Ivanov A. S., Heid R., Mignot J. M., Petrova A. E. and Alekseev P. A. **Physical Review B**, vol. 82(14), pp., (2010)

82) *Measurement of strong phonon softening in Cr with and without Fermi-surface nesting by inelastic x-ray scattering.* Lamago D., Hoesch M., Krisch M., Heid R., Bohnen K. P., Boni P. and Reznik D. **Physical Review B**, vol. 82(19), pp., (2010)

83) *Effect of the Pb2+ lone electron pair in the structure and properties of the double perovskites Pb2Sc(Ti0.5Te0.5)O-6 and Pb2Sc(Sc0.33Te0.66)O-6: relaxor state due to intrinsic partial disorder.* Larregola S. A., Alonso J. A., Alguero M., Jimenez R., Suard E., Porcher F. and Pedregosa J. C. **Dalton Transactions**, vol. 39(21), pp. 5159-5165, (2010)

84) *Small-Angle Neutron Scattering of Percolative Perfluoropolyether Water in Oil Microemulsions.* Laurati M., Gambi C. M. C., Giordano R., Baglioni P. and Teixeira J. **Journal of Physical Chemistry B**, vol. 114(11), pp. 3855-3862, (2010)

85) *Compression of random coils due to macromolecular crowding: Scaling effects.* Le Coeur C., Teixeira J., Busch P. and Longeville S. **Physical Review E**, vol. 81(6), pp., (2010)

86) *Dynamics of water in binary and ternary solutions of DNA and porphyrins.* Lebedev V. T., Kulvelis Y. V. and Torok G. **Physics of the Solid State**, vol. 52(5), pp. 1074-1079, (2010)

87) *Amphiphilic Diblock Copolymers with a Moderately Hydrophobic Block: Toward Dynamic Micelles.* Lejeune E., Drechsler M., Jestin J., Muller A. H. E., Chassenieux C. and Colombani O. **Macromolecules**, vol. 43(6), pp. 2667-2671, (2010)

88) *Asymptotic energy profile of a wave packet in disordered chains.* Lepri S., Schilling R. and Aubry S. **Physical Review E**, vol. 82(5), pp., (2010)

89) *Magnetic excitations in multiferroic LuMnO3 studied by inelastic neutron scattering.* Lewtas H. J., Boothroyd A. T., Rotter M., Prabhakaran D., Muller H., Le M. D., Roessli B., Gavilano J. and

Publications

Bourges P. **Physical Review B**, vol. 82(18), pp., (2010)

90) *Hidden magnetic excitation in the pseudogap phase of a high-T-c superconductor*. Li Y., Baledent V., Yu G., Barisic N., Hradil K., Mole R. A., Sidis Y., Steffens P., Zhao X., Bourges P. and Greven M. **Nature**, vol. 468(7321), pp. 283-285, (2010)

91) *Macroscopic Quantum Coherence of the Spin Triplet in the Spin-Ladder Compound Sr14Cu24O41*. Lorenzo J. E., Regnault L. P., Boullier C., Martin N., Moudden A. H., Vanishri S., Marin C. and Revcolevschi A. **Physical Review Letters**, vol. 105(9), pp., (2010)

92) *Effect of Nanoparticle Size on the Morphology of Adsorbed Surfactant Layers*. Lugo D. M., Oberdisse J., Lapp A. and Findenegg G. H. **Journal of Physical Chemistry B**, vol. 114(12), pp. 4183-4191, (2010)

93) *v(4) from ideal and viscous hydrodynamic simulations of nuclear collisions at the BNL Relativistic Heavy Ion Collider (RHIC) and the CERN Large Hadron Collider (LHC)*. Luzum M., Gombeaud C. and Ollitrault J. Y. **Physical Review C**, vol. 81(5), pp., (2010)

94) *A Generic Phase Diagram for R_2PdSi_3 (R = Heavy Rare Earth)?* M F. and Frontzek M F. T., P Link[2], A Schneidewind[1,2], J M Mignot[3], J U Hoffman[4] and M Loewenhaupt[1]. **Journal phys; conf series**, vol. 251, pp. 012026, (2010)

95) *Magnetic properties and neutron diffraction study of $(Ni_xMn_{l-x})_3[Cr(CN)_6]_2$ molecule-based magnets*. M M. and Mihalik M V. K. a., S Mat'aš[1,]2, M Zentkov[å]1, O Prokhenko1 and G

96) *Synthesis, Magnetic Structure, and Properties of a Layered Cobalt-Hydroxide Ferromagnet, Co-5(OH)(6)(SeO4)(2)(H2O)(4)*. Maalej W., Vilminot S., Andre G. and Kurmoo M. **Inorganic Chemistry**, vol. 49(6), pp. 3019-3024, (2010)

97) *Self-similar assemblies of globular whey proteins at the air-water interface: Effect of the structure*. Mahmoudi N., Gaillard C., Boue F., Axelos M. A. V. and Riaublanc A. **Journal of Colloid and Interface Science**, vol. 345(1), pp. 54-63, (2010)

98) *Dynamics in Clays - Combining Neutron Scattering and Microscopic Simulation*. Malikova N., Dubois E., Marry V., Rotenberg B. and Turq P. **Zeitschrift Fur Physikalische Chemie-International Journal of Research in Physical Chemistry & Chemical Physics**, vol. 224(1-2), pp. 153-181, (2010)

99) *The neutron diffraction study, calorimetry and spontaneous polarization of pyridinium perrhenate at 350, 300 and 100 K*. Maluszynska H., Cousson A. and Czarnecki P. **Journal of Physics-Condensed Matter**, vol. 22(23), pp., (2010)

100) *Nonlinearity and isotope effect in temporal evolution of mesoscopic structure during hydration of cement*. Mazumder S., Sen D., Bahadur J., Klepp J., Rauch H. and Teixeira J. **Physical Review B**, vol. 82(6), pp., (2010)

101) *Spin ice and soft spin ice ground state under high pressure: comparative study by neutron scattering*. Mirebeau I., Goncharenko I. and Cao H. **High Pressure Research**, vol. 30(1), pp. 3-11, (2010)

102) *Neutron study of the short range order inversion in Fe1-xCrx*. Mirebeau I. and Parette G. **Physical Review B**, vol. 82(10), pp., (2010)

103) *Pressure dependence of phonon modes across the tetragonal to collapsed-tetragonal phase transition in CaFe2As2*. Mittal R., Heid R., Bosak A., Forrest T. R., Chaplot S. L., Lamago D., Reznik D., Bohnen K. P., Su Y., Kumar N., Dhar S. K., Thamizhavel A., Ruegg C., Krisch M., McMorrow D. F., Brueckel T. and Pintschovius L. **Physical Review B**, vol. 81(14), pp., (2010)

104) *Does Molecular Self-Association Survive in Nanochannels?* Morineau D. and Alba-Simionesco C. **Journal of Physical Chemistry Letters**, vol. 1(7), pp. 1155-1159, (2010)

105) *Radiolysis of water in nanoporous gold*. Musat R., Moreau S., Poidevin F., Mathon M. H., Pommeret S. and Renault J. P. **Physical Chemistry Chemical Physics**, vol. 12(39), pp. 12868-12874, (2010)

106) *Neutron Diffraction Residual Stress Evaluation and Numerical Modeling of Coating Obtained by PTA Process*. Nady A., Bonefoy H., KloseK V., Mathon M. H. and Lodini A., Thermec 2009, Pts 1-4. Chandra, T., Wanderka, N., Reimers, W. and Ionescu, M. 638-642**:** pp. 594-599, (2010)

107) *Various Modes of Void Closure during Dry Sintering of Close-Packed Nanoparticles*. Nawaz Q. and Rharbi Y. **Langmuir**, vol. 26(2), pp. 1226-1231, (2010)

108) *Spin dynamics in the electron-doped Kondo insulator Yb1-xZrxB12 (x=0.2)*. Nemkovski K. S., Alekseev P. A., Mignot J. M., Goremychkin E. A., Nikonov A. A., Parfenov O. E., Lazukov V. N., Shitsevalova N. Y. and Dukhnenko A. V. **Physical Review B**, vol. 81(12), pp., (2010)

109) *Spin dynamics in Yb- and Sm-based systems with the nonmagnetic ground state*. Nemkovski K. S., Alekseev P. A., Mignot J. M. and Lazukov V. N. **Physics of the Solid State**, vol. 52(5), pp. 936-940, (2010)

110) *Connection between slow and fast dynamics of molecular liquids around the glass transition*. Niss K., Dalle-Ferrier C., Frick B., Russo D., Dyre J. and Alba-Simionesco C. **Physical Review E**, vol. 82(2), pp., (2010)

111) *Revealing the solid-like nature of glycerol at ambient temperature*. Noirez L. and Baroni P. **Journal of Molecular Structure**, vol. 972(1-3), pp. 16-21, (2010)

112) *Self-Assembly and Foaming Properties of Fatty Acid-Lysine Aqueous Dispersions*. Novales B., Riaublanc A., Navailles L., Houssou B. H., Gaillard C., Nallet F. and Douliez J. P. **Langmuir**, vol. 26(8), pp. 5329-5334, (2010)

113) *Enhanced drug loading in polymerized micellar cargo.* Ogier J., Arnauld T., Carrot G., Lhumeau A., Delbos J. M., Boursier C., Loreau O., Lefoulon F. and Doris E. **Organic & Biomolecular Chemistry**, vol. 8(17), pp. 3902-3907, (2010)

114) *Comment on "Preeminent Role of the Van Hove Singularity in the Strong-Coupling Analysis of Scanning Tunneling Spectroscopy for Two-Dimensional Cuprate Superconductors".* Onufrieva F. and Pfeuty P. **Physical Review Letters**, vol. 105(9), pp., (2010)

115) *Study of the Orthorhombic Polymeric Phase of C-60 Under High Pressure Using Synchrotron X-Ray Powder Diffraction.* Papoular R. J., Dmitriev V., Davydov V. A., Rakhmanina A. V., Allouchi H. and Agafonov V. **Fullerenes Nanotubes and Carbon Nanostructures**, vol. 18(4-6), pp. 392-395, (2010)

116) *First Observation of the FCC to Trigonal/Rhombohedral Transition of Pure Dimerized C-60 Under High Pressure.* Papoular R. J., Le Parc R., Dmitriev V., Davydov V. A., Rakhmanina A. V. and Agafonov V. **Fullerenes Nanotubes and Carbon Nanostructures**, vol. 18(4-6), pp. 386-391, (2010)

117) *Symmetry of spin excitation spectra in the tetragonal paramagnetic and superconducting phases of 122-ferropnictides.* Park J. T., Inosov D. S., Yaresko A., Graser S., Sun D. L., Bourges P., Sidis Y., Li Y. A., Kim J. H., Haug D., Ivanov A., Hradil K., Schneidewind A., Link P., Faulhaber E., Glavatskyy I., Lin C. T., Keimer B. and Hinkov V. **Physical Review B**, vol. 82(13), pp., (2010)

118) *Self-Assembly in Solution of a Reversible Comb-Shaped Supramolecular Polymer.* Pensec S., Nouvel N., Guilleman A., Creton C., Boue F. and Bouteiller L. **Macromolecules**, vol. 43(5), pp. 2529-2534, (2010)

119) *Role of transverse temperature gradients in the generation of lamellar eutectic solidification patterns.* Perrut M., Parisi A., Akamatsu S., Bottin-Rousseau S., Faivre G. and Plapp M. **Acta Materialia**, vol. 58(5), pp. 1761-1769, (2010)

120) *Enhancing permittivity of ferroelectric superlattices via composition tuning.* Pertsev N. A., Janolin P. E., Kiat J. M. and Uesu Y. **Physical Review B**, vol. 81(14), pp., (2010)

121) *Spin dynamics in the geometrically frustrated multiferroic CuCrO2.* Poienar M., Damay F., Martin C., Robert J. and Petit S. **Physical Review B**, vol. 81(10), pp., (2010)

122) *Microemulsion nanocomposites: phase diagram, rheology and structure using a combined small angle neutron scattering and reverse Monte Carlo approach.* Puech N., Mora S., Phou T., Porte G., Jestin J. and Oberdisse J. **Soft Matter**, vol. 6(21), pp. 5605-5614, (2010)

123) *Influence of the Formulation Process in Electrostatic Assembly of Nanoparticles and Macromolecules in Aqueous Solution: The Interaction Pathway.* Qi L., Fresnais J., Berret J. F., Castaing J. C., Destremaut F., Salmon J. B., Cousin F. and Chapel J. P. **Journal of Physical Chemistry C**, vol. 114(39), pp. 16373-16381, (2010)

124) *Experimental study of the relation between the permeability of kaolinite and its deformation at micro and macro scale.* Raynaud S., Vasseur G., Celerier B., Loggia D., Ghoreychi M., Mathon M. H. and Mazerolle F. **International Journal of Rock Mechanics and Mining Sciences**, vol. 47(4), pp. 559-567, (2010)

125) *The Fermi surface and band folding in La2-xSrxCuO4, probed by angle-resolved photoemission.* Razzoli E., Sassa Y., Drachuck G., Mansson M., Keren A., Shay M., Berntsen M. H., Tjernberg O., Radovic M., Chang J., Pailhes S., Momono N., Oda M., Ido M., Lipscombe O. J., Hayden S. M., Patthey L., Mesot J. and Shi M. **New Journal of Physics**, vol. 12, pp., (2010)

126) *Flow-Induced Ordering in Cubic Gels Formed by P2VP-b-PEO-b-P(GME-co-EGE) Triblock Terpolymer Micelles: A Rheo-SANS Study.* Reinicke S., Karg M., Lapp A., Heymann L., Hellweg T. and Schmalz H. **Macromolecules**, vol. 43(23), pp. 10045-10054, (2010)

127) *Natural rubber-clay nanocomposites: Mechanical and structural properties.* Rezende C. A., Braganca F. C., Doi T. R., Lee L. T., Galembeck F. and Boue F. **Polymer**, vol. 51(16), pp. 3644-3652, (2010)

128) *Methods for probing the long-range dynamic of confined polymers in nanoparticles using small-angle neutron scattering.* Rharbi Y., Yousfi M., Porcar L. and Nawaz Q. **Canadian Journal of Chemistry-Revue Canadienne De Chimie**, vol. 88(3), pp. 288-297, (2010) 522 *Homogeneous Dispersion of Magnetic Nanoparticles Aggregates in a PS Nanocomposite: Highly Reproducible Hierarchical Structure Tuned by the Nanoparticles' Size.* Robbes A. S., Jestin J., Meneau F., Dalmas F., Sandre O., Perez J., Boue F. and Cousin F. **Macromolecules**, vol. 43(13), pp. 5785-5796, (2010)

129) *Long-range order and low-energy magnetic excitations in CeRu2Al10 studied via neutron scattering.* Robert J., Mignot J. M., Andre G., Nishioka T., Kobayashi R., Matsumura M., Tanida H., Tanaka D. and Sera M. **Physical Review B**, vol. 82(10), pp., (2010)

130) *Study of C-60 Peapods After a High-Pressure-High-Temperature Treatment.* Rols S., Papoular R. J., Davydov V. A., Rakhmanina A. V., Autret C. and Agafonov V. **Fullerenes Nanotubes and Carbon Nanostructures**, vol. 18(4-6), pp. 412-416, (2010)

131) *A neutron powder diffraction study of the helimagnetic structure of TlCo2Se2-xSx.* Ronneteg S., Berger R. and Andre G. **Journal of**

Magnetism and Magnetic Materials, vol. 322(6), pp. 681-685, (2010)

132) *Molecular simulation of aqueous solutions at clay surfaces*. Rotenberg B., Marry V., Malikova N. and Turq P. **Journal of Physics-Condensed Matter**, vol. 22(28), pp., (2010)

133) *Pressure-Induced Structural Transition in LuFe2O4: Towards a New Charge Ordered State*. Rouquette J., Haines J., Al-Zein A., Papet P., Damay F., Bourgeois J., Hammouda T., Dore F., Maignan A., Hervieu M. and Martin C. **Physical Review Letters**, vol. 105(23), pp., (2010)

134) *Glycodynamers: Dynamic Polymers Bearing Oligosaccharides Residues - Generation, Structure, Physicochemical, Component Exchange, and Lectin Binding Properties*. Ruff Y., Buhler E., Candau S. J., Kesselman E., Talmon Y. and Lehn J. M. **Journal of the American Chemical Society**, vol. 132(8), pp. 2573-2584, (2010)

135) *On the behaviour of water hydrogen bonds at biomolecular sites: Dependences on temperature and on network dimensionality*. Russo D., Copley J. R. D., Ollivier J. and Teixeira J. **Journal of Molecular Structure**, vol. 972(1-3), pp. 81-86, (2010)

136) *Lattice dynamics in ZrB12 and LuB12: Ab initio calculations and inelastic neutron scattering measurements*. Rybina A. V., Nemkovski K. S., Alekseev P. A., Mignot J. M., Clementyev E. S., Johnson M., Capogna L., Dukhnenko A. V., Lyashenko A. B. and Filippov V. B. **Physical Review B**, vol. 82(2), pp., (2010)

137) *Magnetic structures of the ternary silicide $Nd_6Ni_{1.67}Si_3$*. S T. and E Gaudin G. A., F Bourée and B Chevalier. **Journal physics; conf series**, vol. 200, pp. 032074, (2010)

138) *Turbulent velocity spectra in superfluid flows*. Salort J., Baudet C., Castaing B., Chabaud B., Daviaud F., Didelot T., Diribarne P., Dubrulle B., Gagne Y., Gauthier F., Girard A., Hebral B., Rousset B., Thibault P. and Roche P. E. **Physics of Fluids**, vol. 22(12), pp., (2010)

139) *Biocompatible and Biodegradable Poly(trimethylene carbonate)-b-Poly (L-glutamic acid) Polymersomes: Size Control and Stability*. Sanson C., Schatz C., Le Meins J. F., Brulet A., Soum A. and Lecommandoux S. **Langmuir**, vol. 26(4), pp. 2751-2760, (2010)

140) *Evolution of the conducting phase topology at the percolation threshold in colossal magnetoresistance manganites: A magnetic small-angle neutron scattering study*. Saurel D., Simon C., Pautrat A., Martin C., Dewhurst C. and Brulet A. **Physical Review B**, vol. 82(5), pp., (2010)

141) *Field-induced magnetic structures in Tb2Ti2O7 at low temperatures: From spin-ice to spin-flip structures*. Sazonov A. P., Gukasov A., Mirebeau I., Cao H., Bonville P. and Grenier B. **Physical Review B**, vol. 82(17), pp., (2010)

142) *Foaming properties of protein/pectin electrostatic complexes and foam structure at nanoscale*. Schmidt I., Novales B., Boue F. and Axelos M. A. V. **Journal of Colloid and Interface Science**, vol. 345(2), pp. 316-324, (2010)

143) *Low-temperature structural phase transition in deuterated and protonated lithium acetate dihydrate*. Schroder F., Winkler B., Haussuhl E., Cong P. T., Wolf B., Avalos-Borja M., Quilichini M. and Hennion B. **Journal of Chemical Thermodynamics**, vol. 42(8), pp. 957-961, (2010)

144) *All-Manganite Tunnel Junctions with Interface-Induced Barrier Magnetism*. Sefrioui Z., Visani C., Calderon M. J., March K., Carretero C., Walls M., Rivera-Calzada A., Leon C., Anton R. L., Charlton T. R., Cuellar F. A., Iborra E., Ott F., Imhoff D., Brey L., Bibes M., Santamaria J. and Barthelemy A. **Advanced Materials**, vol. 22(44), pp. 5029-+, (2010)

145) *Thermoresponsive Amphiphilic Diblock Copolymers Synthesized by MADIX/RAFT: Properties in Aqueous Solutions and Use for the Preparation and Stabilization of Gold Nanoparticles*. Sistach S., Beija M., Rahal V., Brulet A., Marty J. D., Destarac M. and Mingotaud C. **Chemistry of Materials**, vol. 22(12), pp. 3712-3724, (2010)

146) *Water-clay surface interaction: A neutron scattering study*. Sobolev O., Buivin F. F., Kemner E., Russina M., Beuneu B., Cuello G. J. and Charlet L. **Chemical Physics**, vol. 374(1-3), pp. 55-61, (2010)

147) *Is ambient water inhomogeneous on the nanometer-length scale?* Soper A. K., Teixeira J. and Head-Gordon T. **Proceedings of the National Academy of Sciences of the United States of America**, vol. 107(12), pp. E44-E44, (2010)

148) *Possible room-temperature ferromagnetism in K-doped SnO2: X-ray diffraction and high-resolution transmission electron microscopy study*. Srivastava S. K., Lejay P., Barbara B., Pailhes S., Madigou V. and Bouzerar G. **Physical Review B**, vol. 82(19), pp., (2010)

149) *Ca2+-triggered coelenterazine-binding protein from Renilla muelleri: spatial structure and properties*. Stepanyuk G., Malikova N., Liu Z. J., Markova S., Frank L., Lee J. and Vysotski E. **Febs Journal**, vol. 277, pp. 264-264, (2010)

150) *Incommensurate Magnetic Order and Dynamics Induced by Spinless Impurities in YBa2Cu3O6.6*. Suchaneck A., Hinkov V., Haug D., Schulz L., Bernhard C., Ivanov A., Hradil K., Lin C. T., Bourges P., Keimer B. and Sidis Y. **Physical Review Letters**, vol. 105(3), pp., (2010)

151) *The glass transition and relaxation behavior of bulk water and a possible relation to confined water*. Swenson J. and Teixeira J. **Journal of Chemical Physics**, vol. 132(1), pp., (2010)

152) *Pink Noise of Ionic Conductance through Single Artificial Nanopores Revisited*. Tasserit C.,

Koutsioubas A., Lairez D., Zalczer G. and Clochard M. C. **Physical Review Letters**, vol. 105(26), pp., (2010)

153) *Around the composition Gd4Co3: Structural, magnetic and magnetocaloric properties of Gd6Co4.85(2)*. Tence S., Gaudin E. and Chevalier B. **Intermetallics**, vol. 18(6), pp. 1216-1221, (2010)

154) *Hydrogenation Inducing Ferromagnetism in the Ternary Antiferromagnet NdCoSi*. Tence S., Matar S. F., Andre G., Gaudin E. and Chevalier B. **Inorganic Chemistry**, vol. 49(11), pp. 4836-4842, (2010)

155) *Spin-Flop Transition and Magnetocaloric Effect through Disconnected Magnetic Blocks in Co-III/Co-IV Oxybromides*. Toulemonde O., Roussel P., Isnard O., Andre G. and Mentre O. **Chemistry of Materials**, vol. 22(12), pp. 3807-3816, (2010)

156) *Temperature-Dependent Structure of alpha-CD/PEO-Based Polyrotaxanes in Concentrated Solution in DMSO: Kinetics and Multiblock Copolymer Behavior*. Travelet C., Hebraud P., Perry C., Brochon C., Hadziioannou G., Lapp A. and Schlatter G. **Macromolecules**, vol. 43(4), pp. 1915-1921, (2010)

157) *Magnetoelastic coupling in the frustrated antiferromagnetic triangular lattice CuMnO2*. Vecchini C., Poienar M., Damay F., Adamopoulos O., Daoud-Aladine A., Lappas A., Perez-Mato J. M., Chapon L. C. and Martin C. **Physical Review B**, vol. 82(9), pp., (2010)

158) *Giant Magnetic Hardness in the Synthetic Mineral Ferrimagnet K2Co3II(OH)(2)(SO4)(3)(H2O)(2)*. Vilminot S., Baker P. J., Blundell S. J., Sugano T., Andre G. and Kurmoo M. **Chemistry of Materials**, vol. 22(13), pp. 4090-4095, (2010)

159) *Photoelectron Generation by Photosystem II Core Complexes Tethered to Gold Surfaces*. Vittadello M., Gorbunov M. Y., Mastrogiovanni D. T., Wielunski L. S., Garfunkel E. L., Guerrero F., Kirilovsky D., Sugiura M., Rutherford A. W., Safari A. and Falkowski P. G. **Chemsuschem**, vol. 3(4), pp. 471-475, (2010)

160) *Dynamics of the interfacial film in bicontinuous microemulsions based on a partly ionic surfactant mixture: A neutron spin-echo study*. Wellert S., Altmann H. J., Richardt A., Lapp A., Falus P., Farago B. and Hellweg T. **European Physical Journal E**, vol. 33(3), pp. 243-250, (2010)

161) *Structural Determinants Underlying Photoprotection in the Photoactive Orange Carotenoid Protein of Cyanobacteria*. Wilson A., Kinney J. N., Zwart P. H., Punginelli C., D'Haene S., Perreau F., Klein M. G., Kirilovsky D. and Kerfeld C. A. **Journal of Biological Chemistry**, vol. 285(24), pp. 18364-18375, (2010)

162) *Magnetic resonance in the model high-temperature superconductor HgBa2CuO4+delta*. Yu G., Li Y., Motoyama E. M., Zhao X., Barisic N., Cho Y., Bourges P., Hradil K., Mole R. A. and Greven M. **Physical Review B**, vol. 81(6), pp., (2010)

163) *Two- and three-dimensional magnetic correlations in the spin-1/2 square-lattice system Zn2VO(PO4)(2)*. Yusuf S. M., Bera A. K., Kini N. S., Mirebeau I. and Petit S. **Physical Review B**, vol. 82(9), pp., (2010)

164) *Effect of crowding on the conformation of interwound DNA strands from neutron scattering measurements and Monte Carlo simulations*. Zhu X. Y., Ng S. Y., Gupta A. N., Feng Y. P., Ho B., Lapp A., Egelhaaf S. U., Forsyth V. T., Haertlein M., Moulin M., Schweins R. and van der Maarel J. R. C. **Physical Review E**, vol. 81(6), pp., (2010)

Instrumentation

Very Intense Polarized (VIP) neutron diffractometer at the LLB

A. Gukasov, S. Rodrigues, B. Gillon, J-L. Meuriot, T. Robillard, A. Laverdunt, G. Exil, F. Prunes, F. Coneggo and G. Koskas

Léon Brillouin Laboratory,CEA-CNRS, CE Saclay, 91191 Gif sur Yvette, France

Polarized neutron diffraction (PND) is an important technique to investigate interatomic or intermolecular magnetic interactions. PND takes full advantage of the neutron magnetic moment and gives a direct access to the spin density distribution in the unit cell. It allows obtaining valuable information about magnetic form factors, spin/orbital moment ratios, spin density distributions, wave functions of unpaired electrons and others. In a typical procedure of spin density measurements a pre-oriented single crystal is placed at low temperature under an applied vertical magnetic field of several Tesla. A monochromatic beam of polarized neutrons, with polarization direction parallel or antiparallel to the applied field (+ or -), impinges on the crystal, which has been set at Bragg position. A single detector (that is normally carried out by a lifting arm) goes to the expected position of the diffracted beam corresponding to a reflection of scattering vector q and the intensities I+ and I- corresponding to the two states of the incident polarization are measured. The ratio of the measured intensities R=(I+/I-), the so-called flipping ratio, is used to deduce the magnetic structure factor M_q, providing the nuclear structure factor N_q is known. Once a large number of magnetic structure factors M_q, is found, the reconstruction of the spin density in the unit cell is performed using Fourier synthesis, Maximum Entropy Methods (MEM), multipoles or wave function refinements.

The major limitation of the PND instruments is the data acquisition time. On the first generation PND instruments like D3, 5C1, D23 several days of beam time are needed for a density reconstruction, depending on the sample volume and the smallness of the magnetic moment. This is necessary to collect one by one hundreds of flipping ratios, in order to obtain a high resolution spin density map.

VIP - Very Intense Polarized neutron diffractometer is an upgrade of the former 5C1

diffractometer. It is the second instrument delivered in 2010 in the framework of the LLB **CAP2010-2015** instrumentation road maps. The aim of the project was to decrease the measurement time of spin densities by a factor of 5 to 20, depending on the crystal lattice parameters. This can be achieved by using large Position Sensitive Detector (PSD) which allows measuring the flipping ratios on several reflections simultaneously. The technique using a large PSD for integrated intensities measurements was already successfully implemented on the diffractometer D19 at the ILL for unpolarized neutrons. Here we report on the first implementation of PSD on a polarized neutron diffractometer VIP.
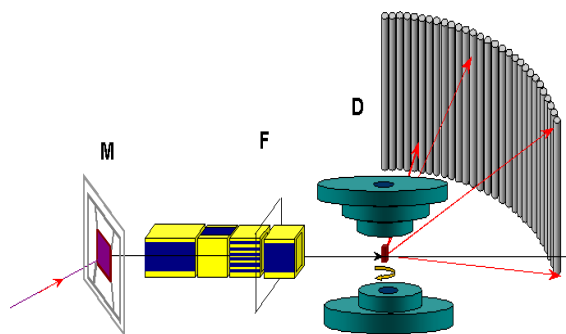
Fig. 1. Schematic layout of VIP
(M) is a polarizer, (F) is a flipper, (D) PSD

VIP is installed on the beam tube located on the hot source of the ORPHEE reactor in replacement of the 5C1 diffractometer (Fig.1). At present the Heussler polarizing monochomator of 5C1 of dimension 50x50 mm^2 is used to select the neutrons of wavelength λ= 0.84 Å. In 2012 it will be replaced by a new focusing Heussler monochromator of dimension 90x90 mm^2. Neutrons scattered by the crystal in the directions satisfying Bragg condition are collected by 64 position sensitive detectors (15 bar of ^{3}He) of 19 mm in diameter covering scattering angles of 25° in vertical and 80° in horizontal directions (0.6 sterad).

Instrumentation

Fig. 2 VIP diffractometer

Rotating of sample and collecting of 2D diffraction patterns allows us to record both integrated intensities and flipping ratios up to $\sin(\vartheta/\lambda) \sim 0.8$ Å^{-1} in the horizontal plane and $\sin(\vartheta/\lambda) \sim 0.2$ Å^{-1} in the vertical one. Then flipping ratios are re-measured with a longer exposition time for the frames having low statistical accuracy to reach the required one. Once the data collection is finished, the vertical axis of the crystal can be oriented into the horizontal plane and the missing reflection intensities along the originally vertical crystal axis can be measured. To reduce the scattering from the sample environment a radial collimator is installed in the detector shielding (Fig. 2). It consists of 64 foils coated with Gd oxide (Eurocollimators Ltd.) and covers full scattering range. The radial collimator reduces considerably the scattering from the sample environment in particular at high diffraction angles, which is of great importance for the performance of the diffractometer when using samples of small volume. Another important gain in efficiency of PND instruments with PSD is due to a simplification of the measurement procedure, since some of time consuming processes like crystal orientation, lattice parameters refinement can be done during collection procedure or even later.

Fig. 3 Radial collimator

A- Data acquisition is realized by means of a EuroPsd microprocessor module designed at the LLB. The module assures connection between the driving computer and the ILL PSD interface via the IEEE 488 bus. It is able to sustain very high acquisition rates (up to 5 Mhz) and to run different histogramming modes, like polarized neutrons, time-of-flight (TOF) and time resolved modes. The module is equipped by the on-board memory adapted for detector sizes up to 512x512 channels. This makes the acquisition being totally independent from the performance and capacities of the driving computer.

B-Data are collected with the new software "Pingouin". This solution is built around a .NET kernel in charge of visualization and control/command, an evolved XML scheme to manage configuration and a Python engine to execute user scripts. Automatically updated from repository server, the kernel is common on all the detectors of the laboratory. So, the full implementation of specifics functionalities of "VIP" detector requires less than 800 lines of Python code and concerns only the business algorithms (scan, measurement, etc.). Thus, "Pingouin" provides to engineers a full solution quick, easy and reliable to manage detectors. We chose an industrial standard XML (Extended Markup Language) to store the data collected from the PSD. This standard describes in an easy and intuitive way how the information is stored. It's another advantage is that it comes with readymade parsers and standard XML editors. The XML file created by the LLB acquisition software contains compressed data collected from the PSD and all current parameters of the diffractometer: date, time, angles, monitor counts, temperature etc.

The visualization program written in JAVA allows for the quasi-instantaneous visualization and access to any selected frame due to the XML standard, providing tabulation files. The same program assures reading of frame

content, binning/summation of frames and creation of dynamic mask of strongest pixels. Program for indexing, integration and flipping ratio calculations is written in Fortran 90.

For the crystals having small lattice parameters the gain from the use of the PSD can be small. In this case we consider a possibility to simultaneously use several single crystals of different orientation. Particularly, if crystals are mounted at different heights, the Friedel pairs can be used to define zero offsets in the horizontal plane and to separate reflections belonging to different crystals.
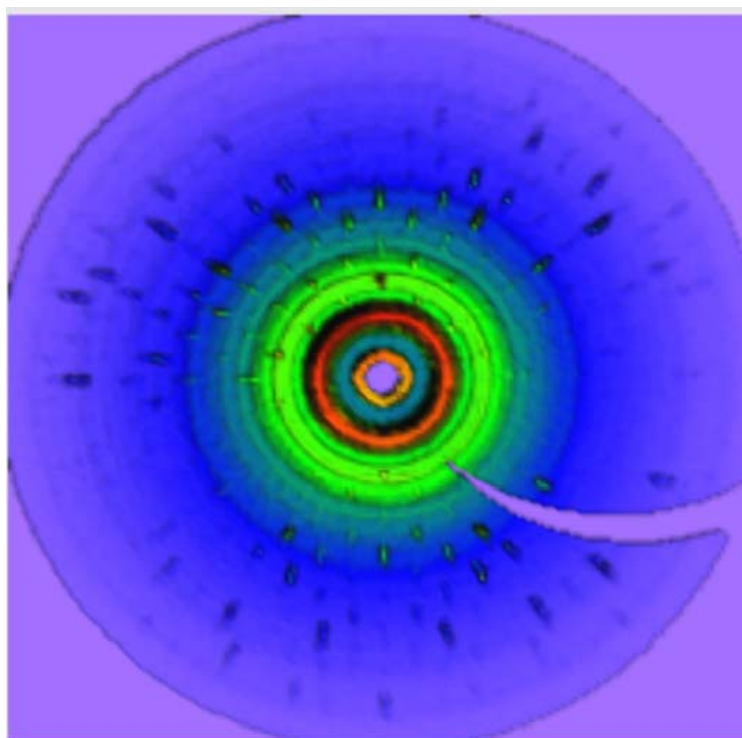

Fig. 4 Typical two dimensional cut in the reciprocal space measured on VIP.

Instrumentation

The new Very Small-Angle Neutron Scattering Instrument "Très Petits Angles" at Laboratoire Léon Brillouin.

S. Désert, V. Thévenot, A. Hélary, P. Permingeat, A. Gabriel, G. Exil, F. Coneggo, P. Lambert, A. Brûlet

Laboratoire Léon Brillouin UMR12 CEA-CNRS, CEA Saclay, 91191 Gif Sur Yvette Cedex, France.

Small-angle neutron scattering (SANS) has been successfully used since the 1970's in an increasing number of research area (physics, biology, material science, etc.) to investigate structures at typical length-scales ranging from 0.5 to 100nm. At LLB, SANS experiments performed on three spectrometers operating since the early 1980's represent over one third of total beam-time requests. Numerous experiments have been performed in soft matter (polymers, polyelectrolytes, micelles, copolymers, vesicles, gels, etc.), biological systems (membranes, proteins), materials science (chemical demixing, precipitates, porous materials, memory shape alloys, etc.) and magnetic materials (critical magnetic fluctuations near transitions, vortices in superconductors, nanomagnets, microphase separation in manganites, etc.).

In order to meet growing demands (arising also from the success of nanosciences) to study larger objects, up to 1000nm size, SANS instrument capabilities need to be developed towards smaller minimum momentum transfer Q. The objective is the Very Small-Angle Neutron Scattering (VSANS) Q range, 10^{-3} nm^{-1} < Q < 10^{-2} nm^{-1}.

VSANS

The success of the SANS technique relies on pinhole-collimated beams of sufficient beam current and low background to measure the scattered intensity profile over a large dynamic range of both intensity and scattering angles. The circular apertures also provide excellent bidirectional resolution that allows determination of the orientational-dependence of the anisotropic scattering produced by many aligned materials. This pinhole collimated instrumentation is however limited by insufficient beam current in the VSANS Q range. So, various advanced focusing methods from refractive lenses and ellipsoidal shaped mirrors to multiple confocal converging beams have been proposed in order to increase the scattering intensity. Some of them are currently being either developed in new VSANS instruments (KWS3 at FRMII) or implemented on existing SANS instruments (NIST, ILL, J-Parc, FRMII …). Two different kinds of VSANS instruments are known:

• Conventional extremely long pinhole instruments (80m for D11 at ILL), for which $Q_{min} \approx 5 \times 10^{-3}$ nm^{-1} and $\Delta Q \approx 4 \times 10^{-3}$ nm^{-1}.

• Focusing instruments like KSW3 in FRMII using toroidal and elliptical mirrors, $\Delta Q \approx 10^{-3}$ nm^{-1} and $Q_{min} \approx 10^{-3}$nm^{-1}. The Q resolution is really improved on this instrument, but the sample size required to benefit from the focusing is very large, 80×20 mm^2.

An alternative to these systems is the multi-aperture converging pinhole collimator. This system relies upon the use of multiple sets of pinholes having the same focal point on the detector but which prevent cross-talk between the different imaginary channels. Such a method is appealing because it allows a direct improvement in the Q resolution without too much loss in the flux on the sample and one obtains 2D data that do not need to be desmeared. It is also almost independent on the wavelength: so, it allows varying continuously the Q range by simply changing the wavelength. Disadvantage is the difficulty in machining and aligning the various apertures and the Fraunhofer diffraction from these small apertures. Collimation can be also tightened through multiple converging slits. Advantage is the gain in intensity; disadvantage is still the Fraunhofer diffraction from the small sample aperture but also slit smearing considerations.

The new instrument "Très Petits Angles" (TPA) built at LLB is a multi-beam type VSANS machine[1]. Our objective was to reduce

by about one order of magnitude both the minimum accessible momentum transfer Q down to $2 \cdot 10^{-3}$ nm^{-1}, and its related resolution ΔQ. Multiple pinhole and multiple slit collimations have been designed for the instrument.

Instrument description

The original design of TPA first includes a high definition Image Plate detector of Marresearch GmbH; the pixels size is $0.15*0.15$mm^2. Image plate suffers from an overwhelming gamma background; cautions taken against γ radiation emission are heavy concrete around the detector tank, ^{6}Li instead of ^{10}B and Cd at any other strategic places of the instrument. For the same reason, a double m = 3 super-mirrors monochromator[1] allows to select the wavelength between 0.5 and 1.5 nm (15% FWHM), while decreasing the γ radiation emission compared to a classical mechanical velocity selector. A 3.5 m long trumpet guide (m=2) provided by SwissNeutronics has been installed upstream the instrument in order to reduce the incident divergence of the incoming neutron beam. The most innovative element of the instrument is its multi-beam collimator[2] consisting of a set of 13 masks made out of isotopic Lithium (^{6}Li neutrons absorber) mixed in epoxy resin. Actually, each mask offers two types of collimation: the first collimation includes approximately 600 circular holes with a hexagonal order from 1.28 mm (1st mask) to 0.9 mm (13th mask) in diameter and the second collimation is 15 vertical slits of 1.28 mm to 0.9 mm width (see Fig. 1). The role of this set of masks is to select among all the possible neutron beams going through the various holes only those converging on to the detector located about 6m far from the sample. The various masks are not distributed uniformly along the 2.85m trajectory of the incoming neutron beam. The double SM monochromator is located in between the 1st and the 2nd mask. Most of masks are in the middle of the collimator (Fig. 1b) in order to optimize the cross-talks elimination with a minimum number of masks. Their positions inside the collimator path and the optimum masks number to eliminate cross-talks have been checked by McStas simulations. Changes of symmetry of transmitted beams by varying the horizontal and vertical positions of masks allow us to align accurately each mask. The positioning accuracy of masks is about 100μm as observed on both McStas simulations

and experiments (Fig. 2). Vertical masks adjustments as function of the wavelength allow the correction of gravity effects inside the collimator, while preventing neutrons loss and cross-talks.
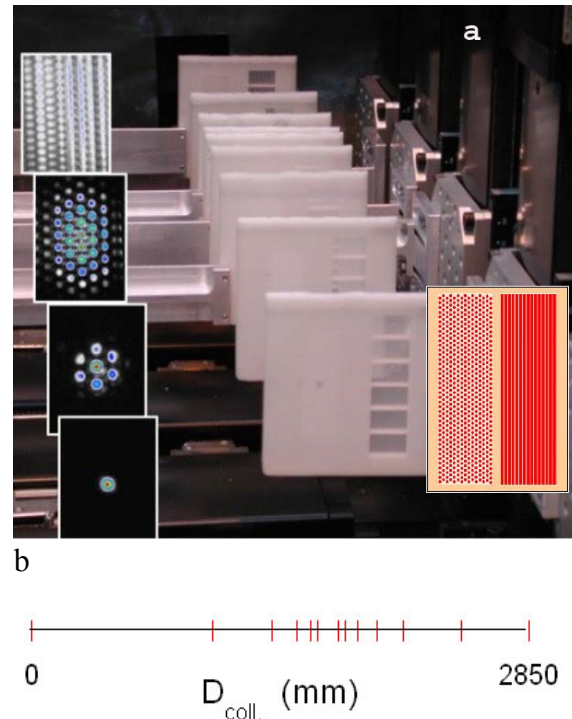
Fig. 1. a) Picture of 9 of the 13 masks inside the collimator. The drawing on the right-hand sideshows the pinholes and slits arrangements. The 4 pictures on the left-hand side show the neutrons beams received on the detector for an increasing number of masks well positioned: the top picture shows the crosstalk when only 2 masks are placed; the picture at the bottom corresponds to the transmitted beam when the 13 masks are set. In-between pictures correspond to intermediate number of masks in.b) Positions of the 13 masks along the horizontal axis of the collimator.

The beam area at the sample position is about 26 mm height and 10 mm width. The overall size of the instrument remains small, 10 m, which in addition to the set of masks inside the collimator has another advantage of reducing the enhancement of the Q resolution in the vertical direction due to the broad wavelength distribution of the incident beam[2]. The beam-stop made of ^{6}Li/epoxy resin has 6mm diameter. The detector tube is filled with helium gas and kept under constant flow to compensate for leaks. Transmission measurements are achieved either by using a

64

single detector placed just before the detector or with the Image Plate.

With this multiple pinhole collimation, we now reach a minimum Q value of $3 \cdot 10^{-3}$ nm^{-1} at 1.2nm wavelength ($\Delta Q = 1.1 \cdot 10^{-3}$ nm^{-1}), close to our initial objective of $2 \cdot 10^{-3}$ nm^{-1} at 1.5nm.
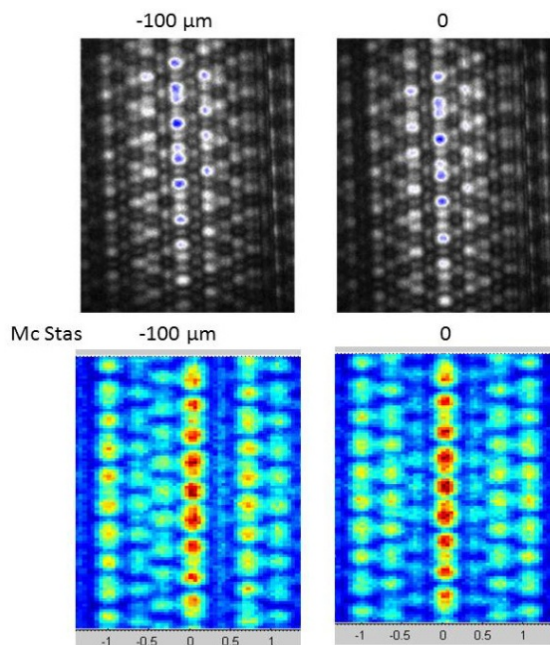

Fig. 2. Images of transmitted beams observed on the detector showing the positioning accuracy of masks. Top images are experiments, bottom are McStas simulations. 0 corresponds to the right mask position: the transmitted beams are symmetric, -100 µm is the shift from the right mask position in the horizontal direction: left-right asymmetry is observed.

First experiments on TPA

Diblock amphiphilic copolymer vesicles. Self-assembled nano-structures of amphiphilic block copolymers in solution (e.g. spherical micelles, vesicles, rod-like micelles, etc.) have great potential in applications, such as surfactants for the stabilization of dispersions, vehicles for encapsulation and controlled release of drugs or as supports for catalysis, etc. Two main methods allow the self-assembly of amphiphilic block copolymers: dissolution (either by direct dissolution of a copolymer or by film rehydration) and the co-solvents way declined in various processes such as dialysis, nano-precipitation and emulsion (used in microfluidic, a very attractive technique for direct drug and\or proteins encapsulation purposes). The morphology and size of self-assembled objects at thermodynamic equilibrium are mainly dictated by the hydrophilic fraction and the molecular interactions, but an inadequate method of preparation will lead either to a low rate of self-assembly or to kinetically freeze objects out of equilibrium.

Fig. 3 shows the scattering curves obtained on two solutions of poly(butadiene)-*g*-poly(ethylene-oxide) (PB-*g*-PEO) block copolymer vesicles, prepared either by direct dissolution (DD) method or by double emulsion (DE) process (microfluidic). SANS curve obtained on PAXY (a classical SANS spectrometer at LLB) allows to precisely determine the membrane thickness 9.5 nm in both cases corresponding to a bilayer of PB-*g*-PEO, while the Q range accessible on TPA shows that vesicles prepared by microfluidic are large aggregates of vesicles with a fractal aggregation dimension $d_f = 2.81$, while those prepared by direct dissolution are single vesicles of more than 500nm radius.
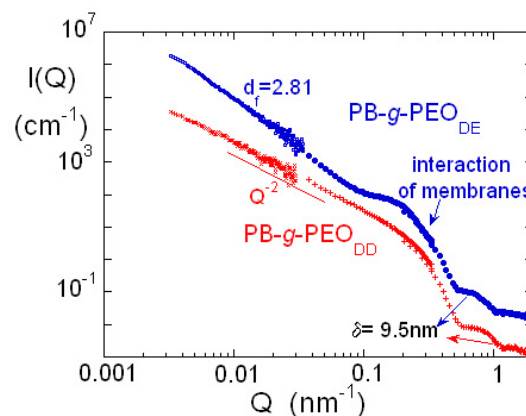
Fig. 3. Scattering curves of solutions of PB-g-PEO block copolymer vesicles measured on PAXY, $Q_{min} = .035$nm^{-1} and on TPA $Q_{min} = .003$nm^{-1}.

Pickering emulsions with clays. Stabilization of emulsion drops by inorganic particles, Pickering emulsions, has been of the object of increasing interest during the last years. An important feature of such emulsions is their incredible stability due to the irreversible adsorption of colloids at the interface. Another interesting aspect is the possibility of functionalising the emulsion droplets through exploitation of the interfacial colloids to create smart materials. The interior of the emulsion droplets could also be exploited, but in the case of simple emulsions this is rather restrictive. The use of lyotropic liquid crystalline (LC) structure as the dispersed phase can improve the potential applications, because of their low viscosity, their high interfacial area, and the presence of both hydrophilic and hydrophobic

regions. Although dispersions of LC phases have been studied over the last ten years, the focus has remained on the structures of both the internal phase and the various organic stabilisers.

Emulsified microemulsion phase of phytantriol (PT) and dodecane (DC) (5% wt.) in water has been stabilised by Laponite clays at low concentrations corresponding to the fluid phases of the Laponite phase diagram (to avoid complications arising from aggregated structures). The VSANS Q range of TPA is peculiarly well suited to the characteristic sizes around 100-300nm of these emulsions, as can be seen on the typical curves shown in Fig. 4. By varying the mixture D_2O/H_2O, we can differentiate the structure of the whole emulsion from the one of Laponite shell.
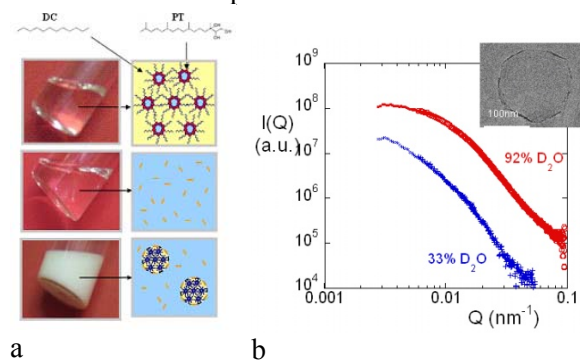

a   b

Fig. 4. a) Phytantriol (PT) and dodecane (DC) mixture (50:50 i.e. in the inverse micro emulsion phase L_2) in water (top scheme) stabilized by Laponite clays (disc-like particles with a mean radius of 12.5 nm and a thickness of 1 nm) to form Pickering emulsions (bottom scheme). b) VSANS curves of 5% emulsions - 4% wt. Laponite in 92% D_2O (matching the laponite) and 33% D_2O obtained at 0.6nm (large symbols) and 1.2nm (small symbols). Measuring times were 2 and 4 hours respectively. The inset is a cryo-TEM image of the stabilized emulsion.

Geological rocks. Sequestration of CO_2 in deep geological reservoirs represents one of the potential methods for reducing anthropogenic emissions to the atmosphere. In the long run, CO_2 dissolves into the local formation of water and participates to a variety of geochemical reactions. Some of these reactions could be beneficial, helping to chemically contain or trap CO_2 as dissolved species and by the formation of new carbonate minerals. Others may be deleterious, and actually aid the migration of CO_2. The overall impact of these competing processes produces changes in mineralogy, porosity, texture and permeability of the rocks.

SANS and VSANS techniques can provide an experimental access to the porous structure of rocks, which is a parameter so important to trap CO_2.

The rocks samples investigated on TPA cover a wide spectrum of lithologies ranging from carbonates ($CaCO_3$, $CaMg(CO_3)_2$), anhydrites (geological formations containing $CaSO_4$) to sandstones (sedimentary rocks composed mainly of sand-sized minerals as quartz and/or feldspar or rock grains) and intrusive ultramafic to intermediate volcanic rocks. Several curves are shown in Fig. 5. Comparison of their micro porosity and their structure deduced from these VSANS curves will help to fully characterize the involved rocks and to evaluate the influence of CO_2 on that structure.
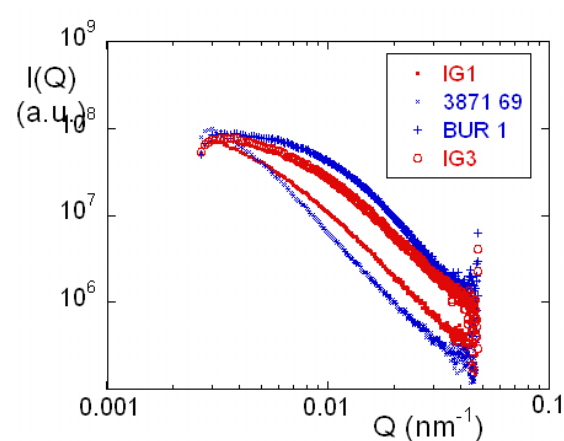
Fig. 5. VSANS curves of different geological rocks. The wavelength was 1.2nm; $Q_{min}<310^{-2}nm^{-1}$. The measuring times were about 2 hrs.

Conclusions

The multi-beam pinhole collimation of TPA allows to reach a minimum Q value of $3 \cdot 10^{-3}$ nm^{-1} at 1.2nm wavelength with a good resolution, $\Delta Q=1.1 \cdot 10^{-3}$ nm^{-1}.

Further developments are going on: single pinhole collimation will be available in September 2011 in order to facilitate the superimposition of VSANS and SANS curves in the range $10^{-2} - 4 \cdot 10^{-2} nm^{-1}$. Commissioning tests of multiple converging slits collimation will be performed at the end of 2011.

Thus, the performances of the TPA instrument enlarge the Q range capabilities of SANS at LLB.

Instrumentation

References

[1] S. Désert, V. Thévenot, A. Gabriel, P. Permingeat, J. Oberdisse, A. Brûlet, J. Appl. Cryst. **40**, 945-949 (2007).
[2] A. Brûlet, V. Thévenot, D. Lairez, S. Lecommandoux, W. Agut, S. Armes, J. Du, S. Désert, J. Appl. Cryst. **41**, 161–166 (2008).

The Orphée Reactor

A- General presentation and historical background
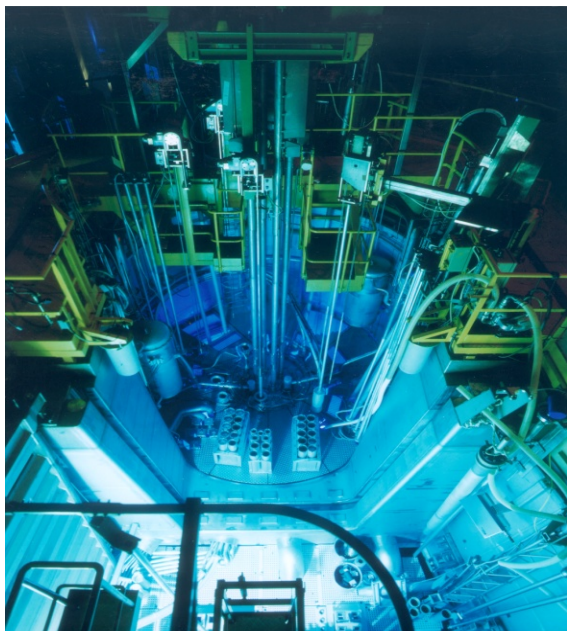
The Basic Nuclear Installation n°101 located at CEA Saclay Centre, comprises the experimental 14 MW thermal power ORPHEE reactor and the buildings used the Léon Brillouin Laboratory (LLB).

After the creation of LLB in 1974, the ORPHEE reactor was built between 1976 and 1980 as a, national-based, sister facility of the High Flux Reactor (RHF) of the Laue Langevin Institute (ILL) in Grenoble. The decision to build the reactor stemmed from the continuous expansion of European and international neutronic research in the 70s. The ORPHEE design directly benefited from the safety, construction and operation feedback of previous generation reactors like RHF and was contemporary to the development of the PWR equipment program in France. The reactor first went critical on December 19th 1980. The designers' projections purposely resulted into a moderate investment cost - moderate operation cost facility, ensuring both reliable operation, good safety record and high performances.

Though the first five years of operation were perturbed by technical problems of youth rapidly solved, the compact design of the reactor enables the construction of very high performances spectrometers. User access on an open basis was already set up in 1983 with the organisation of the first "Tables Rondes". The construction of the LLB building (563) in 1986 and the first participation to the European programs in early 1993 finalized the way of operation of the LLB-Orphée entity.

During the long shutdown of the RHF-ILL in 1990-1993, Orphée operates up to 250 days a year. Up to now, since its first divergence, the reactor has been operated circa 5500 days.

B- Reactor technical characteristics

ORPHEE is a « pool » type reactor. The 14-MWth compact, light-water moderated, core provides up to 3.10^{14} n/cm^2/s thermal flux in the surrounding heavy water reflector tank. Core life cycle duration is 100 days. The core and the heavy water tank are immerged in a pool filled with demineralised light water. This ensures radiological shielding and facilitates handling from above the pool. The reactor hosts 9 horizontal channels (feeding 20 neutron beams) and 9 vertical channels (comprising 4 pneumatic channels for activation analysis and 5 irradiation pits for radio-isotope and other industrial productions). The heavy water tank is equipped with three local moderators: two cold sources (liquid hydrogen at 20K) and one hot source (graphite at 1400 K) which provide neutrons of respectively lower and higher energy

ORPHEE neutrons are currently supplied to 27 experimental areas. The experimental areas are located around the reactor, either in the reactor building (11 of them) or along the neutron guides of the guides hall (16 of them). One experimental area with specific radiological shielding has been designed for industrial neutronography (mostly used by the aeronautical or space industry).

The ORPHEE reactor is operated by the Nuclear Energy Division of CEA (CEA/DEN) and is run by a 60 people team, about half of which work on a shift basis. This facility benefits from the support of the radiological protection teams and security teams of CEA Saclay Centre

Instrumentation

C- Reactor safety

The safety design of the reactor enables to ensure permanent control of the three main safety functions: reactivity control, residual heat removal and containment of radioactive material. The design includes the following elements:

- Permanent reactor monitoring by a safety system using 3 completely independent channels. If necessary, 2 channels out of 3 will automatically trigger the reactor emergency shutdown.
- Once the reactor has been stopped, the residual power is removable by purely passive natural convection between the core and the reactor pool.
- The core and the core cooling circuit are located in the reactor building made of reinforced concrete.

Three barriers are placed between dangerous products and the environment. These barriers are: the reactor fuel cladding, the reactor main cooling circuit plus the reactor pool, and the reactor building. The reactor building has also been designed to sustain any accident which could occur to the reactor.

The supervision of the impact of the installation onto the environment is included in the Saclay Centre environmental monitoring program.

D- 2010 safety reassessment

The reactor safety case was reassessed twice since 1980. 2008 and 2009 had seen the preparation of the second safety reassessment. To this aim, a major non-destructive inspection programme was carried out. In parallel, substantial safety study work was carried out with notable support of, the CEA specialists from the Nuclear Energy Division technical departments of the Saclay Centre. The resulting work underwent CEA internal review and control beginning of the year 2009. Results of these actions confirmed the very satisfactory technical and safety condition of the reactor after 29 years of operation. The reassessment file was submitted to the French regulatory body on March 31st 2009. Some additional clarifications were than given to the IRSN (Institut de Radioprotection et de Sûreté Nucléaire) that did submit a technical report by July 2010 to the "Groupe Permanent" (GP), the group in charge of the final evaluation. After two final meetings with the CEA in September, the GP issued its final report to the French safety authorities on October 23rd. Though some improvement of safety were asked, the report points out that the initial reactor safety features remain in good adequation with up-to-date safety practices.

E- Future operations

This good report on the safety of the reactor opens up a future of at least ten years of operations. The main works to be performed are the replacement of the various thimbles of the beams that becomes fragile after 30 years of irradiation. This work has already been started in 2008 by the replacement of the 4F thimble that took place as scheduled. It will be continued during the next years doing roughly one thimble each year. When all completed, this type of replacements should not occur again before 2035. On the same line, cold sources have also to be replaced each 15 years. This will be done during the summer 2011.

All these maintenance operations will enable us to keep the Orphée reactor in a very well state. With that point and with the amount of fuel that we already have, we are prepared to reach the next safety reassessment in 2020 in good conditions.

Figures & Facts

Ph. D students of LLB

Ph. D THESES STARTED IN 2010

	LEROY Marie-Alix. *"Tunnel coupling between nanometric antiferromagnetic films."* *Supervision : S. Andrieu (U. Nancy) /A. Bataille (LLB)* Materials and Nanosciences: Fundamental Studies and Applications
FANG Weiqing *"Elaboration of composites based on magnetic threads for the fabrication of permanent magnets."* *Supervision : F. Boué (LLB)* Soft Matter and Biophysics	
	GUENNOUNI Zineb *"Nanostructures of polymers metallized by radiolysis and/or photoreduction"* *Supervision : M. Goldman (U. Paris VI)/F. Cousin (LLB)* Materials and Nanosciences: Fundamental Studies and Applications
BOUTY Adrien *"Study of elastomer-nanoparticules composites"* *Supervision : F. Boué (LLB)* Soft Matter and Biophysics	

Figures & Facts

CURRENT PHD STUDENTS

BHOWMIK Debsindhu – started in 2008
« Dynamic at the microscopic scale in complex fluids under confinement »
Supervision : P. Turq (PECSA, Paris) / N. Malikova (LLB)
Soft Matter and Biophysics

BOURGEOIS Julie – started in 2008
« RFe_2O_4 –type ferrites with mixed valence »
Supervision : C. Martin (CRISMAT, Caen) / F. Damay (LLB)
Strongly Correlated Quantum Materials and Magnetism

FAMEAU Anne-Laure –started in 2008
"From volume to interface: impact from volume structures on the foaming and emulsifying properties
of hydroxylised fatty acids assemblies: toward new detergents"
Supervision: F. Boué (LLB)
Soft Matter and Biophysics

ROBBES Anne-Sophie – started in 2008
« Magnetic nanocomposites: control of the dispersion by grafting and orientation of charges under
external field »
Supervision : F. Boué (LLB)
Materials and Nanosciences: Fundamental Studies and Applications

SAÏD-MOHAMED Cynthia – started in 2008
« Reversible modulation of distances between nanoparticles by a thermosensitive polymer at the
water-air interface and in the thin film »
Supervision : L.-T. Lee (LLB)
Materials and Nanosciences: Fundamental Studies and Applications

DUBOIS Matthieu – started in 2009
« Multiscale analysis of the microstructural and mechanical state in a copper-based memory shape
alloy by neutron diffraction"
Supervision: M.H. Mathon (LLB)
Materials and Nanosciences: Fundamental Studies and Applications

HATNEAN Monica – started in 2009
« Magnetic and structural study of magnetoelectric $GaFeO_3$ compounds »
Supervision : L. Pinsard (ICCMO, Orsay) / S. Petit (LLB)
Strongly Correlated Quantum Materials and Magnetism

SHI Li – started in 2009
« Study by neutron, X-Ray and light scattering of the complexation in mix of macromolecular and
supramolecular polyelectrolytes: flexibility, association and dynamics."
Supervision: E. Buhler (U. Paris 7)/F. Boué (LLB)
Soft Matter and Biophysics

ZHONG Shengyi – started in 2009
« Study of deformation heterogeneities in ODS steels in correlation with the distribution of nano-
reinforcements. »
Supervision : M.-H. Mathon (LLB)
Materials and Nanosciences: Fundamental Studies and Applications

THESIS DEFENDED IN 2010

LE CŒUR Clémence – 8 March 2010
« Influence of cytoplasmic crowding on the stability and diffusion of proteins »
Supervision : J. Teixeira (LLB)
Soft Matter and Biophysics

TASSERIT Christophe – 15 March 2010
« Transport of ions and objects in nanopores »
Supervision : D. Lairez (LLB)
Soft Matter and Biophysics

FABREGES Xavier – 5 October 2010
« Study of magnetic properties and of spin-lattice coupling in hexagonal $RMnO_3$ multiferroic compounds »
Supervision: I. Mirebeau (LLB)
Strongly Correlated Quantum Materials and Magnetism

CHAHINE Gilbert – 15 November 2010
« Remarkable properties and ultraslow dynamics of nanoconfined liquid crystals."
Supervision: R. Lefort (Inst. Phys. Rennes) / J.M. Zanotti (LLB)
Materials and Nanosciences: Fundamental Studies and Applications

GAL François – 29 November 2010
« Macromolecular engineering applied to the study of nano-objects based on inorganic nanoparticles grafted with polymers. »
Supervision: C. Reynaud (CEA/IRAMIS/SPAM) / G. Carrot (LLB)
Soft Matter and Biophysics

BALEDENT Victor – 2 December 2010
« Hidden order parameter in the pseudo-gap phase of High Critical Temperature Supraconductors. »
Supervision : Ph. Bourges (LLB)
Strongly Correlated Quantum Materials and Magnetism

DE ALMEIDA-DIDRY Sonia – 14 December 2010
« Synthesis of the under-doped phase in the High Critical Temperature supraconducting system $Bi_2Sr_2CaCu_2O_{8+\delta}$ and study by neutron scattering »
Supervision: I. Laffez & F. Giovannelli (LEMA, Blois) / Y. Sidis (LLB)
Strongly Correlated Quantum Materials and Magnetism

The 2010 SFN thesis prize was awarded to **Chloé CHEVIGNY** for her thesis defended in October 2010 at the Université Paris-Sud. This thesis, co-directed by F. Boué and J. Jestin (LLB) was untitled *"Polymers-grafted particules nanocomposites: from synthesis in colloidal solution to the study of macroscopic properties"*

POST-DOCTORAL FELLOWSHIPS

ZIGHEM Fatih – 2008 -2010
« Elaboration of High Temperature permanent magnets based from nano threads organised from a bottom-up approach »
G. Chaboussant   Materials and Nanosciences: Fundamental Studies and Applications

KOUTSIOUMPAS Alexandros – 2009 – 2010.
« Protein folding and translocation though artificial nanopores »
D. Lairez   Soft Matter and Biophysics

MULLER François – 2009 -2011
« Hybrid systems made from cellulosis needles in the presence of biopolymers in water or synthetic polymers obtained by photopolymerisation of metacrylate.”
F. Boué   Soft Matter and Biophysics

THIBIERGE-CRAUSTE Caroline – 2009-2011
« Structure and dynamics of glassifiable liquids and glasses. Organisation in monoalcohols clusters and ultrastable glasses”
C. Alba-Simionesco   Materials and Nanosciences: Fundamental Studies and Applications

CIUAMAKOV Iuri – 2010
« Electron density in a molecular-based magnet: Joint analysis of X-Ray and neutron diffraction data and X-Ray magnetic Compton scattering.”
B. Gillon   Materials and Nanosciences: Fundamental Studies and Applications

LERBRET Adrien – 2010-2011
« Neutron diffraction study of the influence of co-solvents on the stability of biomolecules »
Marie-Claire Bellissent-Funel   Soft Matter and Biophysics

SAZONOV Andrey – 2010-2012
« Application of polarised neutron diffraction for the study of frustrated compounds »
A. Goukassov   Strongly Correlated Quantum Materials and Magnetism

SPONSORING OF WORKSHOPS, CONFERENCES, AND SUMMER SCHOOLS

FLIPPER 2010   *ILL, B. Gillon (LLB)*
Int. Workshop on Single-Crystal Diffraction with Polarised Neutrons
January 26-30th 2010 http://www.ill.eu/news-events/workshops-events/flipper-2010/

FP7-NMI3 project « Polarised neutrons»   *LLB, A. Goukassov*
Febuary 2010, Paris

CONFIT 2010   *ILL, C. Alba Simionesco (LLB)*
4th International Workshop on Dynamics in Confinement
March 2010, Grenoble http://www.ill.eu/news-events/events/confit2010/

SUPRA 2010   *Ph Bourges (LLB)*
Thematic meeting on non-conventionnal superconductivity
April 2010, Gif sur Yvette http://ghmfl.grenoble.cnrs.fr/spip.php?article372

Neutrons et Simulations   N. Malikova (LLB)
June 2010, Rémuzat http://www.sfn.asso.fr/JDN/JDN18/index.html

The power of neutron scattering techniques in nano and bio sciences
J. Jestin et J. Teixeira (LLB)

July 2010, Jaca, Spain http://spins.unizar.es/eventos/JACA2010/index.php

SENSE 2010
**"Superconductivity Explored by Neutron Scattering Experiments"**
October 2010, Grenoble

SEMINARS AT LLB

05/01/2010	Structure magnétique et dynamique de spins dans la delafossite multiferroïque CuCrO$_2$	F. Damay	LLB
12/01/2010	Tuning magnetic quantum phase transitions	H. V. Löhneysen	Karlsruher Institut für Technologie (KIT)
26/01/2010	Observation d'une nouvelle anomalie de phonons dans le chrome par diffusion inélastique de rayons X	D. Lamago	Karlsruher Institut für Technologie (KIT) et LLB
09/02/2010	Susceptibilité locale et aimantation du site atomique : d'une idée à la pratique. Part. 1	A. Goukassov	LLB
16/02/2010	Susceptibilité locale et aimantation du site atomique : d'une idée à la pratique. Part. 2	I. Mirebeau	LLB
10/03/2010	The coupling of protein dynamics to function, the case of myoglobin	W. Doster	Technische Universität München, Physik department
12/03/2010	Structure and dynamics of poly ethylene glycol coated Au nanoparticles	M. Maccarini	ILL, Grenoble, France
30/03/2010	Rôle des fluctuations de spin et des « Cu-O bond stretching phononspour l'appariement supraconducteur et les anomalies électroniques dans les cuprates à haute température critique.	F. Onufrieva	LLB
13/04/2010	Magnetic excitations in superconducting iron arsenides and cuprates: Analogies and differences	V. Hinkov	MPI-FKF Stuttgart
16/04/2010	On how does the presence of hydrophobic groups influence the ion-specific effects in polyelectrolyte solutions	Vojko Vlachy	University of Ljubljana, Ljubljana, Slovenia
18/05/2010	Couplage par effet tunnel entre films antiferromagnétiques.	A. Bataille	LLB
28/05/2010	Phase behavior and surface excitations of polymer-nanoparticle mixtures in bulk and thin films	J. T. Cabral	Imperial College de Londre, UK
01/06/2010	Advances and future perspectives in magnetic x-ray scattering at the ESRF	L. Paolasini	ESRF, Grenoble, France
03/06/2010	Beyond slip : using neutron diffraction and polycrystalline plasticity models to understand plastic deformation in anisotropic materials.	D. W. Brown	Los Alamos
18/06/2010	Ultrafast dynamics following photoionization in water: Electrons and cationic holes	P. Jungwirth	Institute of Organic Chemistry and Biochemistry, Prague
22/06/2010	Anomalous Hall Effect in metallic ferromagnets.	M. Taillefumier	Department of Physics, UIO, Oslo, Norway
23/11/2010	Des mesures neutroniques fournissent, pour les excitations d'un liquide de Fermi à 2D, un résultat inattendu	H. Godfrin	Institut Néel, CNRS et U. J. F., Grenoble
03/12/2010	To click or not to click ?	E. Drockenmuller	Université Lyon I

TRAINING AND EDUCATION

HERCULES Courses (15 -19th Mar. 2010)
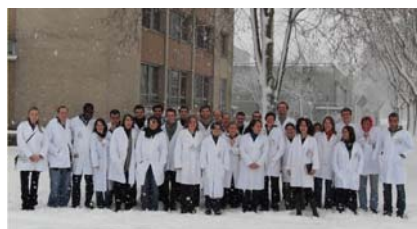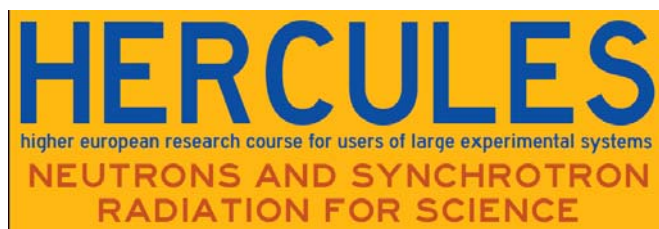
Hercules, the European graduate school for the large scale facilities users, gathers annually about 75 participants over several weeks for lectures tutorials, and practical sessions on the applications of X-Rays and neutron scattering. The last ten days of this 4-weeks formation takes place in the Paris area, at the SOLEIL synchrotron or at the LLB for those participants interested in a reinforced experimental neutron programme. In 2010, 20 students choose to come at LLB where they had the opportunity to exercise on real spectrometers after a general presentation of the installation and a visit of the reactor hall.

http://hercules.grenoble.cnrs.fr

FANs du LLB 2010 (06-09th dec 2010)

From December 6th to 9th, *the LLB* has welcome **35** participants (thesis/post-doctoral students, assistant professors or researcher) to its annual "**F**ormation **A** la **N**eutronique (Formation to Neutron scattering). Like the preceding years, the formation proposed a small introduction to neutron production, and application of neutron scattering in soft and condensed matter. Then, two days were dedicated to discover "in real" in small groups of ~3-5 people two different types of spectrometers among those open at LLB.

http://www-llb.cea.fr/fan

JOURNEES DE LA NEUTRONIQUE (04-10th June 2010)

Every year, the French Neutron Society (SFN), with the help of LLB and ILL centers and Grenoble UJF University, organizes the "Journées de la Neutronique", that gathers the national neutrons community around the "Rossat-Mignot" days and a thematic school. In 2010, the JDN took place at Rémuzat in the Provence region, from the 4th to 10th of June. As usual, the local organizing committee tried to offer a wide scientific program showing the latest developments and topics in the various fields of neutron scattering. The Rossat-Mignot meeting gives an overview of the different research interests from Chemistry up to Physics, Material Sciences, Nanotechnology or Biology. The thematic school, proposed par N. Malikova (LLB) and M. Johnson (ILL), was focused on the combination of neutron scattering and atomic scale simulations for the study of structural and dynamic properties in glasses, porous media, magnetic materials or biological molecules. Practicals on the simulation of electronic properties in condensed matter, but also on optimization of neutrons scattering instruments were proposed to the participants. Presentations from this school were published by the French Physical Society in a special book. At the end of the meeting, the annual SFN prize was awarded to Chloë Chevigny, for her doctoral thesis realized at LLB under the supervision of J. Jestin and F. Boué.
http://www.sfn.asso.fr/

PRACTICALS FOR UNDERGRADUATE STUDENTS

Ecole Centrale Paris (9-10 Dec. 2010)
For two days, the LLB welcome dozen of students in 3rd year at the Ecole Centrale de Paris for practical work on neutron scattering organized by A. Bataille (LLB) and J-M. Gillet (ECP). The themes proposed were Single Crystal and Powder diffraction" (6T2 and G41), and SANS (PACE).
(contact J-M. Gillet : jean-michel.gillet@ecp.fr)

Paris XIII University (10 Dec. 2010)
During the same period as Ecole Centrale Paris, the LLB hosted students from Master M2 "Biomaterials" of Paris XIII University for an initiation to SANS and powder diffraction.
(contact G. Fadda : giulia.fadda@univ-paris13.fr)

Bordeaux-I University – European Master FAME (8 Nov. 2010)
Like in 2009, students of Masters M2 "Physics and Chemistry" and "Material Sciences" from Bordeaux-I University, and from European Master FAME came at LLB for practical works. During their stay, they were initiated to Powder diffraction, Quasi-elastic Neutron Scattering and Inelastic Neutron scattering on G4.2, Mibemol and G4.3 spectrometers. These practical trainings were supervised by doctoral fellows of LLB, and came in complement to lessons on neutrons scattering provided during their Universitary formation.
(contact A. Desmedt : *a.desmedt@ism.u-bordeaux1.fr*)

Marseille-I University (29-30 Mar. 2010)
Two days of practicals for the students of Masters M2 "Advances Materials for Nanosciences and Nanotechnology"were organized at the end of march by V. Coulet (Cezanne University, Marseille). The initiation to neutron scattering was focused on powder diffraction and inélastique neutron scattering.

Beamtime Access

GENERAL LAYOUT OF THE SPECTROMETERS
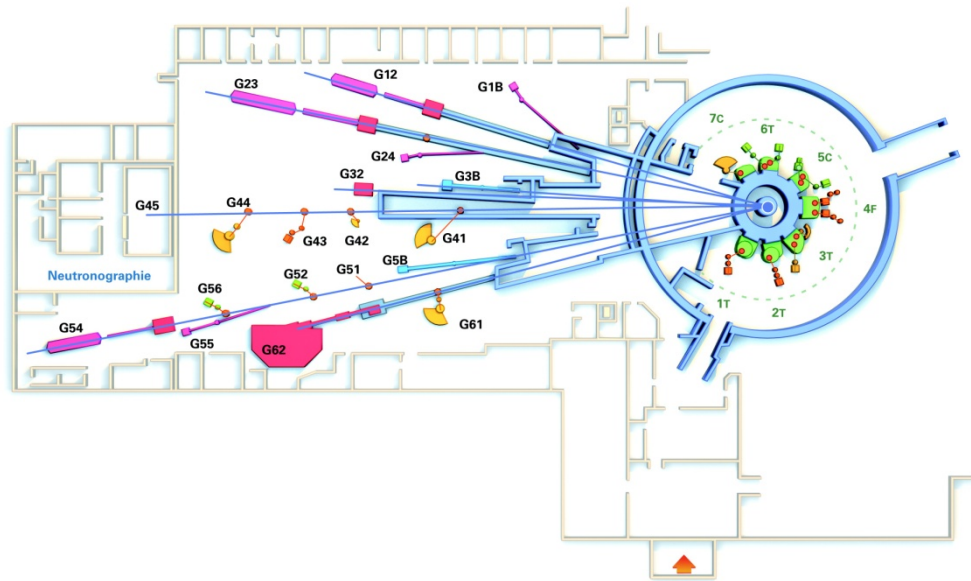
	SPECTROMETERS OPEN TO USERS	CONTACTS
	Powder diffractometers	
3T2	Florence Porcher	florence.porcher@cea.fr
G4.1	Gilles André	gilles.andre@cea.fr
G6.1	Isabelle Mirebeau	isabelle.mirebeau@cea.fr
	Single crystal diffractometers	
5C1	Béatrice Gillon	beatrice.gillon@cea.fr
5C1	Alain Cousson	alain-f.cousson@cea.fr
6T2	Arsen Goukassov	arsen.goukassov@cea.fr
	Diffuse scattering instrument	
7C2	Brigitte Beuneu	brigitte.beuneu@cea.fr
	Small-angle scattering instruments	
G1.2	Didier Lairez	didier.lairez@cea.fr
G2.3	Alain Lapp	alain.lapp@cea.fr
G5.4	José Teixeira	jose.teixeira@cea.fr
G5bis	Sylvain Désert	sylvain.desert@cea.fr
	Diffractometers for material science studies	
6T1	Marie-Hélène Mathon	marie-helene.mathon@cea.fr
G5.2	Vincent Klosek	vincent.klosek@cea.fr
	Reflectometers	
G3bis	Fabrice Cousin	fabrice.cousin@cea.fr
G2.4	Frédéric Ott	frederic.ott@cea.fr
	Triple-axis instruments	
1T	Daniel Lamago / Yvan Sidis (CRG Instrument Karlsruhe/LLB)	daniel.lamago@cea.fr / yvan.sidis@cea.fr
2T	Philippe Bourges	philippe.bourges@cea.fr
4F1	Sylvain Petit	sylvain.petit@cea.fr
4F2	Daniel Petitgrand	daniel.petitgrand@cea.cr
	Quasi-elastic instruments	
G6.2	Jean-Marc Zanotti	jean-marc.zanotti@cea.fr
G1bis	Stéphane Longeville	stephane.longeville@cea.fr
	Neutron radiography	
G4.5	Guy Bayon	guy.bayon@cea.fr

Beamtime Access

THE LLB-ORPHEE NEUTRON SCATTERING AND IMAGING INSTRUMENTS

Powder diffractometers

3T2 "Thermal neutrons" 2-axis (50 detectors) high resolution, mainly for nuclear structure determination.

G4.1 "Cold neutrons" 2-axis (multidetector 800 cells) high flux, mainly for magnetic structure determination

G6.1 "Cold neutrons" 2-axis (multidetector 400 cells) with long wavelength (~5Å) and high flux, for the study of very small powder samples (<1mm^3). Very high pressure cell available (40 GPa).

Single crystal diffractometers

5C1 "Hot neutrons" 2-axis with lifting arm, polarized neutrons, magnetic field (8 Tesla) for spin-density maps determination

5C2 "Hot neutrons" 4-circle for nuclear structure determination.

6T2 "Thermal neutrons" 2-axis, lifting arm and 4-circle, mainly for magnetic structure determination. 12 Tesla magnetic field available, 2D detector.

Diffuse scattering instruments

7C2 "Hot neutrons" 2-axis (multidetector 640 cells) for local order studies in liquid or amorphous systems. Cryostat and furnace available (1.2K to 1300°C).

Small-angle scattering instruments

G1.2 "Cold neutrons" (annular detector, 30 rings) for study of large scale structures in isotropic systems (mainly polymers and colloids).

G2.3 "Cold neutrons" (X-Y detector, 128x128 cells) for study of large scale structures (10 to 500 Å) in anisotropic systems (polymers under stress, metallurgical samples, vortex in superconductors).

G5.4 "Cold neutrons" (X-Y detector, 64x64 cells) for multipurpose studies of large scale structures.

G5bis Very Small Angle Neutrons Scattering spectrometer

Diffractometers for material science studies

6T1 "Thermal neutrons" 4-circle for texture determination.

G5.2 "Cold neutrons" 2-axis for internal strain determination in bulk samples with spatial resolution ~ 1mm^3.

Reflectometers

G3bis "Cold neutrons" reflectometer operating in time-of-flight mode for multipurpose surface studies.

G 2.4 "Cold neutrons" reflectometer with polarized neutrons and polarization analysis for the study of magnetic layers.

Triple-axis instruments

1T "Thermal neutrons" high-flux 3-axis instrument with focussing monochromator and analyser, mainly devoted to phonon dispersion curves measurements. Very high pressure cell (100 Kbar) available.
CRG Instrument operated in collaboration between the INFP Karlsruhe and the L.L.B

2T "Thermal neutrons" high-flux spectrometer with focussing monochromator and analyser, mainly devoted to spin-waves and magnetic excitations studies (1.5 to 80 meV).

4F1
4F2 "Cold neutrons" high flux 3-axis instruments with double monochromator and analyzer, mainly devoted to the study of low-energy (15µeV to 4meV) magnetic excitations. Polarized neutrons and polarization analysis option available.

Quasi-elastic instruments

G62 "Cold neutrons" high resolution (~15µeV at 10Å) time-of-flight instrument for the study of low energy excitations, mainly in disordered systems.

G1bis "Cold neutrons", high resolution and high flux spin-echo instrument. It can study, in a large Q range, slow dynamics of large molecules in biology or long relaxation times like in glassy transition (Fourier times ~ 20ns)

Neutron Radiography

G4.5 Imaging technique : white beam facility for non-destructive control or dynamics imaging.

http://www-llb.cea.fr/fr-en/spectros_p.php

AUXILLIARY SERVICES AVAILABLE

Laboratories for sample preparation:
- Chemistry laboratory
- Biological laboratory

Technical help for:
- Vacuum/Cryogenics
- Cryostat, Furnace (0.1 – 2000 K)
- High pressures (up to 10 GPa)
- High magnetic fields (up to 10 T)
- Mechanics

ACCESS TO BEAMTIME

LLB has been selected in the frame of the European Community – Access activities of the Neutron scattering and Muon spectroscopy Integrated Infrastructure Initiative (NMI3) which supports access to neutron beams for the selected user teams, travel and subsistence fees of visiting scientists. The program is opened to E.C. users and to scientists of the associated states.

http://idb.neutron-eu.net/facilities.php

Beamtime access is free of charge for any experimentalist from the French Scientific community. LLB takes in charge the expenses (travel and stay) of 2 people during the experiment.

Beamtime on the 23 open-access spectrometers can be requested by submission of:

- *An experimental application to a Selection Committee (Normal Procedure)*
This procedure is open to any public/industrial researcher that is interested in using neutron scattering for his research. Results should be free to be totally or partially published in a Scientific Review.

DEADLINE FOR APPLICATION: May 1st and November 1st
http://www-llb.cea.fr/en/fr-en/proposal.php

- *An experimental application to the Directors (Exceptionnal)*
This special procedure should only be used exceptionally for hot topics, confidentiality reasons or if an anomaly in the review procedure is suspected. The delay between the acceptation decision and the realization of the experiment is shortened to the minimum.
There is no deadline for such propositions, which are examined all along the year.
http://www-llb.cea.fr/en/fr-en/proposal.php

- *A fast access application*
This procedure allows a rapid access (1 to 2 months delay) to the spectrometers in order to perform a short experiment (1 day max.). It can be used for feasibility tests, sample characterization, obtaining complementary results…
There is no deadline for such propositions, which are examined all along the year.
http://www-llb.cea.fr/en/fr-en/prop-rap.php

CONTACT AT LABORATOIRE LEON BRILLOUIN

Laboratoire Léon Brillouin
Scientific Office
CEA SACLAY
Bâtiment 563   F - 91191 Gif-sur-Yvette Cedex
Tel. : 33(0) 1 69 08 60 38 • Fax : 33 (0) 1 69 08 82 61
e-mail : experience-llb at cea.fr •
Internet : http://www-llb.cea.fr

SELECTION COMMITEES

Proposals are examined by 5 Selection Committees. Each is composed of 10 to 12 senior scientists that are nominated by the management of LLB for 3 years. At least half of them do not belong to the LLB and 2 or 3 are coming from foreign institutes.

For each spectrometer, LLB gives a beam-time available which is shared out by the committee; each proposal gets a grade A or B or C.

A : The experiment must be done and the committee allocates a beam-time

B : The experiment might be done if there is some extra beam-time,

C : The experiment is refused on scientific arguments.

Selection Committees are asked to take care of the educationnal duty of the LLB when proposal comes from new young searcher.

SELECTION COMMITEES: SCIENTIFIC FOCUS AND SUB-FOCUS

Theme I Chemical physics, biological systems
- I.01   Polymers and Supramolecular Structures
- I.02   Water, aqueous solutions, polyelectrolytes, surfactants
- I.03   System of biological interest, Biophysics
- I.04   Colloids, nanostructures
- I.05   Gels, composite materials
- I.06   Other...

Theme II Crystallographic and magnetic structures
- II.01   Crystalline structures
- II.02   Phases transitions
- II.03   Magnetic Structures
- II.04   High pressures (on powders)
- II.05   Other...

Theme III   Magnetism: Single-crystal systems and thin layers
- III.01   Magnetic thin layers
- III.02   Spin density
- III.03   Systems with strong quantum correlations
- III.04   Extreme conditions (strong fields, high pressures)
- III.05   Magnetic nanosystems
- III.06   Other...

Theme IV Disordered Systems, nanostructured materials and materials
- IV.01   Liquid and amorphous structures
- IV.02   Dynamics of disordered systems
- IV.03   Thin film materials
- IV.04   Nanostructured materials, precipitation, cavities,…
- IV.05   Crystallographic textures
- IV.06   Strains and residual stresses
- IV.07   Other...

Theme V Excitations
- V.01   Magnons
- V.02   Supraconductivity
- V.03   Coupling spin-network
- V.04   Dynamics in frustrated systems
- V.05   Polarized neutrons with polarization analysis
- V.06   Phonons
- V.07   Other…

LLB Reviewing committees

Spring 2010	Automn 2010

COLLEGE 1: Chemical physics, biological systems

Organisers: G. Carrot, N. Malikova | *Organisers: G. Carrot, N. Malikova*

LLB	French users	European users	LLB	French users	European users
F. Cousin	C. Chassenieux	W. Hauessler	F. Cousin	C. Chassenieux	W. Hauessler
D. Lairez	E. Dubois	R. v. Klitzing	D. Lairez	E. Dubois	R. v. Klitzing
	Yvette TRAN	**P. Stepanek [chairman]**		Yvette TRAN	**P. Stepanek [chairman]**
	R Schweins	M. Sferrazza		R Schweins	M. Sferrazza
		M. Weik			F. Gabel

COLLEGE 2: Crystallographic and magnetic structures

Organisers: F. Porcher, N. Rey | *Organisers: F. Porcher, N. Rey*

LLB	French users	European users	LLB	French users	European users
F. Damay	M.H. Lemée-Cailleau	**G. Heger [chairman]**	F. Damay	S. Ravy	**G. Heger [chairman]**
I. Mirebeau	G. Rousse	J. Alonso	I. Mirebeau	G. Rousse	Blanco
	Michaël Josse	L. Chapon		M. Josse	A. Daoud-Aladine

COLLEGE 3: Magnetism: Single-crystal systems and thin layers

Organisers: A. Bataille, F. Ott | *Organisers: A. Bataille, F. Ott*

LLB	French users	European users	LLB	French users	European users
G. André	K. Dumesnil	**J. Campo [chairman]**	G. André	T. Hauet	**J. Campo [chairman]**
	E. Ressouche	K. Temst		E. Ressouche	K. Temst
	O. Mentré			O. Mentré	

COLLEGE 4: Disordered Systems, nanostructured materials and materials

Organisers: V. Klosek, M.H. Mathon | *Organisers: V. Klosek, M.H. Mathon*

LLB	French users	European users	LLB	French users	European users
F. Audonnet	**J.L. Bechade [chairman]**	B. Frick	F. Audonnet	**J.L. Bechade [chairman]**	M. Gonzalez
	L. Cormier	M. Fitzpatrick		L. Cormier	M. Fitzpatrick
	A. Deschamps			A. Deschamps	

COLLEGE 5: Excitations

Organisers: P. Bourges, D. Petitgrand | *Organisers: J. Robert, D. Petitgrand*

LLB	French users	European users	LLB	French users	European users
J. Robert	M. Boehm	**P. Link [chairman]**	D. LAMAGO	**M. Boehm [chairman]**	B. Roessli
	L.-P. Regnault	J. Hlinka		L.-P. Regnault	J. Hlinka,
	P. Foury	A. Huxley		P. Foury	A. Huxley